THIS REPORT HAS BEEN DELIMITED
AND CLEARED FOR PUBLIC RELEASE
UNDER DOD DIRECTIVE 5200.20 AND
NO RESTRICTIONS ARE IMPOSED UPON
ITS USE AND DISCLOSURE.

DISTRIBUTION STATEMENT A

APPROVED FOR PUBLIC RELEASE;
DISTRIBUTION UNLIMITED.

DISCLAIMER NOTICE

THIS DOCUMENT IS BEST QUALITY PRACTICABLE. THE COPY FURNISHED TO DTIC CONTAINED A SIGNIFICANT NUMBER OF PAGES WHICH DO NOT REPRODUCE LEGIBLY.
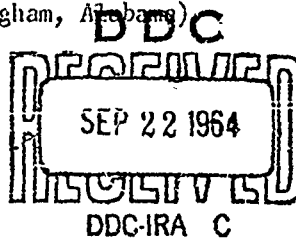
TERMINAL BALLISTIC TARGET ANALYSIS AND STUDY
OF TARGET VULNERABILITY TO VERY HIGH SPEED IMPACT

Technical Documentary Report No. ATL-TDR-64-51
August 1964   Project No. 5841
                                          Task No. 02

Directorate of Armament Development
Det 4, Research and Technology Division
Air Force Systems Command
Eglin Air Force Base, Florida

Qualified requesters may obtain copies from DDC. Orders will be expedited if placed through the libraries or other person designated to request documents from DDC.

When US Government drawings, specifications, or other data are used for any purpose other than a definitely related government procurement operation, the government thereby incurs no responsibility nor any obligation whatsoever; and the fact that the government may have formulated, furnished, or in any way supplied the said drawings, specifications, or other data is not to be regarded by implication or otherwise, as in any manner licensing the holder or any other person or corporation, or conveying any rights or permission to manufacture, use, or sell any patented invention that may in any way be related thereto.

Do not return this copy. Retain or destroy.

KEYWORD LIST
Listed below are keywords which serve as an index
to the contents of this report (AFR 80-29)
Targets
Hypervelocity projectiles
Terminal Ballistics

FOREWORD

Forty-nine targets of various silide materials and of various configurations
were examined to determine the effects of hypervelocity impact by aluminum
projectiles on the targets. Targets were examined visually. Dimensions of
perforations and craters made by projectiles of known mass and velocity were
measured. Specimens from damaged areas were mounted, polished and examined
microscopically. The effects of hypervelocity impact were found to be
confined to a narrow region around impact areas. The results of the target
examinations are presented in this report.

A consideration of new and novel approaches to the analysis of the effects
of hypervelocity impact on targets was made. The results of this work are
discussed.

PUBLICATION REVIEW

This technical documentary report has been reviewed and is
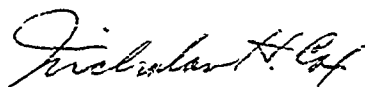approved.

NICHOLAS H. COX
Colonel, USAF
Acting Director

TABLE OF CONTENTS

TABLE OF CONTENTS

1. INTRODUCTION

Under Contract AF 08(635)3641, a series of forty-nine targets subjected to the impact of hypervelocity projectiles were examined to determine the effects of hypervelocity impact. The targets were composed of various metallic materials and configurations as shown in Table 1. The targets were exposed to hypervelocity projectiles at the hypervelocity test facility at Eglin Air Force Base, Florida. A shaped charge technique was used to obtain aluminum projectiles in the range from 27,000 feet per second to 32,000 feet per second. The particle projector consisted of a Composition B shaped-charge with a 42° conical liner of 1100F aluminum alloy. Eccentric initiation was used to obtain particle dispersion. Altitude simulated during firing was approximately 200,000 feet. The distance between the particle accelerator and the target was maintained at eighteen feet and one inch. The angle of obliquity (angle between the projectile velocity and the target face) was 90°.

Targets were given a thorough visual examination. The dimensions of perforations and craters made by projectiles of known mass and velocity were measured. Rockwell hardness measurements were made on the surface of the targets near perforations and in undamaged area. Targets were sectioned, and specimens from the damaged areas were mounted and polished for microscopic examination. Photomacrographs and photomicrographs were made to record changes in metal structure. Microhardness surveys were performed on some specimens.

In addition to the examination utilizing standard laboratory techniques, new and novel means of conducting target analyses were considered.

2. TARGET ANALYSIS

2.1 THIN ALUMINUM TARGETS

Twenty-three of the targets were spaced panel targets in which the first panel was 0.10 inch thick 2024-T3 aluminum. Subsequent panels varied in number and thickness as shown in Table 1. Photographs of typical targets are shown in Figures 1 through 12. Generally, projectiles perforated the initial plate of targets in a string of perforations running diagonally across the plates. Perforations overlapped to form an irregularly shaped continuous perforation in the central portion of the impact area because of close spacing of the impacting projectiles. Perforations produced by projectiles for which the masses and velocities were measured were located at the end of and separated from the main string of perforations. Pitting was severe in the area adjacent to the perforations. A number of small perforations were observed scattered over the target plates.

Damage to the first panel of each target was determined by measuring the dimensions of the perforations produced by projectiles of known mass and velocity. From the dimensions, the areas of the perforations were calculated. These data are summarized in Table 2. Perforation area is plotted as a function of projectile mass in Figure 13. The data show

considerable scatter. Perforation area plotted as a function of the projected area of the impacting projectile produces a smoother relationship as shown in Figure 14. Consequently, the damage to thin 2024-T3 aluminum targets appears to depend primarily on the projected area of the projectile.

Damage to subsequent panels of multiple panel targets varied. Large perforations with petalled edges occurred in 0.1 inch 2024-T3 aluminum second panels at a stand-off distance of two inches (Figure 2). Surface pitting and metallizing of second panels of 0.1 inch 2024-T3 aluminum occurred at stand-off distances of four and twenty-four inches. In general, surface pitting and metallizing were the major effects observed on 0.25 inch 2024-T3 and 0.50 inch 2024-T4 aluminum panels at stand-off distances ranging from two to twenty-four inches. Spallation or scabbing from the rear surface opposite impact points occurred. Extensive pitting, metallizing, and some shallow cratering were observed on 1.0 inch 2024-T4 plates for stand-off distances ranging from two to twenty-four inches. Rear surface spallation occurred only on target 64-04.

Rockwell hardness measurements (15T scale) were made on target surfaces near perforations. The first indentation was made as close to the edge of a perforation as possible. Additional indentations were made at progressively greater distances from the perforation. No change in hardness was evident in damaged areas.

Sections were cut from the edges of perforations, mounted and polished for microscopic examination. A typical pattern of damage was found for 0.1 inch thick 2024-T3 aluminum targets. Grain flow around perforations indicated a displacement of target material from both the front and back surfaces of targets. Typical grain flow patterns at the edges of perforations are shown in Figures 15 through 18. Grain flow extended for a short distance radially from the edges of perforations, generally to a distance approximately equal to the plate thickness. The dividing plane between flow fields was at the mid-plane of the plate. Little or no grain flow was evident at the mid-plane of the plate. Examination of metal structure near perforations at magnifications up to 500X revealed plastic deformation of individual grains in the region of grain flow. Photomicrographs of typical grain structure near perforations are presented in Figures 19 and 20. The structure in damaged areas was examined for evidence of the effects of high temperatures on target material. There was no apparent eutectic melting or grain boundary precipitation. No effects attributable to high temperatures were found.

Microhardness surveys were made on some of the polished specimens obtained from impact areas. A graph of microhardness (Vickers scale) as a function of the distance from the edge of perforation A for target 48-61 is presented in Figure 21. Hardness values indicated a narrow region of work hardened material in the highly deformed area around the perforation. The work hardened area was approximately 0.1 inch wide. A maximum hardness of 176 occurred at 0.05 inch from the edge of the perforation. Based upon similar microhardness surveys on other targets, this effect appears to be typical of thin aluminum target perforation.

2.2 THICK ALUMINUM TARGETS

Six thick aluminum targets were examined. Targets 63-09 and 63-10 were single panel targets of 0.5 inch 2024-T4 aluminum plate. Target 63-95 was a single panel target of 1.0 inch 2024-T4 aluminum plate. Targets 63-98, 63-102, and 63-109 were single panel targets of 2.0 inch 2024-T351 aluminum plate. Each target is discussed individually in this section. Target damage data are summarized in Table 2.

2.2.1 Target 63-09

Target 63-09 was a single panel target of 0.5 inch 2024-T4 aluminum plate. Front and back views of the target are shown in Figures 22 and 23. One projectile with a mass of 1.0 grains and a velocity of 27,800 feet per second was identified. Projectile A perforated the target. The perforation resembled a crater in many respects. The walls sloped inward from a 0.7 inch diameter opening at the front surface to a 0.3 inch diameter opening at the bottom of the perforation. The material around the lip of the perforation was upset slightly above the front surface of the target. Severe spallation or scabbing occurred around the perforation at the rear surface of the target. The depth and diameter of the scab were about 0.1 inch and one inch respectively. The general shape and dimensions of the perforation are shown in the following diagram:
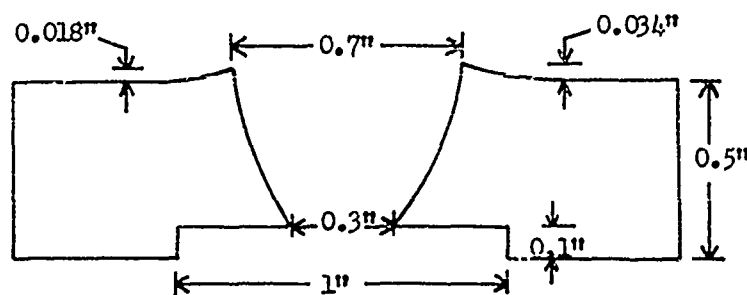

Projectile A would probably not have perforated the target except for the scabbing from the back surface of the plate.

Grain flow about perforation A is shown in Figure 24. Predominant grain flow is toward the back surface of the target. However, for a depth of about 0.1 inch below the front surface of the target, grain flow is toward the front surface of the target. Laminar cracking in the wall of the perforation and scabbing at the back surface are evident. A microhardness traverse was made along the mid-plane of the plate using a Durimet Microhardness Tester with a 100 gram load. The results are plotted in Figure 25. Hardness readings were made at intervals from a point 0.005 inches from the edge of the perforation out to 0.6 inch. Work hardening occurred in the deformed area. The work hardened area extended out to a distance of approximately 0.5 inch. A maximum Vickers hardness of 189 occurred at 0.050 inch from the edge of the perforation.

No evidence such as eutectic melting or grain boundary precipitation was found of high temperature effects on the target upon examination of a polished specimen at high magnification (500X). Individual grains were deformed in a plastic manner around the impact area. What appear to be slip bands were found in the area around perforation A. Multiple slip systems are shown in Figure 26. Electron micrographs of surface replicas of an area near perforation A are presented in Figures 27, 28, and 29. The electron micrographs were prepared by the Electron Microscope Laboratory, Engineering Experiment Station, Georgia Institute of Technology. Structures which may be slip bands are evident in the electron micrographs. Microfissures and alloying constituents are also evident. Damage to the replica may have occurred in the area shown in the upper left corner of Figure 28.

2.2.2 Target 63-10

Target 63-10 was a 0.5 inch 2024-T4 aluminum target. Projectiles A and B had masses of 2.0 and 7.6 grains, respectively, and a common velocity of 29,700 feet per second. Both projectiles perforated the target cleanly as opposed to the crater-like perforation noted in target 63-09. Severe spallation occurred around the peripheries of both perforations at the front and back surfaces of the target as is evident in Figures 30 and 31. The diameters of perforations A and B, excluding the spalled areas, were 0.75 and 1.5 inches, respectively. The general shape and dimensions of the perforations are illustrated in the following diagram:

Perforation A   Perforation B
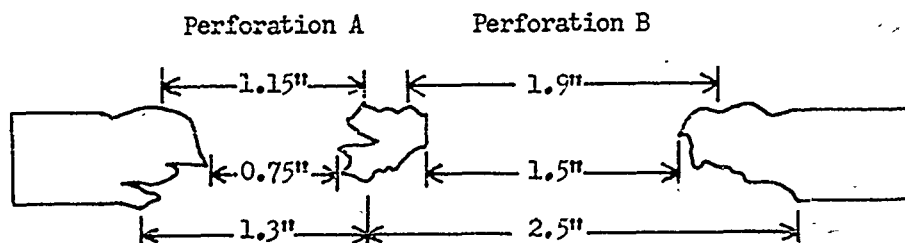
Examination of polished cross-sections through the perforations revealed grain flow toward the front and back surfaces of the target. Grain flow extended outward from the edges of the perforation for about 0.5 inch. Laminar cracking occurred in the walls of the perforation. No effects of high temperatures, such as eutectic melting or grain boundary precipitation, on target material were evident. Slip bands were found in a small number of grains, but they were not so extensive as those observed in Target 63-09.

Three microhardness surveys were made on a section from perforation B. Measurements were made from the edge of the perforation out to unaffected material at 0.050 and 0.250 inch from the front surface and 0.050 inch from the rear surface. The results are presented in Figure 32. The hardness measurements indicate work hardening in the deformed areas.

2.2.3 Target 63-95

Target 63-95 was 1.0 inch 2024-T4 aluminum plate. Figures 33 and 34 are photographs of the target. Projectile A had a mass of 6.4 grains and a velocity of 31,400 feet per second. Crater A was 1.63 inches in diameter at the front surface of the target. A scabbed area 2.5 inches in diameter was observed at the rear surface of the plate. The scab and crater intersected to form a perforation. A cross section through the crater is shown in Figure 35. Laminar cracks originating at the interior surface of the cavity and radiating into the base metal were found. The cracks sloped upward toward the impact surface. Multiple scabbing was predominant toward the rear surface and became indistinguishable from the laminar cracks originating near the bottom of the crater. Grain flow toward the impact surface existed along the upper rim of the crater. Grain flow adjacent to the lower boundary of the crater was nearly parallel to the crater's wall.

2.2.4 Target 63-98

Target 63-98 was a single panel target of 2.0 inch 2024-T351 aluminum alloy. No impact area or projectile data were available for target 63-98. In general, the impacting projectiles formed a line of shallow craters across the target surface as shown in Figure 36. A deep narrow crater was evident near one end of the line of shallow craters. The surface opening of this crater was about 0.67 inch. Figure 37 shows a section through this crater. After sectioning, the depth of the crater was found to be approximately one inch. From the cross sectional view of the crater, it appears to have been formed by the impact of several small projectiles in succession rather than a single projectile of unusual penetrating ability.

2.2.5 Target 63-102

Target 63-102 was a single panel target of 2.0 inch 2024-T351 aluminum alloy. Two projectiles were identified for target 63-102. The mass and velocity of projectile A were 7.8 grains and 31,000 feet per second; of projectile B, 1.7 grains and 30,800 feet per second. Crater A was 1.38 inches in diameter and 0.63 inch deep and had a volume of 7.7 milliliters. Crater B was 1.13 inches in diameter and 0.5 inches deep and had a volume of 4.0 milliliters. A photograph of the target is presented in Figure 38.

Polished cross-sections through craters A and B revealed a few laminar cracks originating at the interior surfaces of the craters and radiating into the base metal. Grain flow toward the impact surface was evident along the upper rims of the craters. Grain flow adjacent to the lower boundary of the craters was approximately parallel to the craters' walls. A cross sectional view through crater A is presented in Figure 39. As a result of compressive forces acting at the bottoms of the craters, severe grain distortion occurred at the bottoms of both craters. Grains were elongated and flattened.

6

2.2.6 Target 63-109

Target 63-109 was a single panel target of 2.0 inch 2024-T351 aluminum alloy. Figure 40 is a photograph of the target. Projectile A with a mass of 3.9 grains and a velocity of 31,500 feet per second produced a crater 1.75 inches in diameter and 0.75 inches deep in target 63-109. The volume of the crater could not be determined by liquid measurement because of interconnection with an adjacent crater produced by an unidentified projectile. A large protrusion about 0.2 inches in height was visible on the rear surface of the target opposite the crater. A cross sectional view through the crater is presented in Figure 41. A number of laminar cracks radiated out into the base metal from the walls of the crater. There were a number of cracks that originated and terminated in the central portion of the plate between the bottom of the crater and the rear surface of the plate. Multiple scabbing occurred near the rear surface of the plate resulting in the protrusion observed in the visual examination. The cracking and scabbing indicate that the plate was subjected to tensile stresses arising from interference of the incident shock wave and the reflected wave from the back surface of the plate of sufficient magnitude to fracture the plate. Severe grain distortion such as was described for Target 63-102 occurred at the bottom of the crater. No significant change in grain structure was found in the central portion of the plate below the crater in the vicinity of the cracks and scab-type fracture.

2.3 MAGNESIUM TARGETS

Thirteen spaced panel magnesium targets were examined. The first panels of eleven of the targets were 0.1 inch AZ31B-H24 magnesium sheet; the first panels of the other two targets were 0.25 inch AZ31B-H24 magnesium sheet. Subsequent panels of targets 63-17, 63-18, and 63-19 were 2024 aluminum alloy. Subsequent panels of the remainder of the targets were AZ31B-H24 magnesium of varying thicknesses. Target configurations are summarized in Table 1. Photographs of typical targets are presented in Figures 42 through 49.

Impacting projectiles perforated the first panels of all targets. Damage was assessed by measuring the dimensions of perforations made by projectiles of known mass and velocity. The areas of the perforations were calculated from the measured dimensions. These data are summarized in Table 2. Figures 50 and 51 are graphs of perforation area as a function of the mass and the projected area of the impacting projectile. Only eleven data points were available for plotting, since no data were available on the projectiles for five targets and the perforations were obscured by interconnecting perforations in two of the targets. The data show considerable scatter in both cases. The data are too limited to draw any definite conclusions concerning the relationship between the characteristics of the impacting projectile and the damage produced in thin magnesium targets.

Damage to subsequent panels of multiple panel magnesium targets varied. Large perforations with petalled edges were formed in 0.1 inch second panels of 2024-T3 aluminum at stand-off distances of two and four inches.

Second panels of 0.1 inch AZ31B-H24 magnesium sheet were perforated by residual fragments from first panels at standoff distances of eight and twenty-four inches. Perforation also occurred in 0.25 inch AZ31B-H24 magnesium second panels at standoff distances of four and twenty-four inches.

Examination of sections cut from the edges of perforations revealed a typical pattern of damage for thin AZ31B-H24 magnesium targets. Metal flowed toward the front and rear surfaces of targets around the peripheries of perforations. Metal flow extended radially from the perforations for distances very nearly equal to the thickness of the target plate. The center plane of the target was the dividing plane for the regions of observed metal flow. Figures 52 through 54 are photomacrographs of typical metal flow at the edges of perforations. Strain or work hardening occurred in the regions of metal flow. A graph of microhardness (Vickers scale) as a function of distance from the edge of perforation B, target 63-18 is shown in Figure 55. A significant increase in hardness was found. The Vickers hardness at a distance of 0.003 inch from the edge of the perforation was 128. The hardness decreased through the affected area and became constant at a value of 65 beyond a distance of 0.2 inch from the perforation. A refinement of grain structure as evidenced by a smaller grain size occurred in the region of metal flow. This effect is illustrated in Figure 56 with photomicrographs of grain structure in an unaffected area and an area near perforation B of target 63-18. Electron micrographs of a surface replica from the area near perforation B of target 63-18 are presented in Figures 57, 58, and 59. A number of micro-fissures and crystallographic planes are evident in the electron micrographs.

2.4 STEEL TARGETS

Targets 63-86, 63-87, and 63-88 were two panel targets of 0.1 inch 4130 steel per MIL-S-18729B. The material was in the annealed condition. Photographs of these targets are presented in Figures 60 through 65. Impacting projectiles perforated the first panel of each target. The front surfaces of second panels were severely pitted. A few small perforations which could not be associated with projectiles of known mass or velocity were noted in second panels. Damage was determined by measuring the dimensions of perforations produced by projectiles which were identified as to mass and velocity. Perforation area was calculated from the dimensions. These data are summarized in Table 2.

A limited region of metal flow was found at the peripheries of perforations. Metal flow toward the front and back surfaces of the targets occurred. Figure 66 is a photomacrograph of a typical section through a perforation. A microhardness survey was made from the edge of perforation A in target 63-87 along the mid-plane of plate one. The data are plotted in Figure 67. Work hardening occurred in the deformed area near the perforation. The Vickers hardness at a distance of 0.003 inch from the perforation was 208. The hardness decreased through the region of metal flow and became constant at a value of about 173 at a distance of 0.09 inch from the perforation.

No significant change in structure was observed in the vicinity of perforations. The material was in the annealed condition. Structure is not subject to change unless heated above its upper critical temperature. Change in structure is also dependent upon time at temperature. Assuming that sufficient energy was deposited in the target at perforations to raise the temperature above the upper critical point, heat would be dissipated rapidly in the surrounding material. The material would not be above the upper critical point for a significant period of time. Therefore, the structure observed did not reveal any significant details.

Target 63-104 consisted of three panels of 0.1 inch stainless steel. Spectrochemical analysis identified the material as type 410 stainless steel. Projectiles A and B with masses of 6.1 and 1.5 grains and velocities of 31,100 and 30,700 feet per second, respectively, perforated the first panel of the target as shown in Figure 68. The second panel of the target is shown in Figure 69. The second plate was shattered into a number of pieces. Damage to the third plate was minor.

Perforation A in panel one was elliptical with principal axes of 1.25 and 0.63 inches. Perforation B was circular with a diameter of 0.63 inches. The areas of perforations A and B were 0.61 and 0.31 square inches, respectively. Spallation or scabbing occurred at the front and back edges of the perforations. Metal flow is limited to the center edges of the perforations as shown in Figure 70. Specimens of material at the edges of the perforations were examined for change in martensite. No further tempering of the martensite or phase change to another microstructure was observed.

2.5 TITANIUM TARGETS

Targets 63-97, 63-99, and 63-100 were multiple panel targets of 0.1 inch titanium. Spectrographic analysis of the target material indicated it to be an alloy containing six percent aluminum and four percent vanadium. Figures 71 through 77 are photographs of the targets. Impacting projectiles perforated the first panels of the targets. The second panels were also perforated at stand-off distances of two inches for targets 63-97 and 63-99 and four inches for target 63-100. Data were available for only one projectile impacting on target 63-99. Projectile A had a mass of 7.1 grains and a velocity of 30,900 feet per second. The perforation produced by this projectile was elliptical with principal axes of 1.13 and 0.63 inches. The perforation area was 0.56 square inches.

A limited region of metal flow was found at the edges of perforations. Metal flow toward the front and rear surfaces of target panels occurred with essentially no flow at the center of the panel. Figure 78 is a photomacrograph of a section through a perforation in target 63-100. A photomicrograph of the structure near the edge of a perforation in target 63-100 is shown in Figure 79. There was no significant difference observed in the microstructure in the vicinity of perforations and in unaffected areas of the targets.

3. NEW AND NOVEL TECHNIQUES

The problem of developing new and novel techniques for examining impacted targets has been studied, and attempts have been made to apply several of the proposed techniques on an experimental scale. When the analysis program was proposed, a variety of possible nonmetallurgical testing techniques were discussed. Among the examination techniques proposed for study were the following: Electrical properties (resistivity and/or conductivity measurements), observations of optical properties, measurement of thermal properties, photoelastic analyses, and x-ray diffraction studies. A review of each of these possible techniques will reveal the degree of success attained with some and the reasons for eliminating others.

The original R & D Exhibit, on which the program proposal was based, stated that "targets will consist of a wide variety of metallic and plastic target panels and composite structural panels." Examination techniques must necessarily be tailored to the particular material under study. In the case of electrical properties, the applicable techniques resolve into resistivity measurements for metallic materials and conductivity measurements for nonmetallic materials. Since only metallic, and these primarily aluminum and magnesium, targets were submitted, the conductivity measurements were not attempted. Investigations were conducted into possible techniques for measuring changes in resistivity in impacted areas. These investigations were made on the basis of theoretical hypotheses concerning the effects of shock wave phenomena.

It was hypothesized that impact shock waves propagated through the targets would leave regions of local strain and associated discontinuities which might be detected by resistivity measurements. Such discontinuities occur when a projectile impacts at a speed greater than the dilatational wave velocity and sets up impact shock waves which interact with reflected shock waves. These discontinuities should be observable as abrupt changes in electrical resistivity in target materials normally homogeneous and isotropic. It was anticipated that the changes in resistivity might be measured as a function of radial distance from a reference electrode in the center of a crater, and that a plot of equal-resistivity curves might be interpreted in the light of a micrometallurgical examination.

An experiment was performed on a crater in a semi-infinite target of 2024 aluminum to test the feasibility of the method. The rear surface of the target was thoroughly cleaned with fine emery cloth to insure proper electrical contact with a copper plate. The copper contact plate, cut slightly larger than the target, was cleaned on both sides with emery cloth and four leads of standard 16 gage copper wire were soldered to the approximate mid-point of each side. The four leads were then cut to the same length and soldered to an identical single wire connecting them with one terminal of a Wheatstone bridge capable of measuring 0.001 ±0.001 ohm. Several random resistance measurements made over the surface of the copper plate fell within 0.001 ohm of one another, thus assuring that the electrode plate and its lead wires would not contribute spurious resistances.

Another lead from the Wheatstone bridge terminated in a meter test probe. The probe was filed sharp and mounted in a ring stand clamp. Under the test probe, the target was mounted on a lab jack which could be raised to establish

contact. A series of resistance measurements, made around several imaginary circles concentric with the crater, averaged 0.063 ohm, but the measurements were not reproducible to within ±0.01 ohm and were not recorded.

The lack of reproducibility in the resistance measurements was attributed to contact potentials caused by the probe and to contact pressure variations. The small changes in the resistance of the target material apparently were masked by these small pressure variations.

Novel techniques based on the examination of optical properties had to be eliminated from consideration, since all the targets submitted were opaque.

Consideration of techniques based on observing deviations from normal thermal properties (limited by practical considerations to thermal conductivity) of targets was influenced by the result of the electrical experiments. The thermal conductivity of metals is due principally to electron transport, since phonons are too easily scattered by electrons. It follows, therefore, that good electrical conductors are also good thermal conductors. The high electrical conductivity of the target materials, eliminating reliable measurement of changes in electrical properties, also rendered impractical the measurement of changes in thermal properties and the mapping of isothermal curves.

Photoelastic analysis offers a sensitive means of determining residual surface strain. Sensitivities of ±10 microinches per inch for strain magnitude and ±2° for principal strain directions can be obtained using standard instrumentation. Laminated targets comprised of thin plates separated only by photoelastic films might reveal some internal strain distributions. The disadvantage of photoelastic analysis is that the films must be applied to the target before impact. None of the targets was so prepared, so this particular technique could not be investigated.

Finally, x-ray diffraction studies can provide information about grain orientation, crystal transformations, strain, and lattice distortion. Micrographs made for various targets revealed little evidence of extensive alterations in microstructure. However, preliminary x-ray diffraction analyses were made on two target plates having craters, 63-9 and 64-4. The former was a 1/2-inch aluminum plate and the latter, a 3/4-inch aluminum plate. The first reports indicated no observable differentiation between the impacted area and an unaffected area. More careful analysis of the traces, based on differences in peak heights, areas, and displacements, indicated that sample 64-4 had some change in crystal orientation, strain, and possibly lattice distortion. Sample 63-9 had the same changes but to a lesser extent. No changes in lattice parameters were indicated by the traces. The results of these preliminary examinations did not seem to justify the additional cost of more elaborate analyses. The x-ray diffraction analyses were performed by the Georgia Institute of Technology, Engineering Experiment Station, Atlanta, Georgia.

Mention was made in the Third Quarterly Technical Report of a possible investigation of energy transmission at audio frequencies. As stated at that time, the energy equation for a sound wave in a given material is

$$E = 2\pi^2 f dn^2 a^2,$$

where E is the energy, d is the density of the material, n is the frequency, and a is the amplitude of the sound wave. It can be seen that the only material property entering into the equation is the density. A considerable change in density would be required to measurably alter the transmitted energy. Such a density change would have been manifested as a change of the lattice parameters in the impacted area. Since the x ray diffraction work indicated no such change, it must be concluded that any changes in energy transmission would be negligibly small. Accordingly no experimental apparatus was designed to test the hypothesis.

4. CONCLUSIONS

Target damage assessment is complicated by the interplay of many variables such as size, shape, mass, velocity and orientation of impacting projectiles; target panel thickness and spacing; and target material properties. Therefore, no direct correlation between any two variables is possible without a consideration of other variables mentioned above. The following qualitative conclusions, based upon data which are limited with respect to several variables, appear to be warranted:

1. Damage Pattern

   Damage to thin panel targets of 2024-T3 aluminum alloy, AZ31B-H24 magnesium alloy, 4130 steel, and 6Al-4V titanium alloy was limited to a narrow region around perforations. The pattern of damage is typical for 0.1 inch panels. Metal flow around perforations indicates displacement of target metal from the front and back surfaces of targets. The regions of metal flow extend radially from the edges of perforations to a distance approximately equal to the plate thickness. The dividing plane between flow fields is at the mid-plane of target plates. An increase in hardness occurs in regions of metal flow. No changes in structure attributable to the effects of high temperatures on target materials occur.

2. Perforation Size

   Damage to the first panel (0.1 inch) of multiple panel targets of aluminum and magnesium as measured by the areas of perforations produced by projectiles of known mass and velocity appears to depend primarily upon the projected area of impacting projectiles. For 2024-T3 aluminum targets, the ratio of perforation area to projected area of an impacting projectile varies from ten (10) for small projected areas to approximately six (6) for large projected areas for a velocity range of 30,000 to 32,000 feet per second. With AZ31B-H24 magnesium targets the ratio of perforation area to projected area of an impacting projectile varies from about twenty (20) for small projected areas to about twelve (12) for large projected areas for a velocity range of 26,000 to 32,000 feet per second. A comparison of the ratio of perforation area to projected area of the impacting projectile indicates that a projectile with a given projected area produces twice the damage in 0.1 inch AZ31B-H24 magnesium plates as in 0.1 inch 2024-T3 aluminum plates.

3. Effect on Back Up Panels

   Based upon the targets examined, damage to secondary target panels depends upon spacing between panels, panel thicknesses and target material. The effect of spacing is shown on 2024 aluminum targets where large perforations with petalled edges occurred in 0.1 inch second panels of 2024-T3 aluminum at a panel spacing of two inches, whereas surface pitting and metallizing occurred at spacings of four and twenty four inches. The effect of back up material thickness is shown by comparing the 0.1 inch panel to a 1.0 inch

thick panel. Pitting, metallizing and shallow cratering were observed for 1.0 inch 2024-T4 aluminum second panels at spacings ranging from two to twenty four inches. Material variation is shown by comparing the perforation pattern just described on aluminum alloys to that of higher hardness materials such as titanium, annealed 4130 alloy steel, and high strength stainless steel. It was generally observed that with increased hardness the effect on the back up panel progressed from perforations to pitting and metallizing and then to shattering of the panel.

PLATE 1
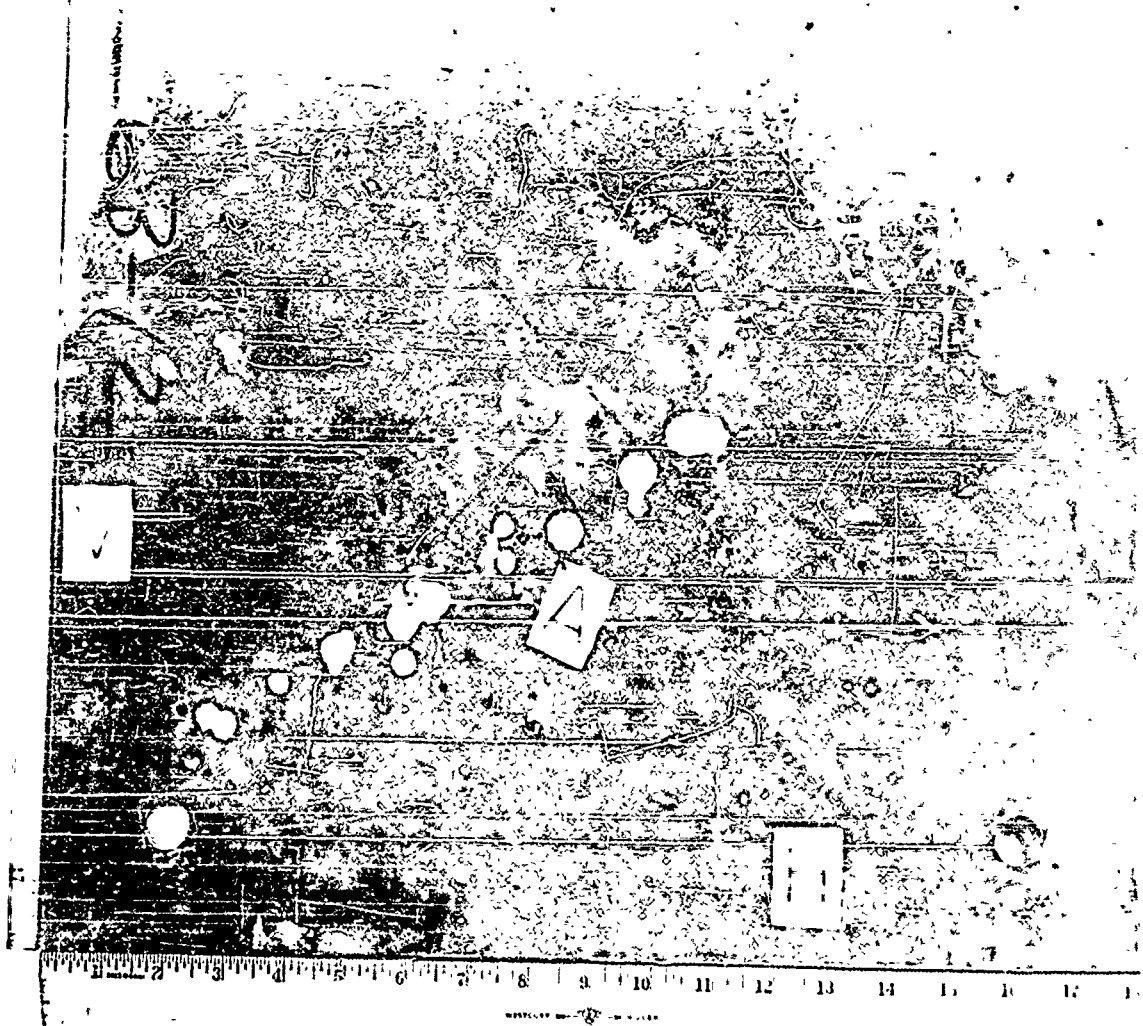
FIGURE 1   TARGET 63-12, PLATE 1, 2024-T3
ALUMINUM, 0.1 INCH THICK

PLATE 2 65-12
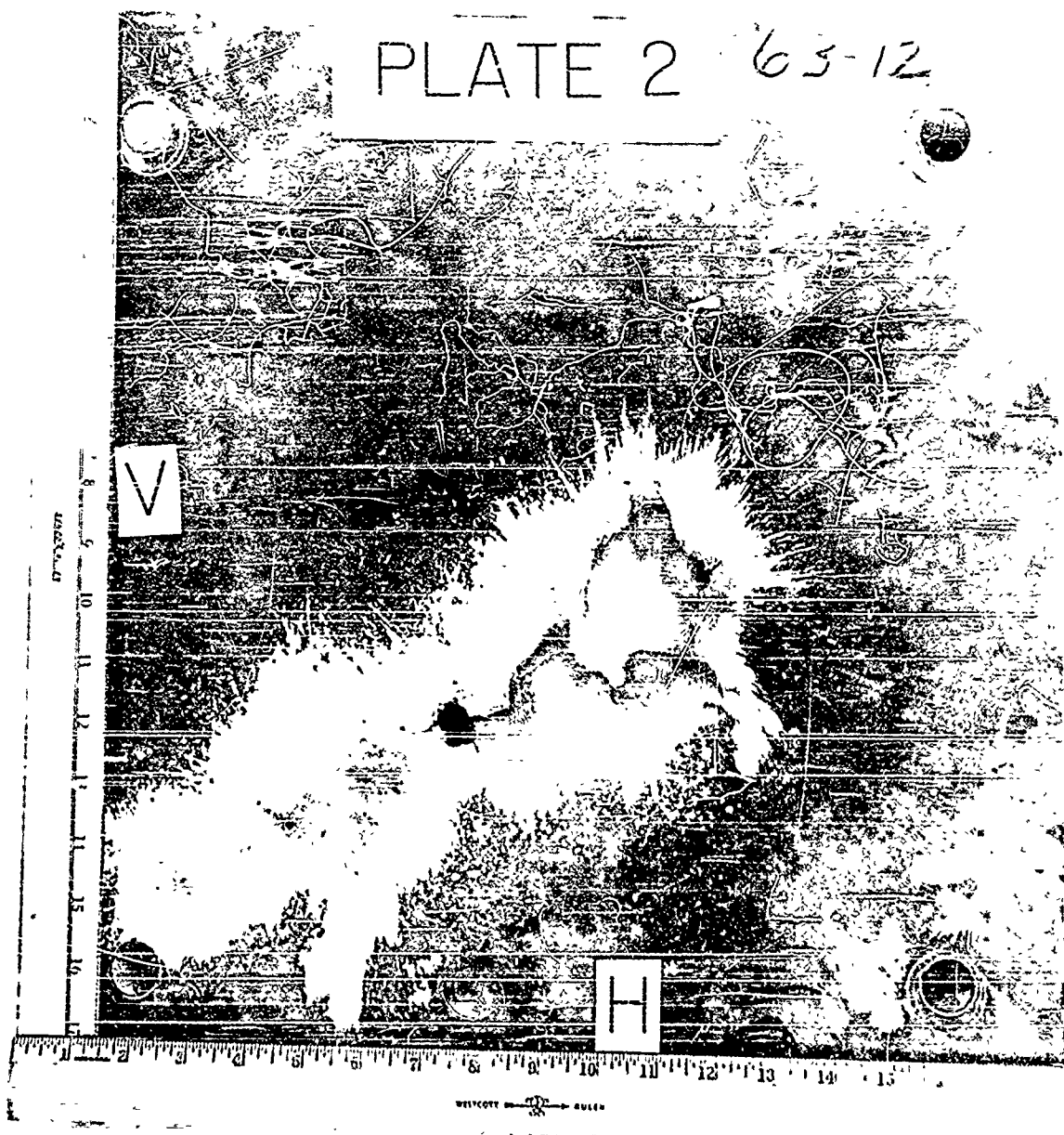
FIGURE 2   TARGET 63-12, PLATE 2, 2024-T3
ALUMINUM, 0.1 INCH THICK
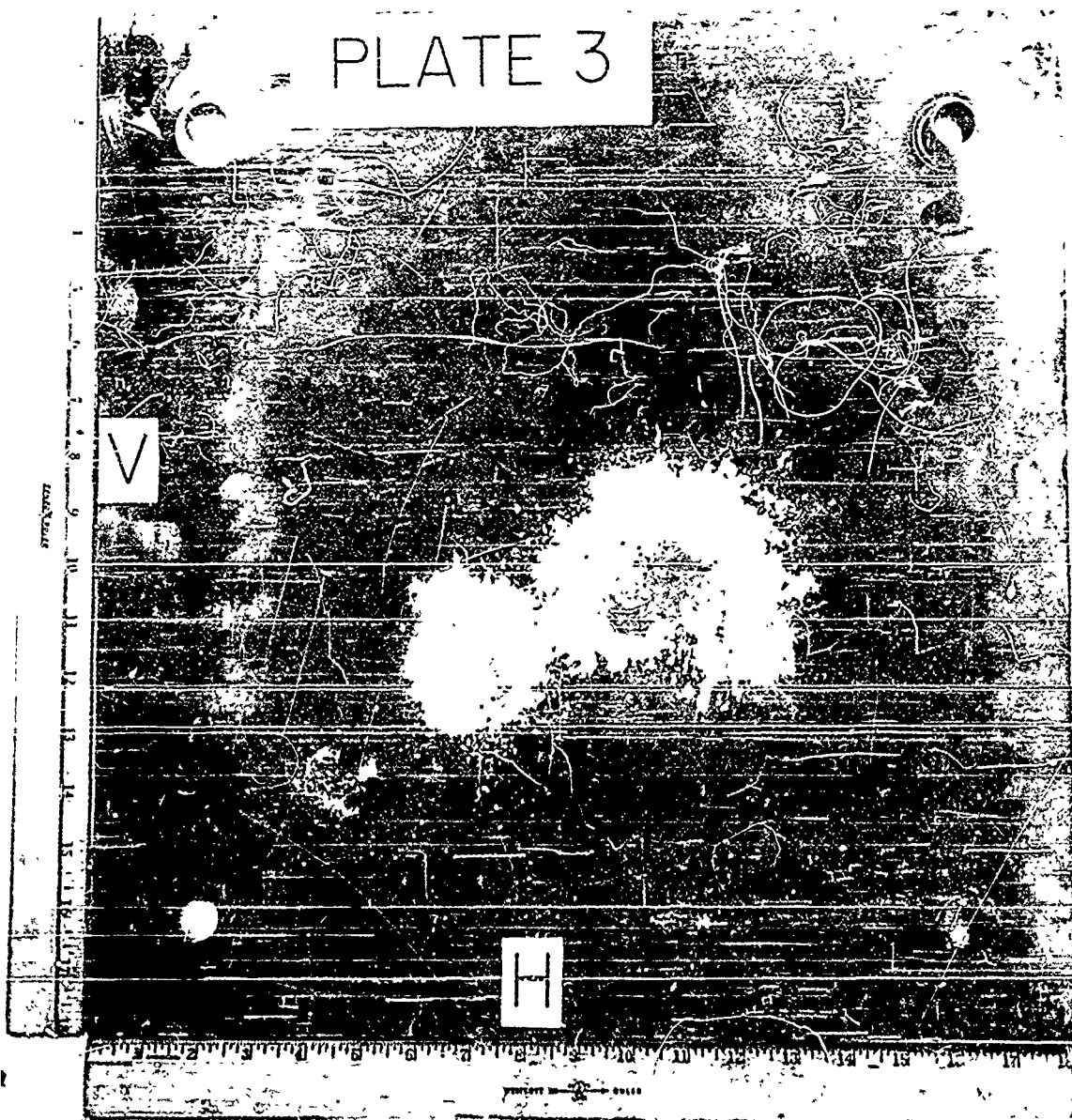
FIGURE 3   TARGET 63-12, PLATE 3, 2024-T3
ALUMINUM, 0.1 INCH THICK
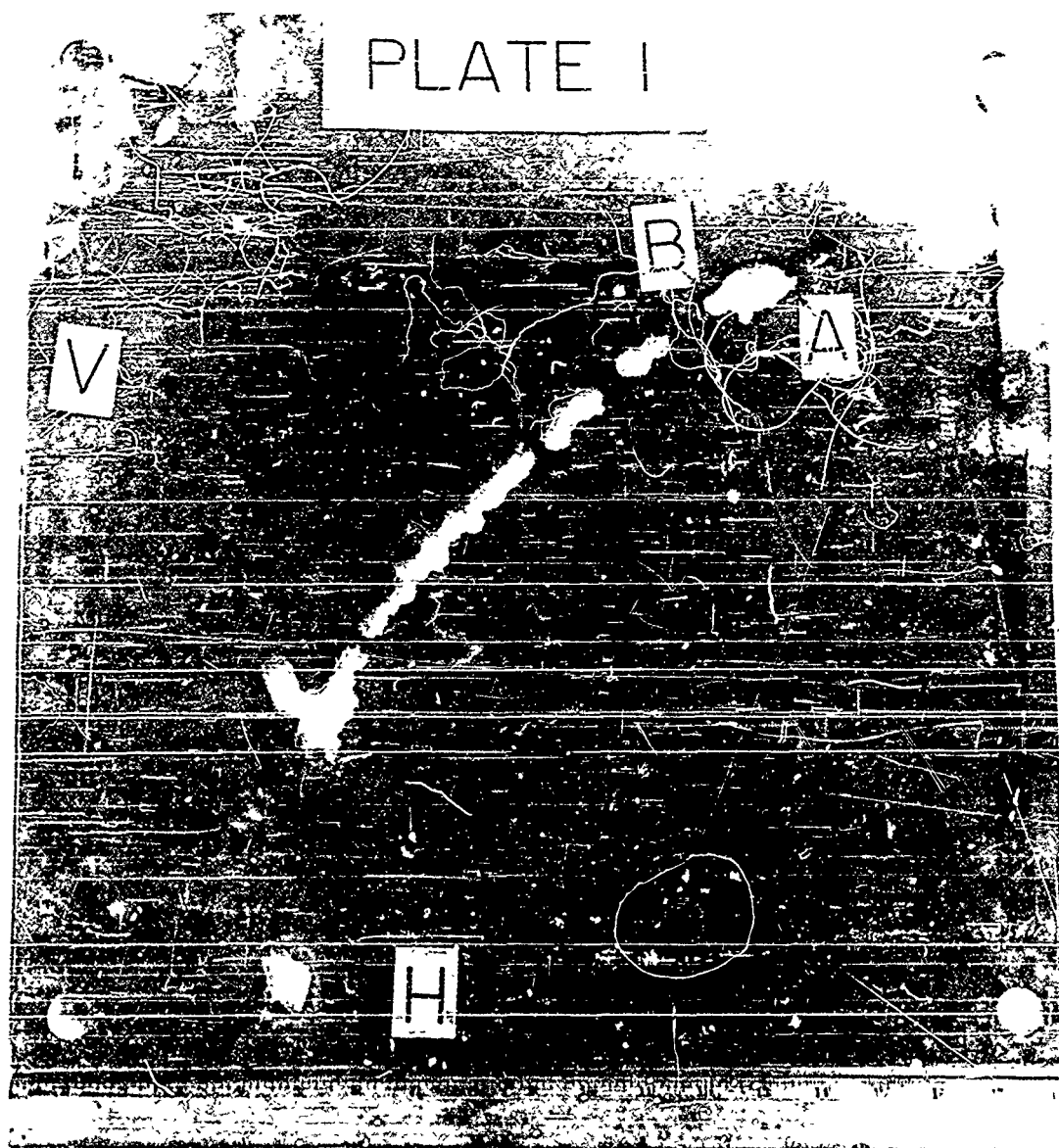
FIGURE 4   TARGET 63-51, PLATE 1, 2024-T3
ALUMINUM, 0.1 INCH THICK
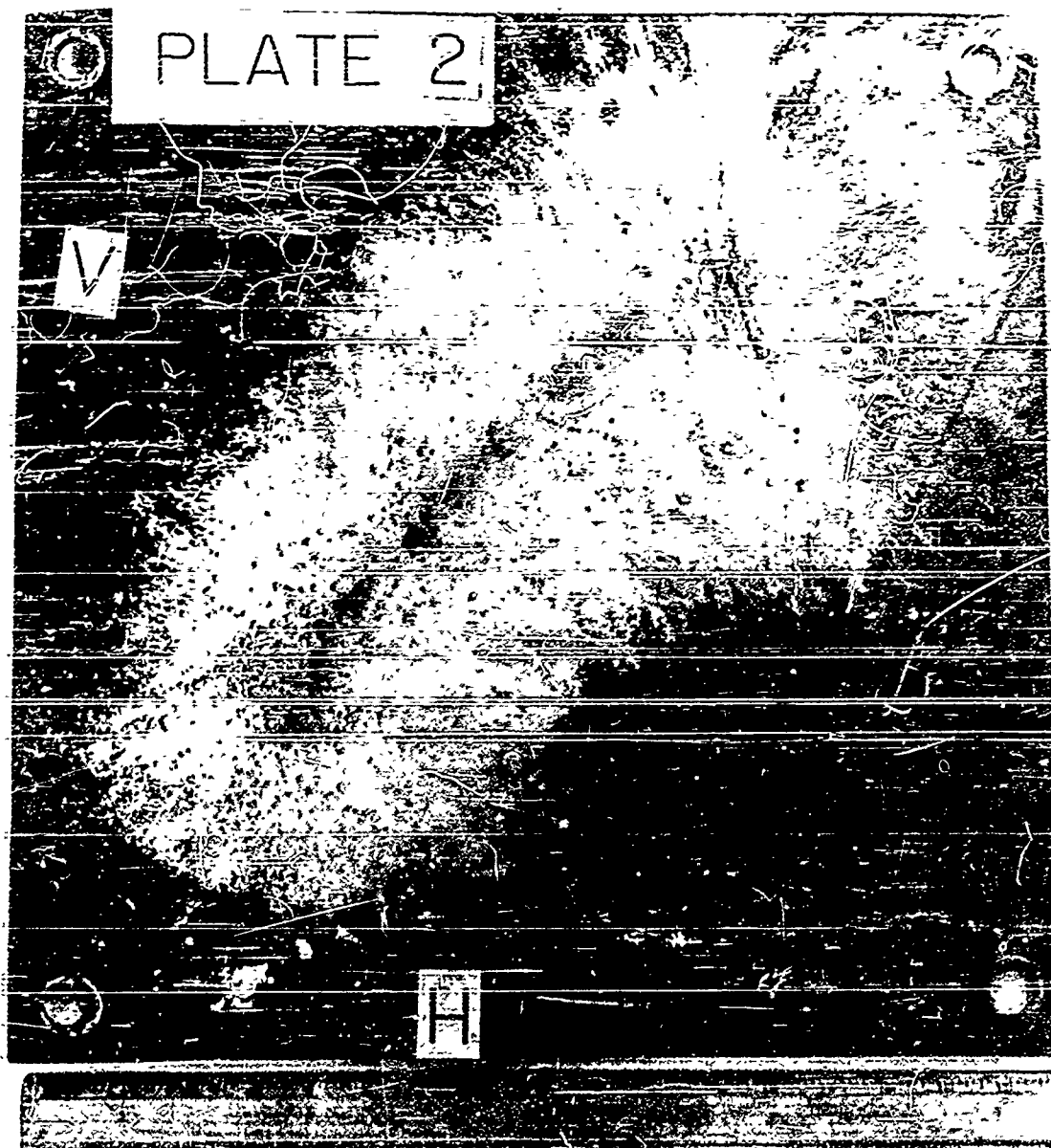
FIGURE 5 TARGET 63-51, PLATE 2, 2024-T3
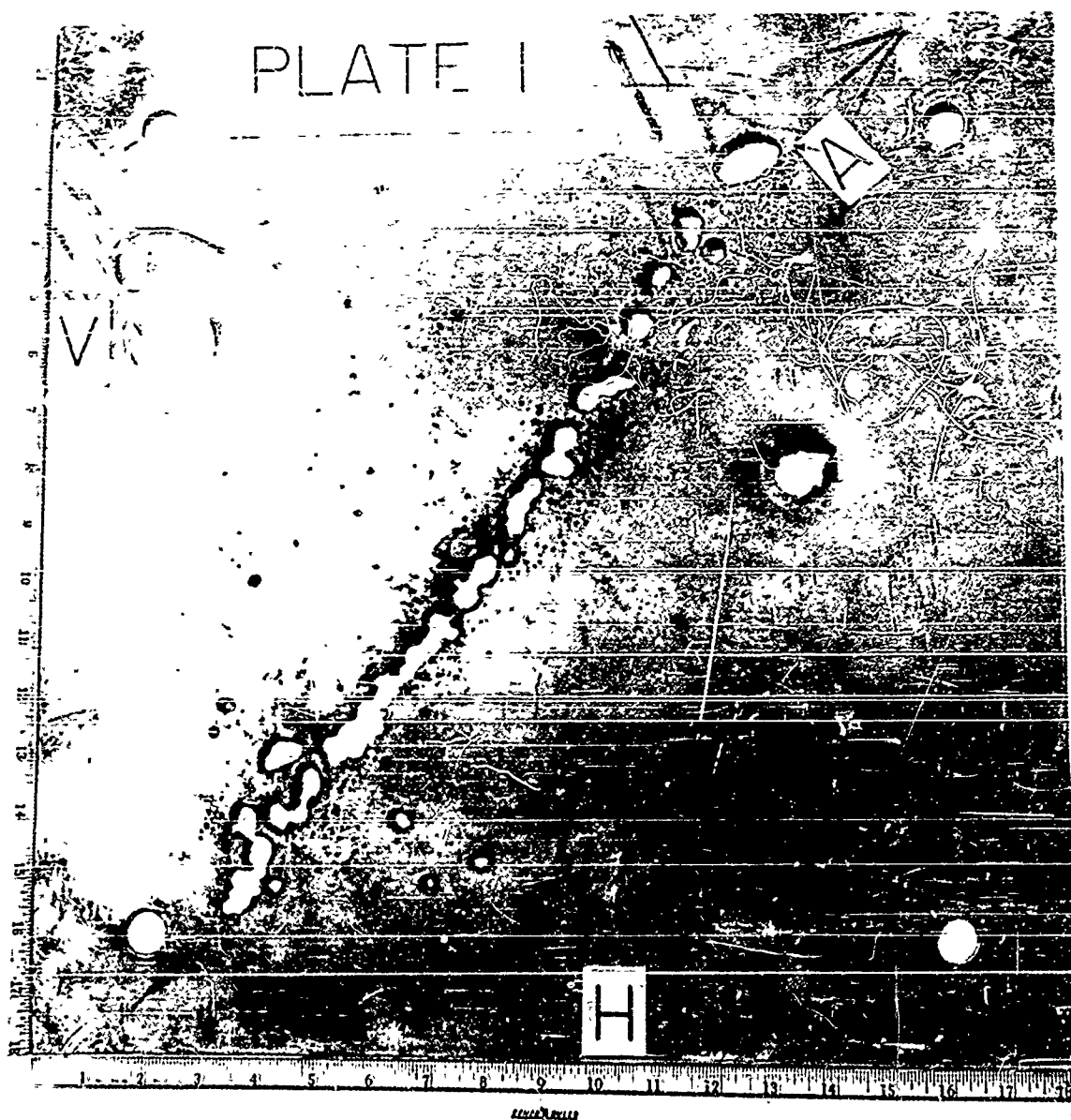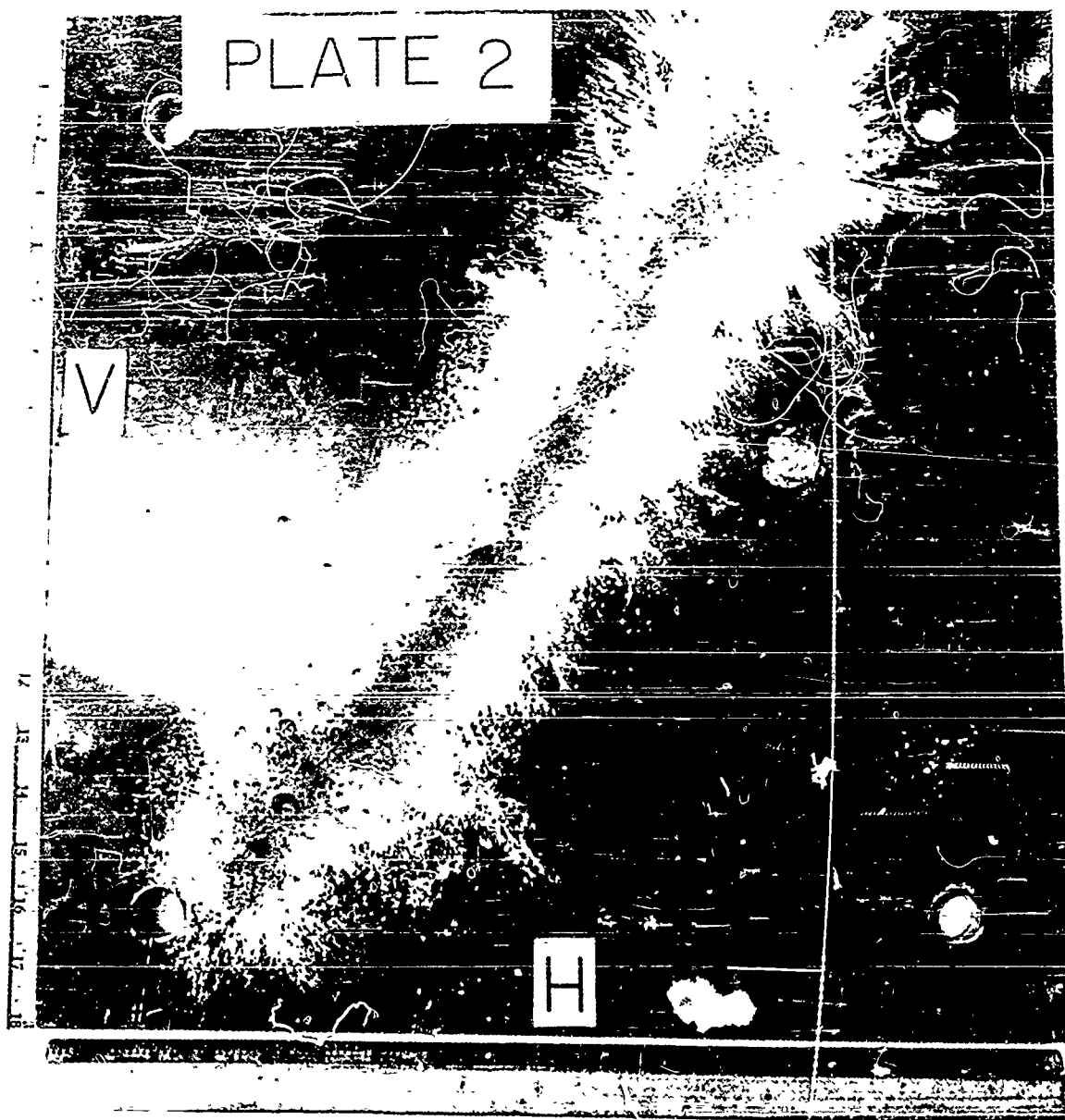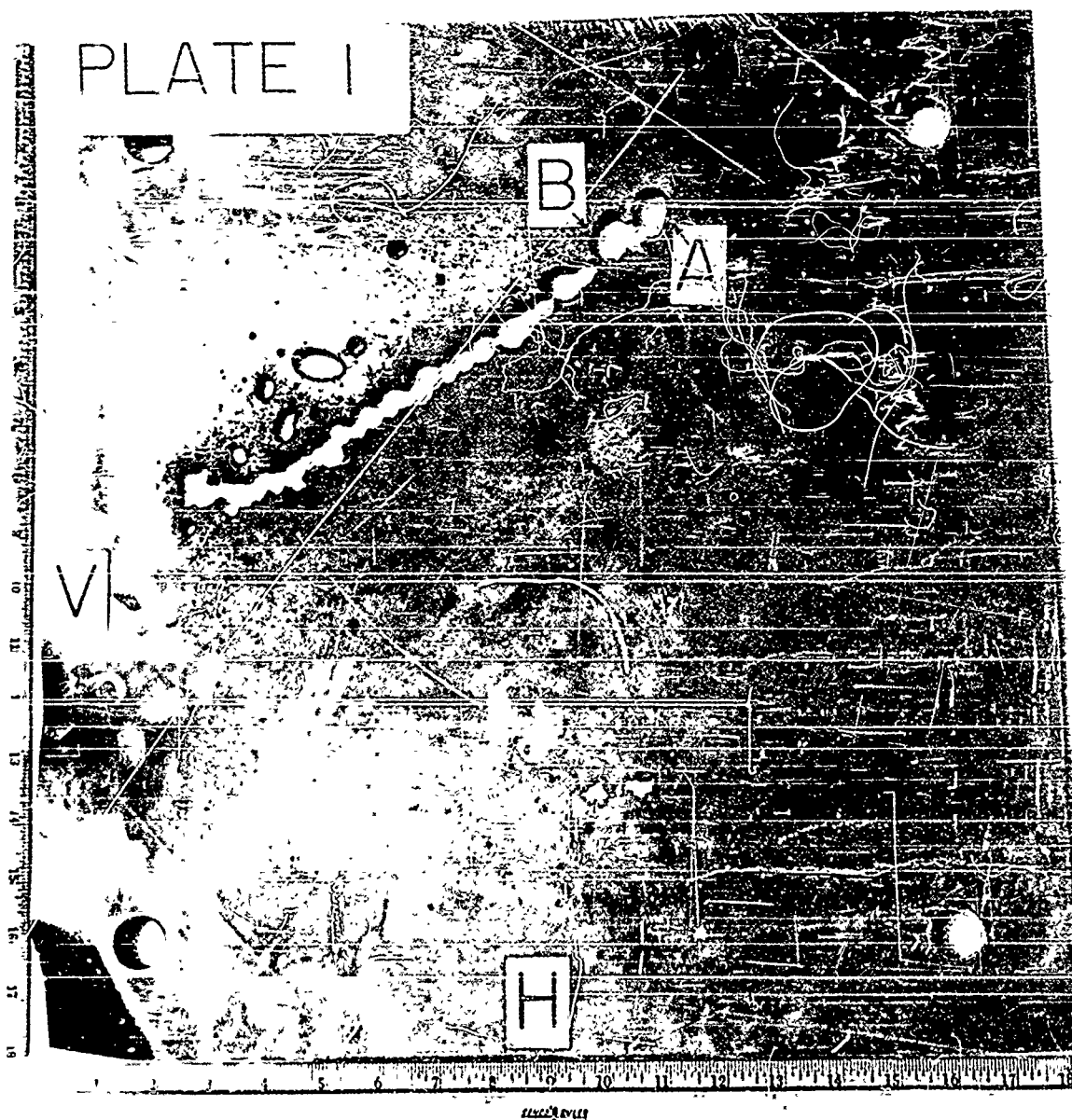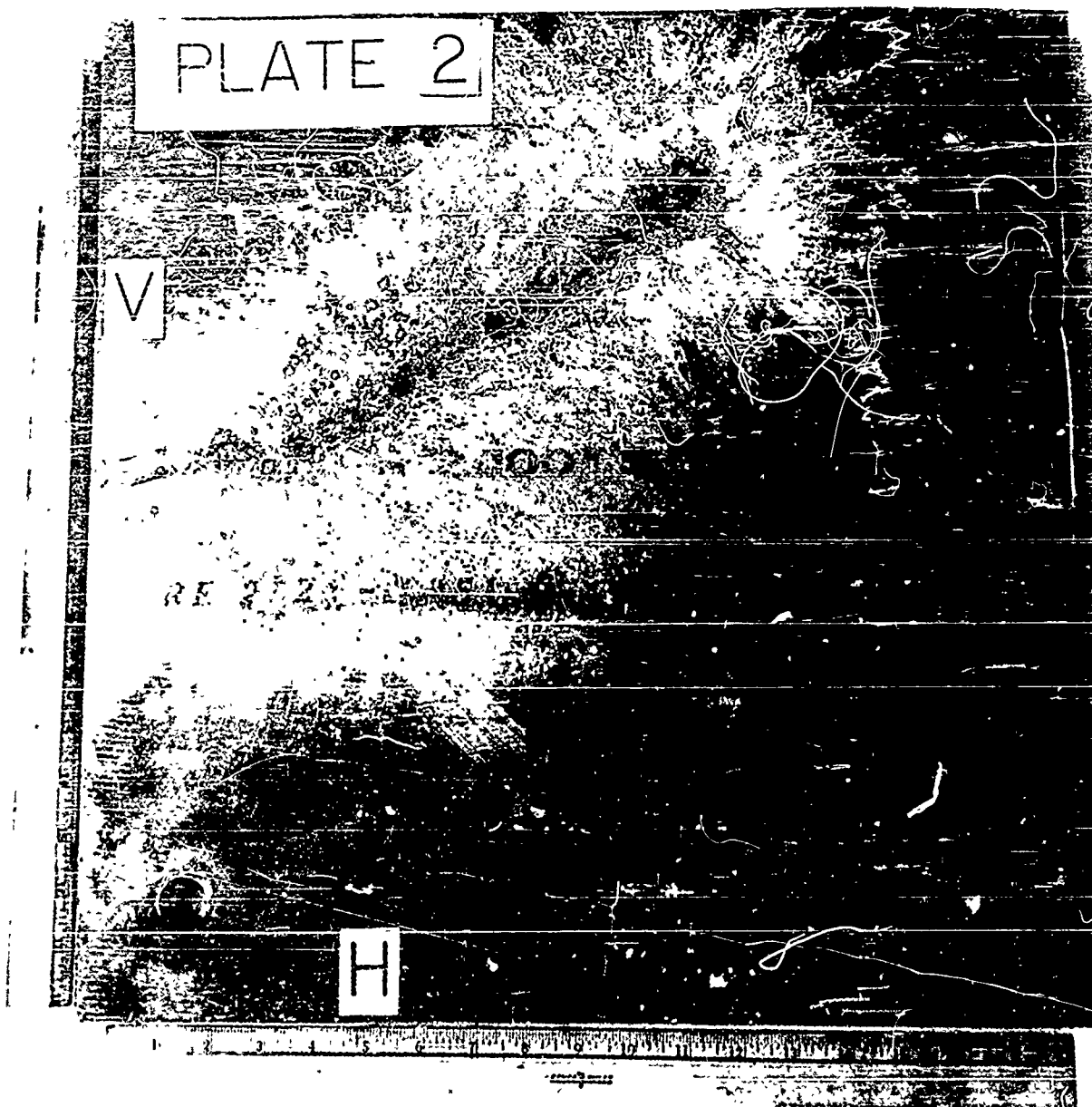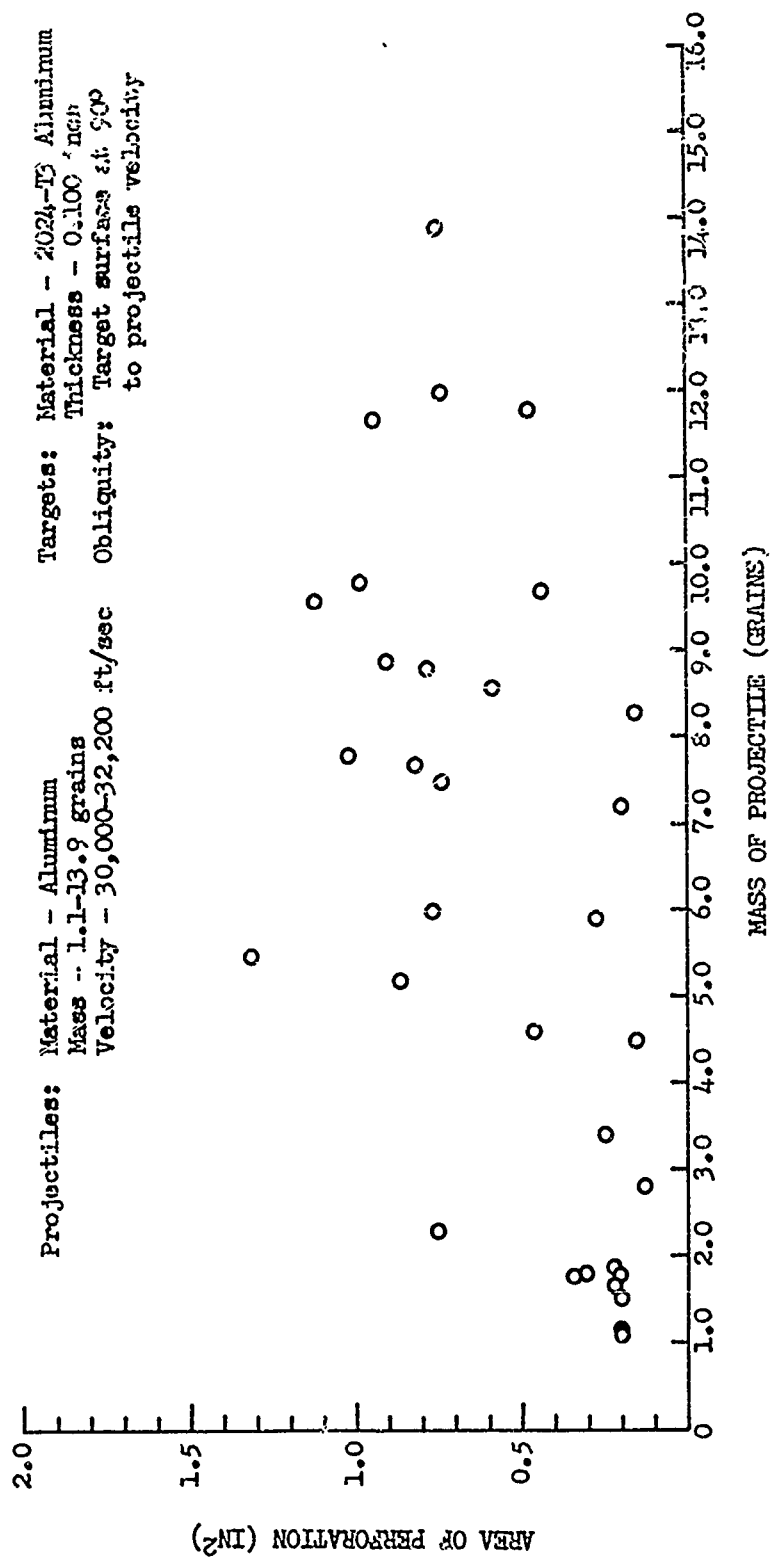ALUMINUM, 0.25 INCH THICK
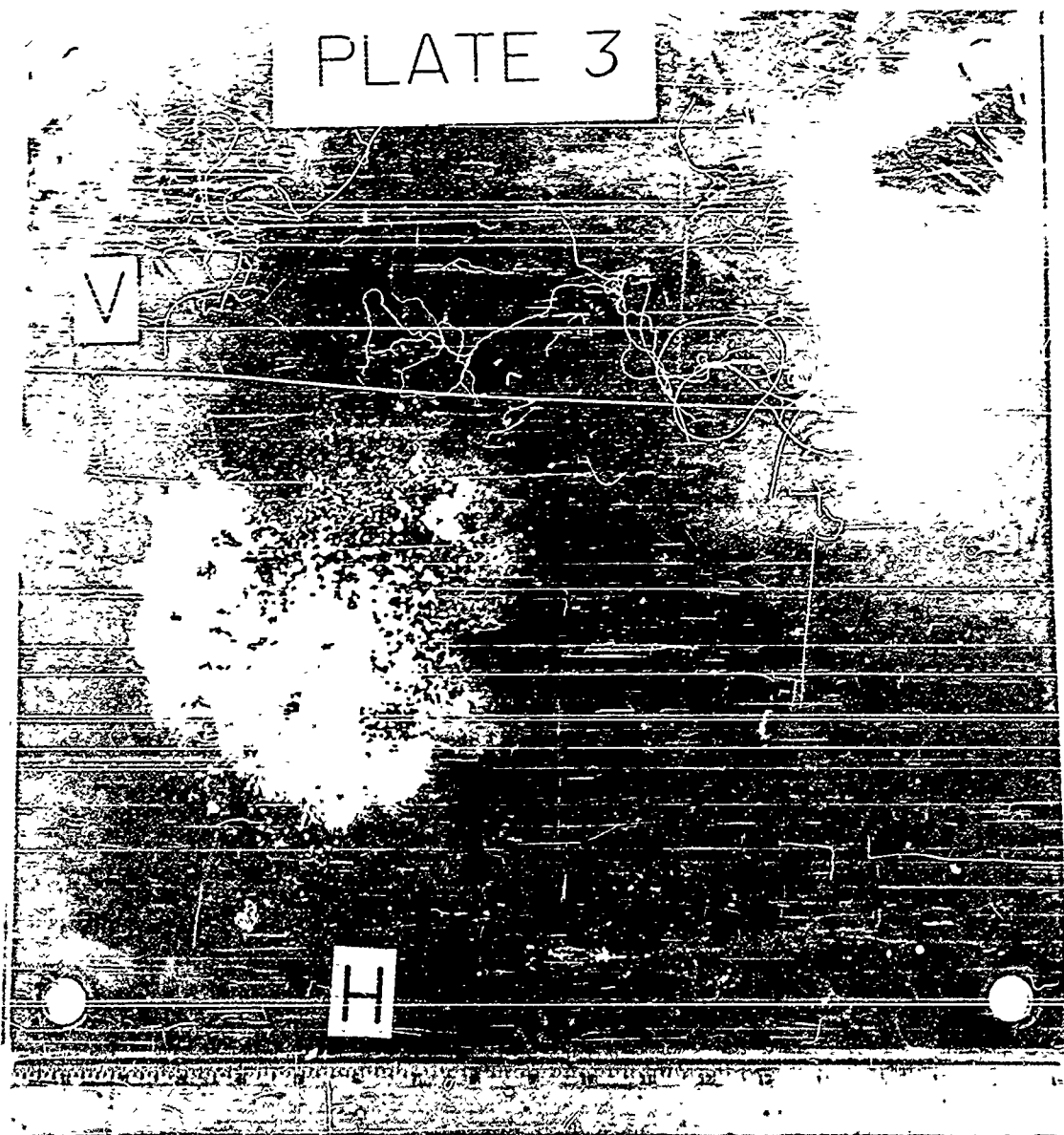
FIGURE 6   TARGET 63-51, PLATE 3, 2024-T3
ALUMINUM, 0.25 INCH THICK
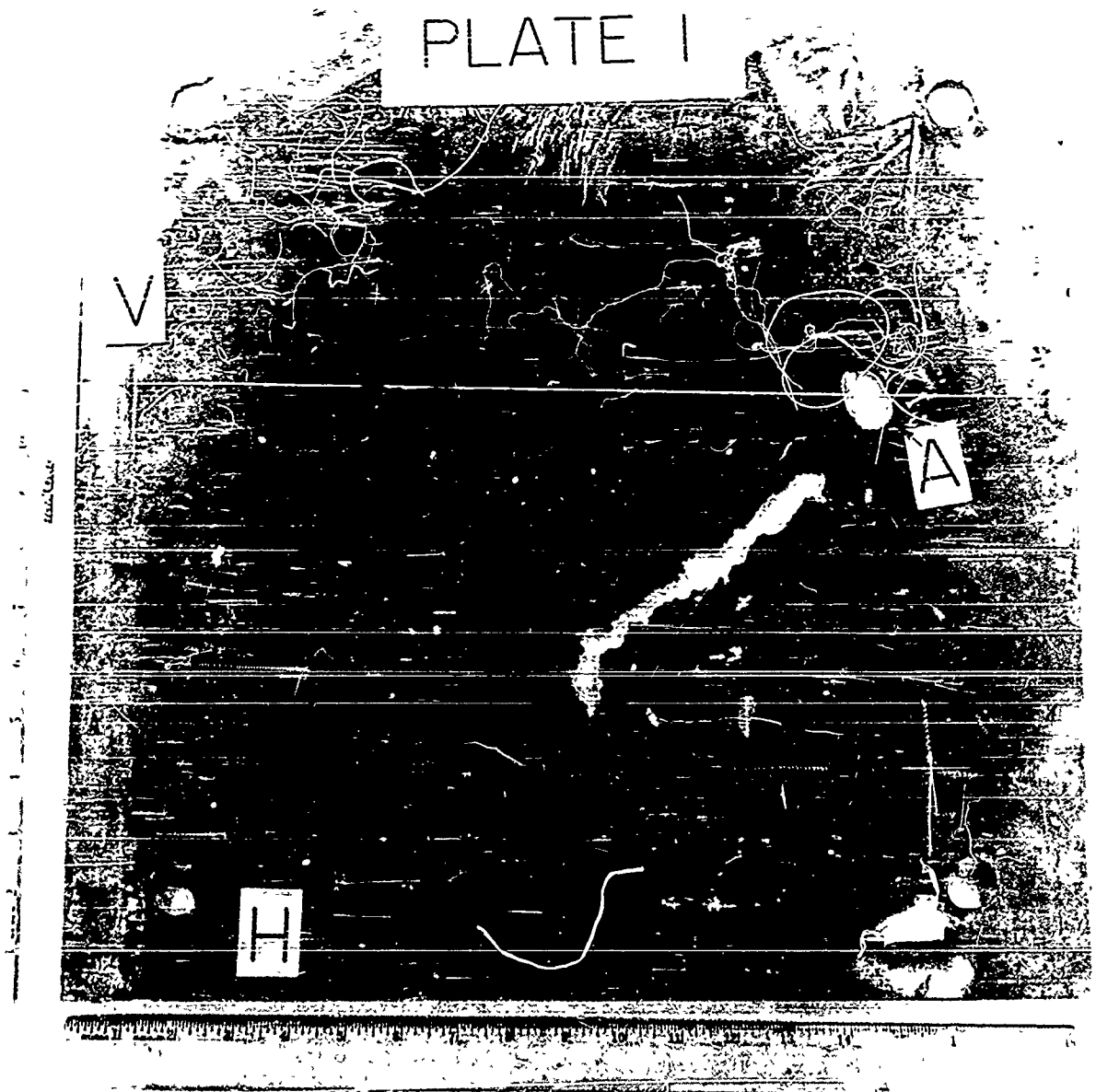
FIGURE 7   TARGET 63-62, PLATE 1, 2024-T3
ALUMINUM, 0.1 INCH THICK
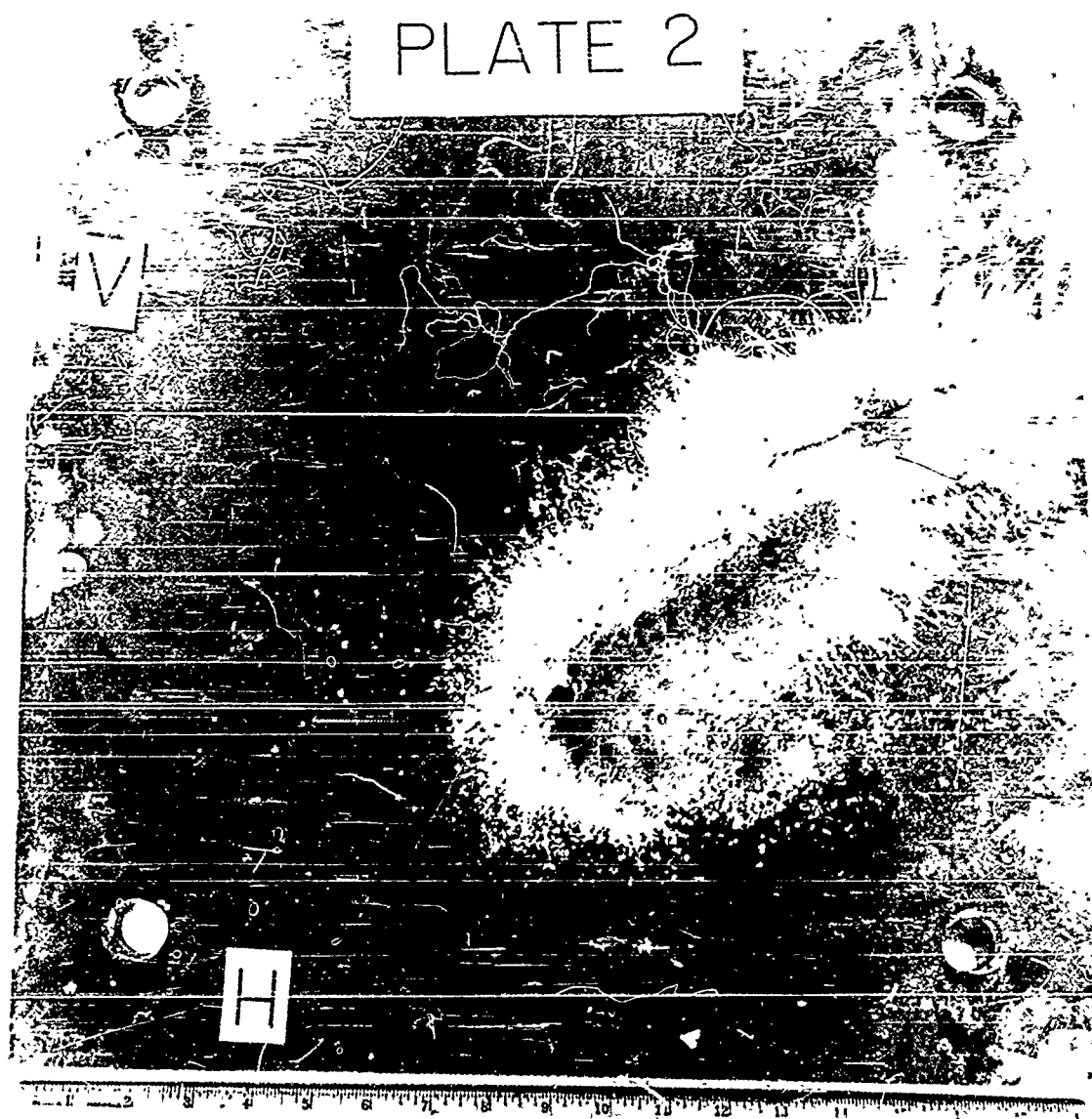
FIGURE 8   TARGET 63-62, PLATE 2, 2024-T4
ALUMINUM, 0.5 INCH THICK

FIGURE 9   TARGET 63-94, PLATE 1, 2024-T3
ALUMINUM, 0.1 INCH THICK

FIGURE 10   TARGET 63-94, PLATE 2, 2024-T4
ALUMINUM, 1.0 INCH THICK

FIGURE 11 TARGET 64-09, PLATE 1, 2024-T3
ALUMINUM, 0.1 INCH THICK

FIGURE 12   TARGET 64-09, PLATE 2, 2024-T351
ALUMINUM, 2.0 INCH THICK

Projectiles: Material – Aluminum
Mass – 1.1–13.9 grains
Velocity – 30,000–32,200 ft/sec

Targets: Material – 2024–T3 Aluminum
Thickness – 0.100 inch
Obliquity: Target surface at 90°
to projectile velocity

FIGURE 13   PERFORATION AREA AS A FUNCTION OF PROJECTILE MASS
FOR THIN ALUMINUM TARGETS

MASS OF PROJECTILE (GRAINS)

AREA OF PERFORATION (IN²)

Projectiles: Material - Aluminum
Mass - 1.1-13.9 grains
Velocity - 30,000-32,000 ft/sec

Targets: Material - 2024-T3 Aluminum
Thickness - 0.100 inch
Obliquity: Target Surface at 90° to
projectile velocity

AREA OF PERFORATION (IN²)
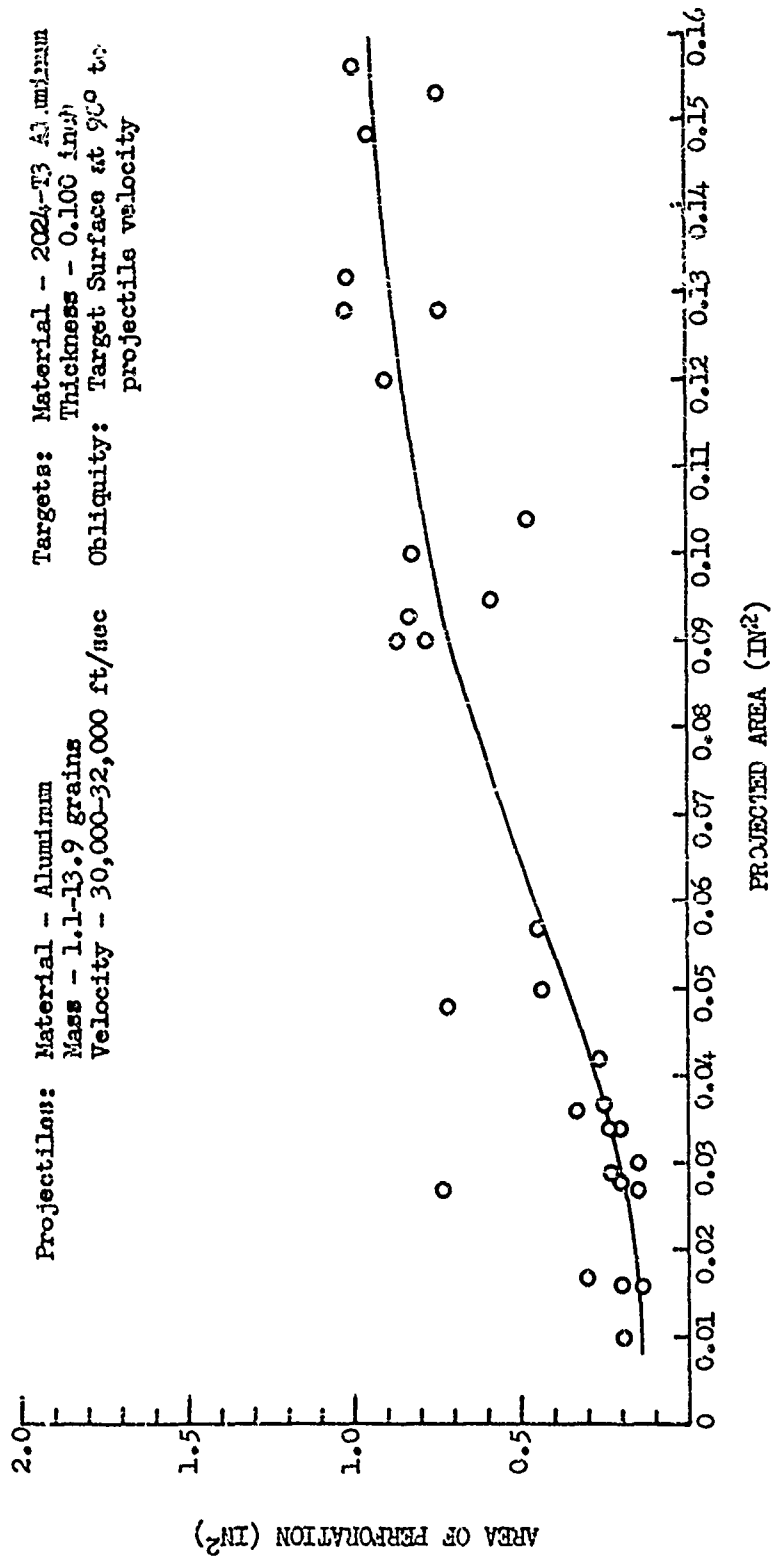
PROJECTED AREA (IN²)

FIGURE 14   PERFORATION AREA AS A FUNCTION OF PROJECTED AREA
OF PROJECTILE FOR THIN ALUMINUM TARGETS
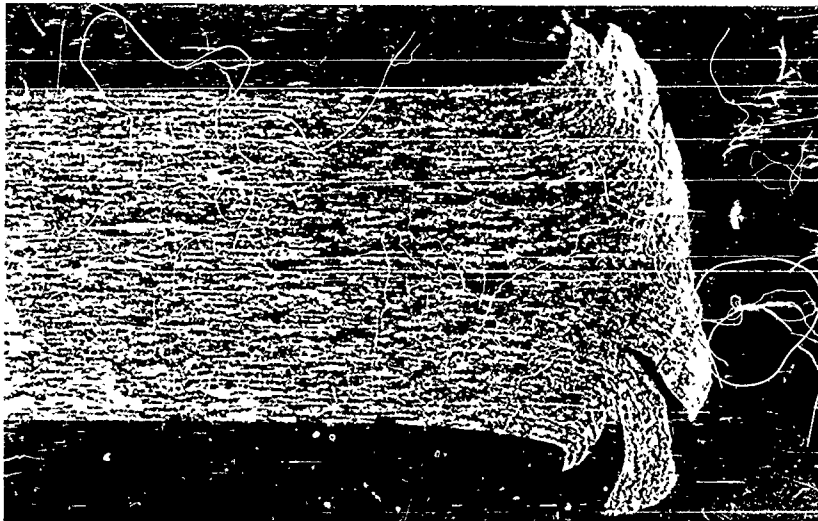
FIGURE 15   PERFORATION A, TARGET EB-61, 0.1 INCH
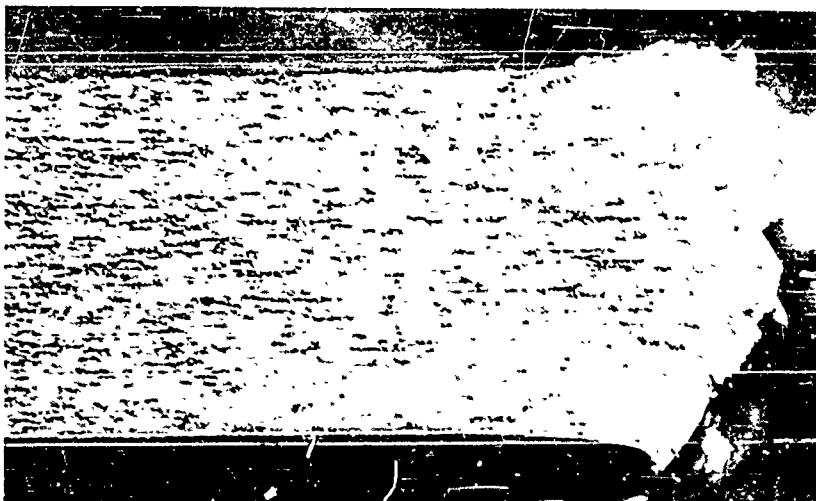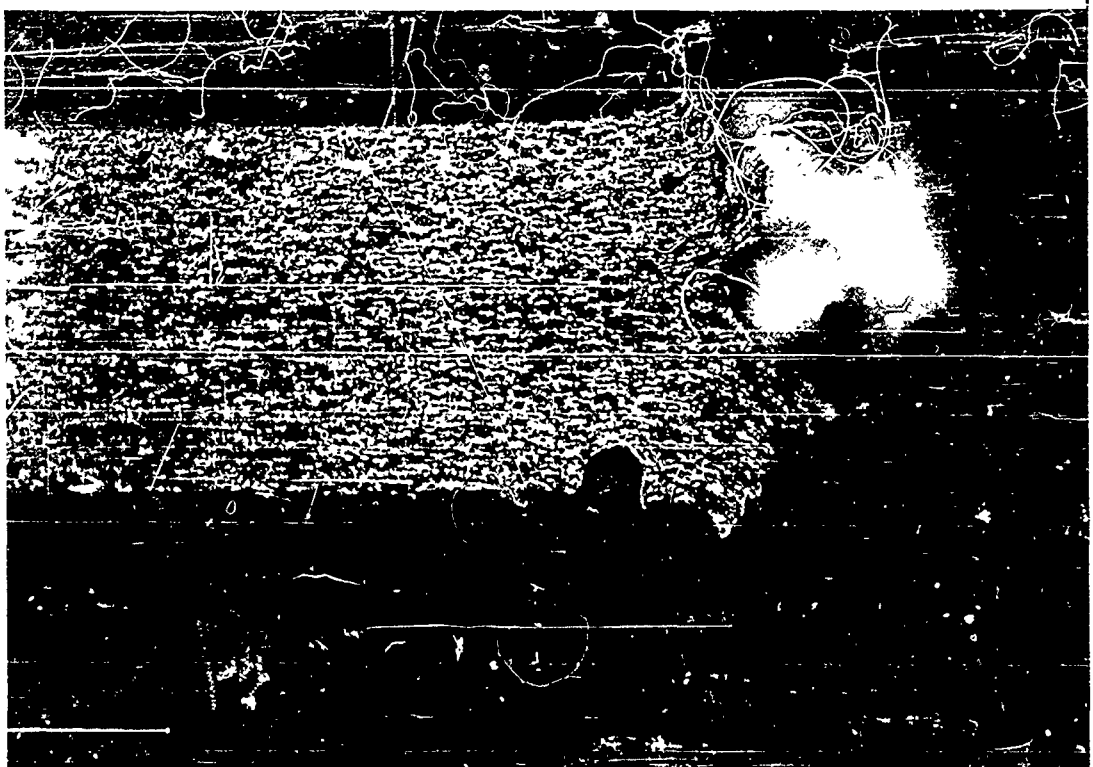2024-T3 ALUMINUM (20X)

FIGURE 16   PERFORATION A, TARGET 63-83, 0.1 INCH
2024-T3 ALUMINUM (20X)

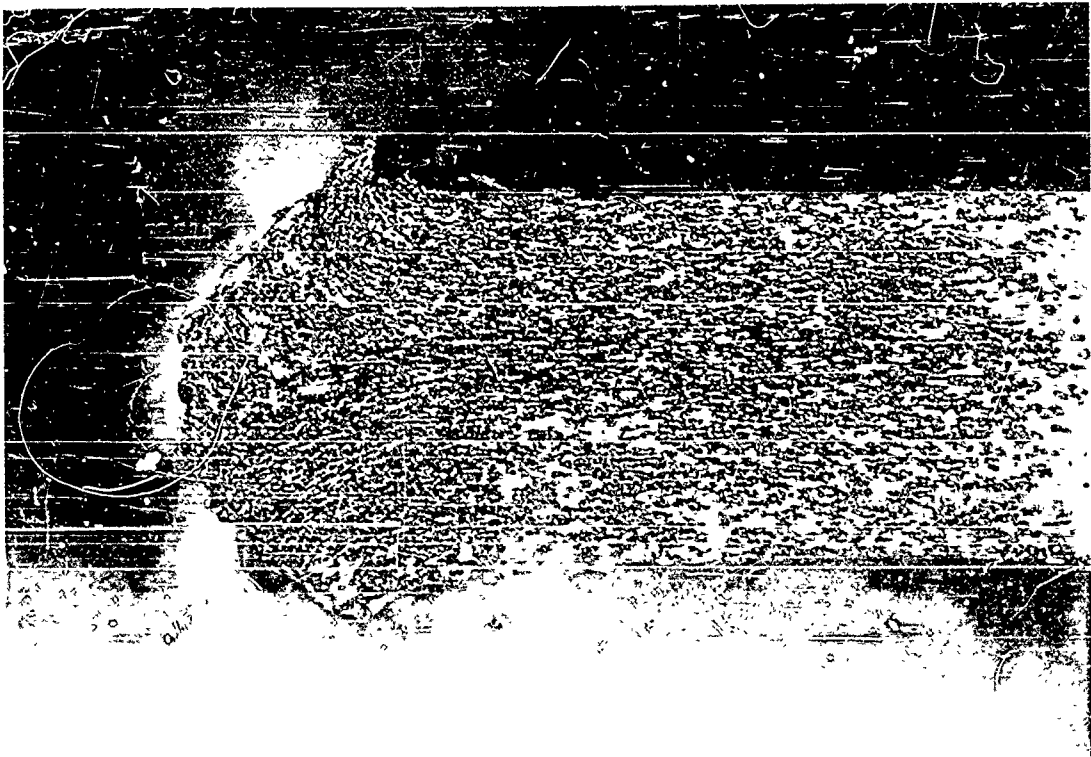FIGURE 17 PERFORATION B, TARGET 64-03, 0.1 INCH
2024-T3 ALUMINUM (20X)

FIGURE 18   PERFORATION A, TARGET 64-03, 0.1 INCH
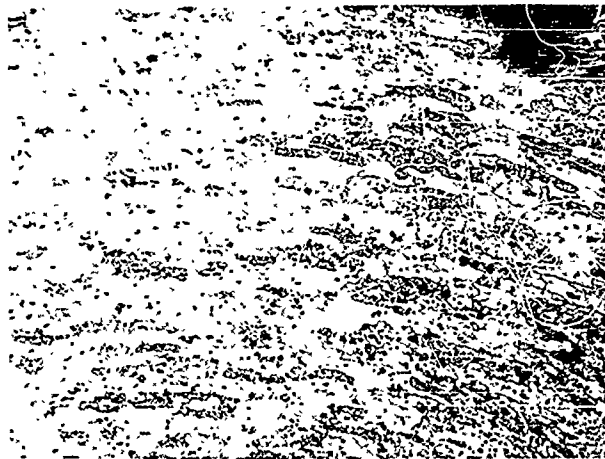2024-T3 ALUMINUM (20X)

FIGURE 19   MICROSTRUCTURE AT CENTER EDGE OF PERFORATION A,
TARGET EB-61 (100X, KELLER'S ETCH)

FIGURE 20   MICROSTRUCTURE AT REAR EDGE OF PERFORATION A,
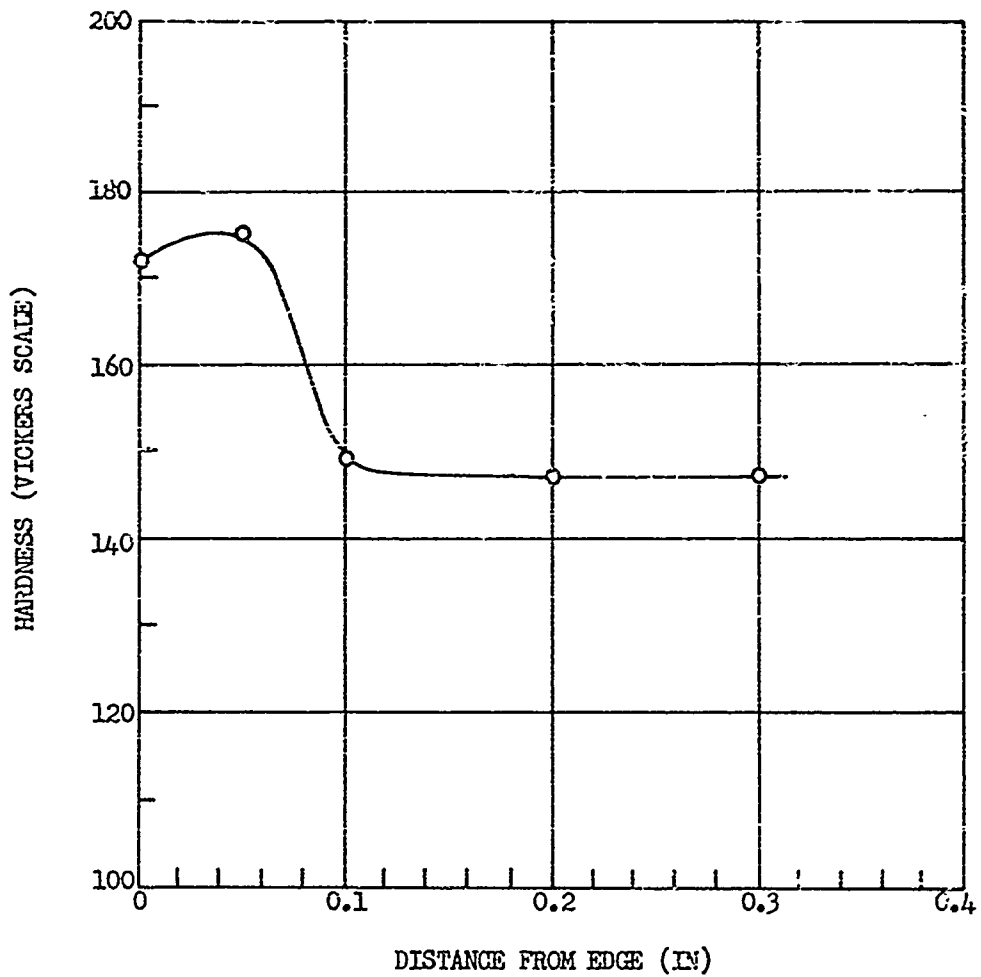TARGET EB-61 (100X, KELLER'S ETCH)

FIGURE 21   HARDNESS OF A FUNCTION OF DISTANCE FROM THE EDGE
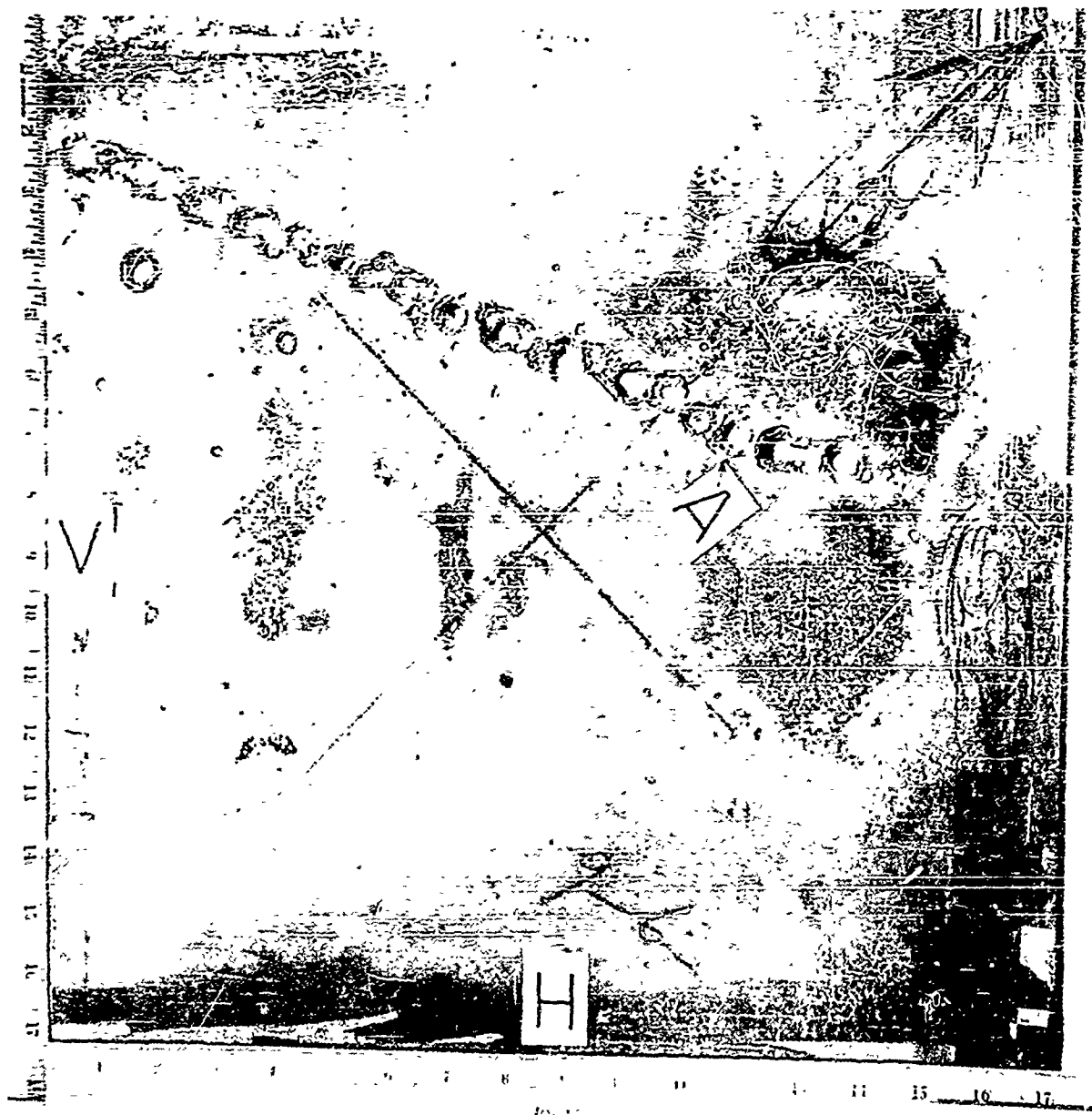OF PERFORATION A, TARGET EB-61

FIGURE 22   TARGET 63-09, 2024-T4 ALUMINUM,
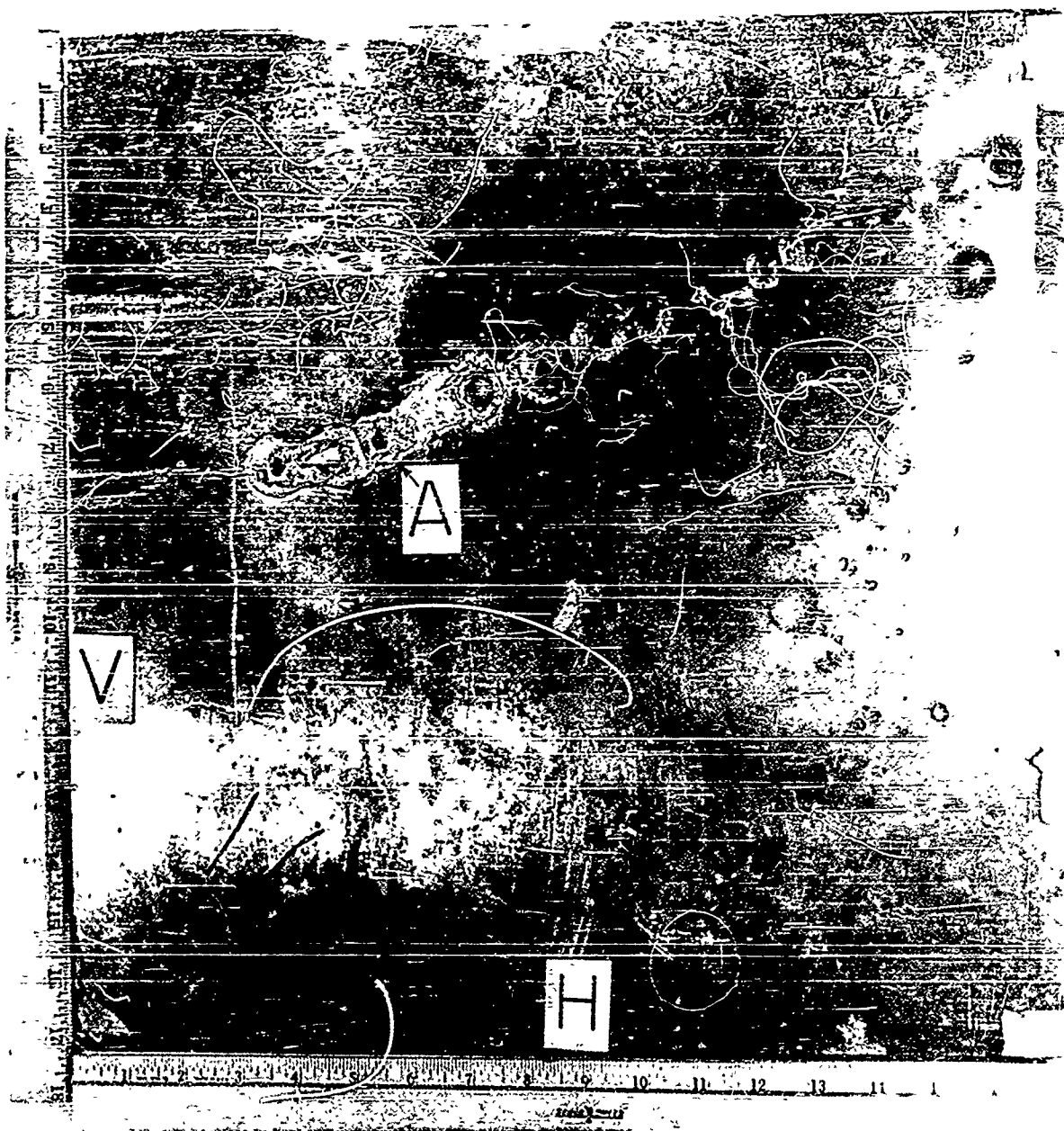0.5 INCH THICK, FRONT VIEW

FIGURE 23   TARGET 63-09, 2024-T4 ALUMINUM,
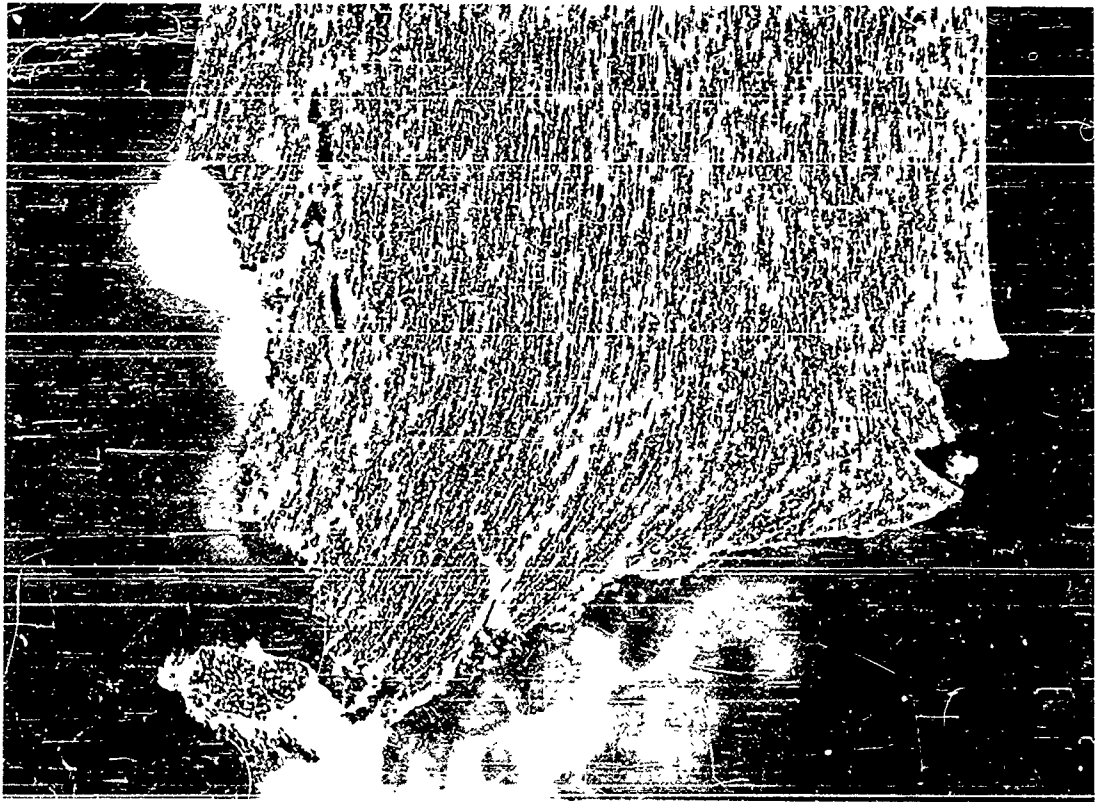0.5 INCH THICK, REAR VIEW

FIGURE 24   PERFORATION A, TARGET 63-09, 2024-T4
ALUMINUM, 0.5 INCH THICK (10X)
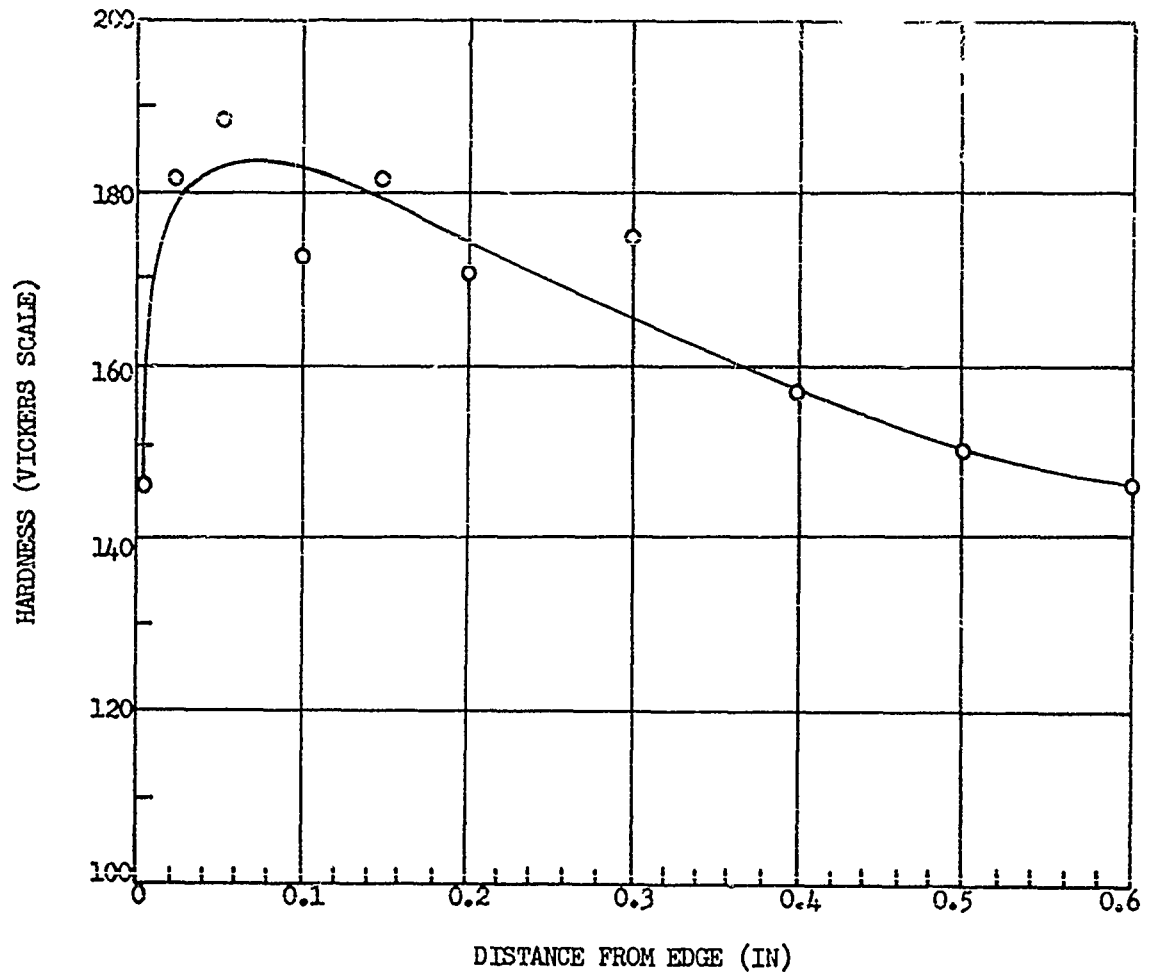
FIGURE 25   HARDNESS AS A FUNCTION OF DISTANCE
FROM THE EDGE OF PERFORATION A,
TARGET 63-09

Magnification: 100X   Magnification: 250X
Etchant: Keller's   Etchant: Keller's

FIGURE 26   SLIP SYSTEMS NEAR PERFORATION A,
             TARGET 63-09, 2024-T4 ALUMINUM,
             0.5 INCH THICK

$$\overline{1\mu}$$

FIGURE 27   ELECTRON MICROGRAPH OF STRUCTURE NEAR
PERFORATION A, TARGET 63-09, 2024-T4
ALUMINUM, 0.5 INCH THICK (9900X)

1μ

FIGURE 28 ELECTRON MICROGRAPH OF STRUCTURE NEAR
PERFORATION A, TARGET 63-09, 2024-T4
ALUMINUM, 0.5 INCH THICK (9900X)

1μ

FIGURE 29   ELECTRON MICROGRAPH OF STRUCTURE NEAR
PERFORATION A, TARGET 63-09, 2024-T4
ALUMINUM, 0.5 INCH THICK (30,700X)

FIGURE 30   TARGET 63-10, 2024-T4 ALUMINUM,
0.5 INCH THICK, FRONT VIEW
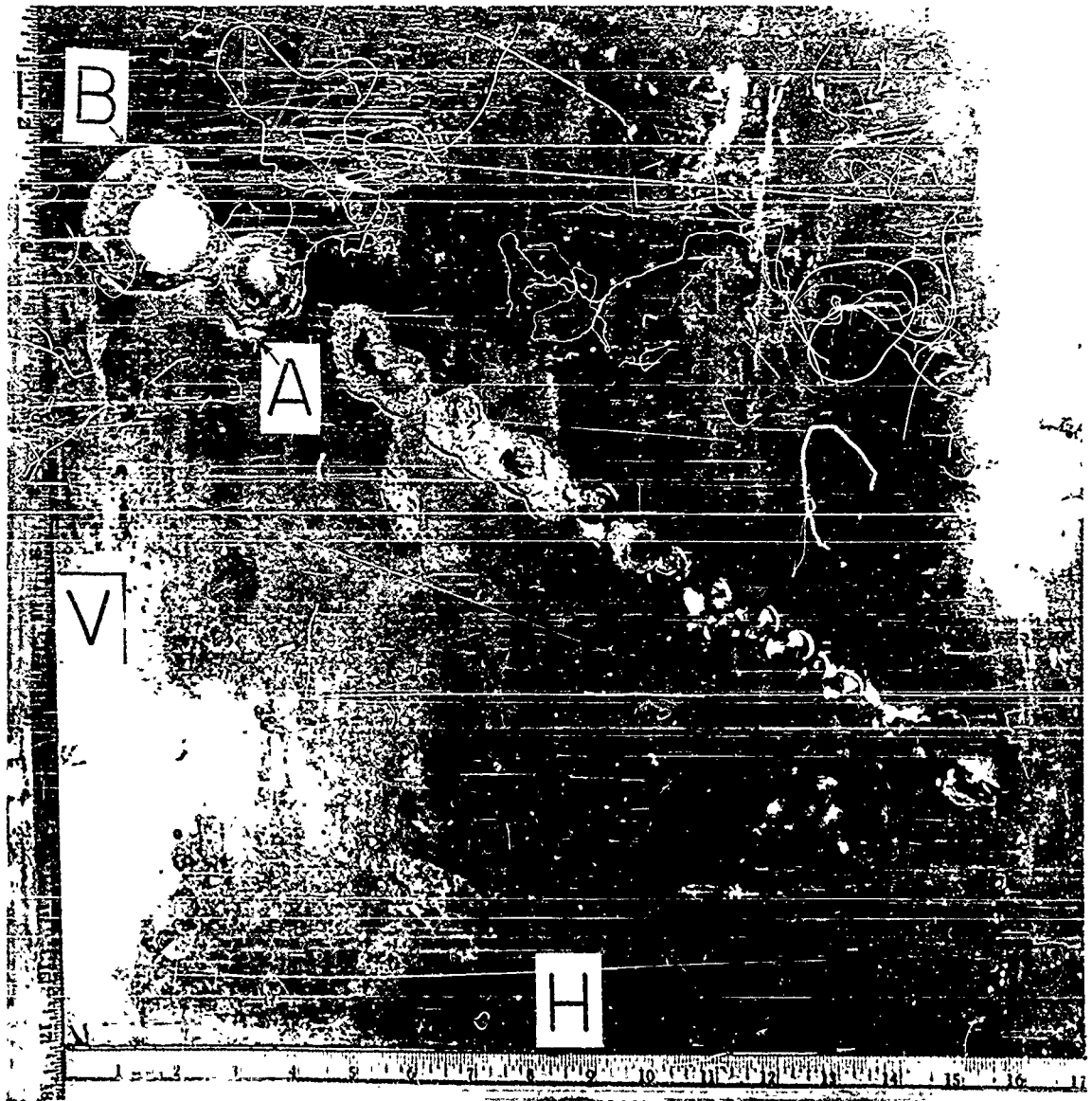
FIGURE 31 TARGET 63-10, 2024-T4 ALUMINUM,
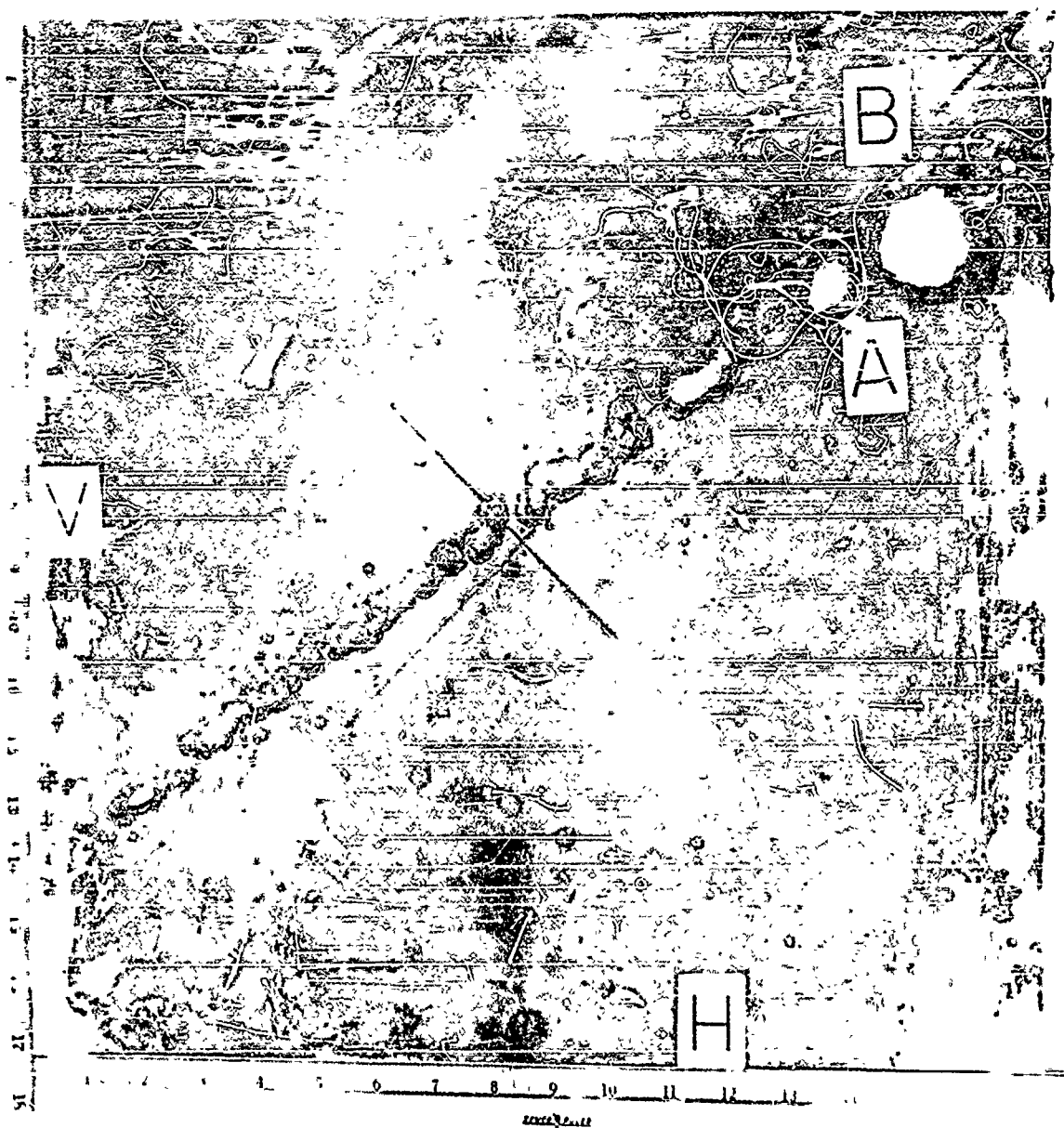0.5 INCH THICK, REAR VIEW

Durimet Microhardness Tester
Load: 100 grams

○ — 0.050" from front surface
□ — 0.250" from front surface
△ — 0.050" from back surface

HARDNESS (VICKERS SCALE)

DISTANCE FROM EDGE (IN)
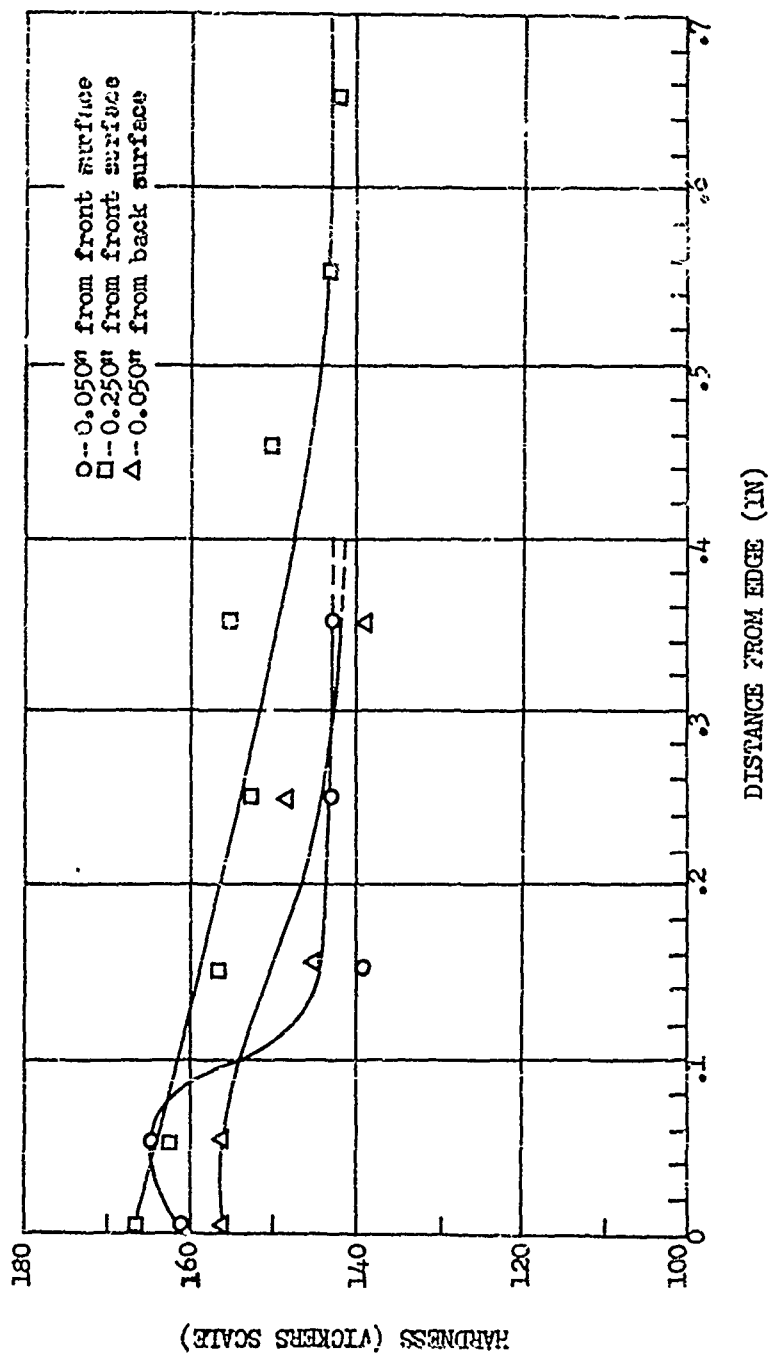
FIGURE 32   HARDNESS AS A FUNCTION OF DISTANCE FROM THE EDGE OF
PERFORATION B, TARGET 63-10
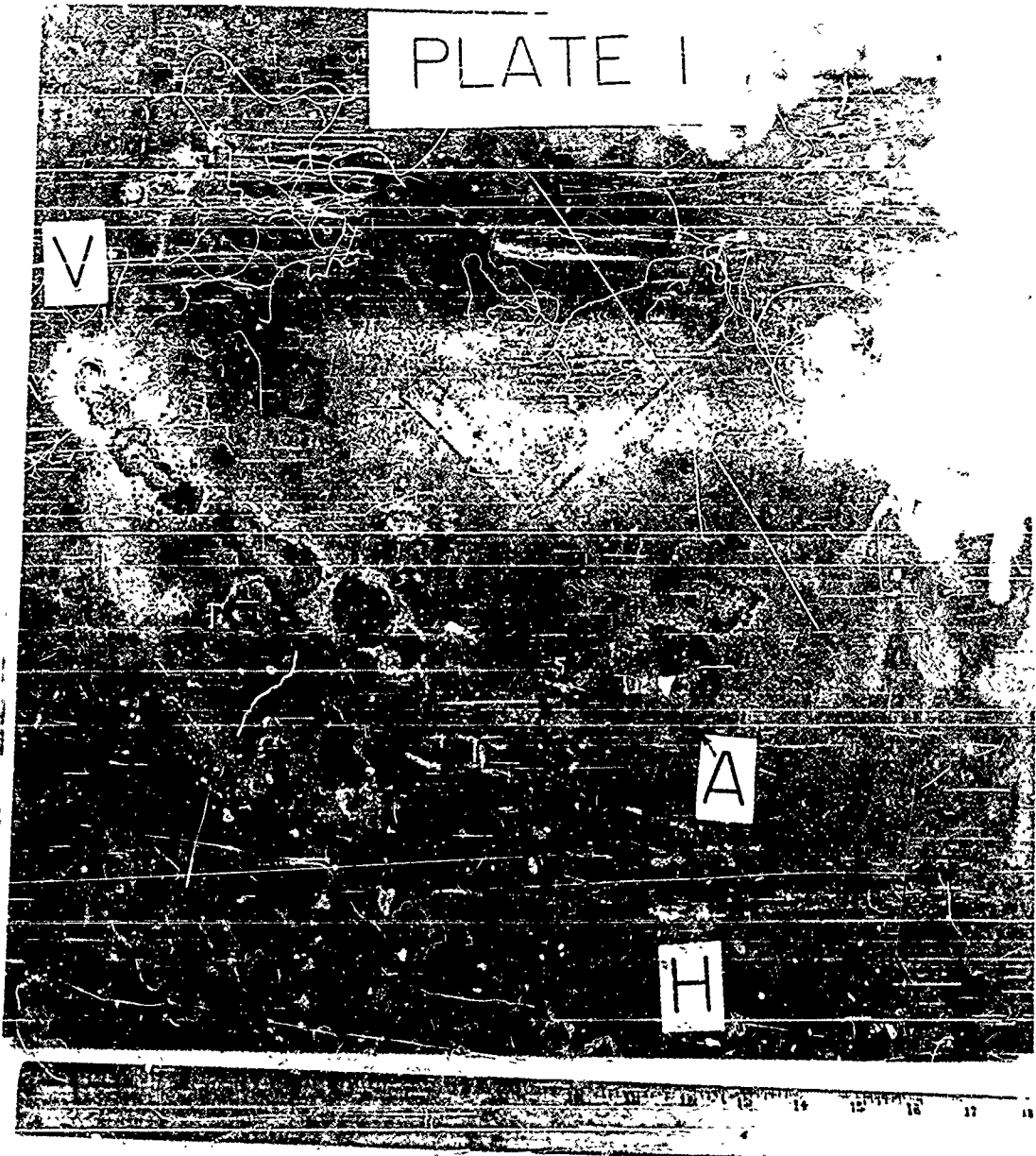
FIGURE 33   TARGET 63-95, 2024-T4 ALUMINUM,
1.0 INCH THICK, FRONT VIEW

FIGURE 34 TARGET 63-95, 2024-T4 ALUMINUM,
1.0 INCH THICK, REAR VIEW

FIGURE 35   PERFORATION A, TARGET 63-95, 2024-T4
ALUMINUM, 2.0 INCH THICK (2X)
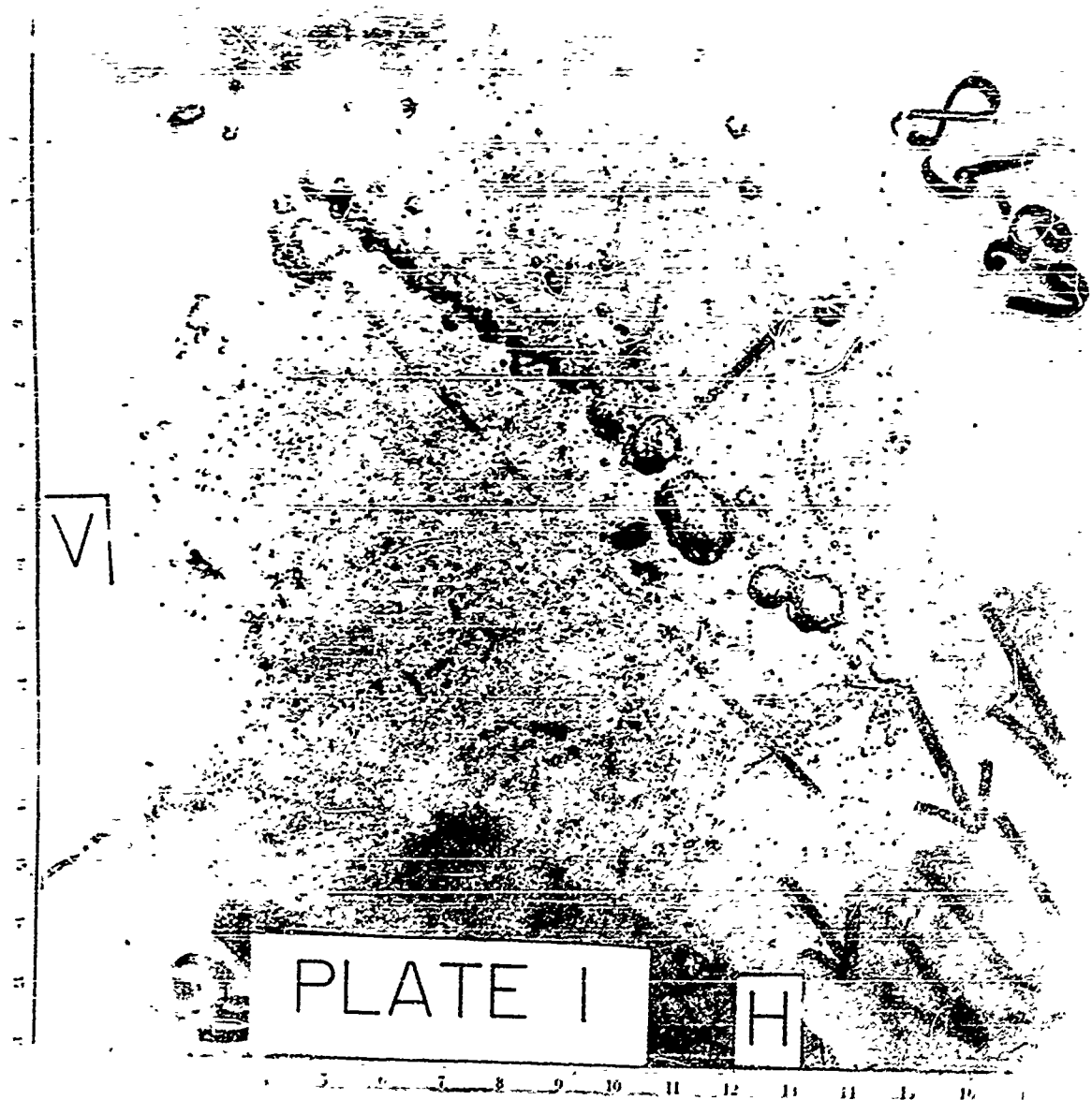
FIGURE 36   TARGET 63-98, 2024-T351 ALUMINUM,
2.0 INCH THICK

FIGURE 37 CRATER IN TARGET 63-09, 2024-T351
ALUMINUM, 2.0 INCH THICK (1.5X)
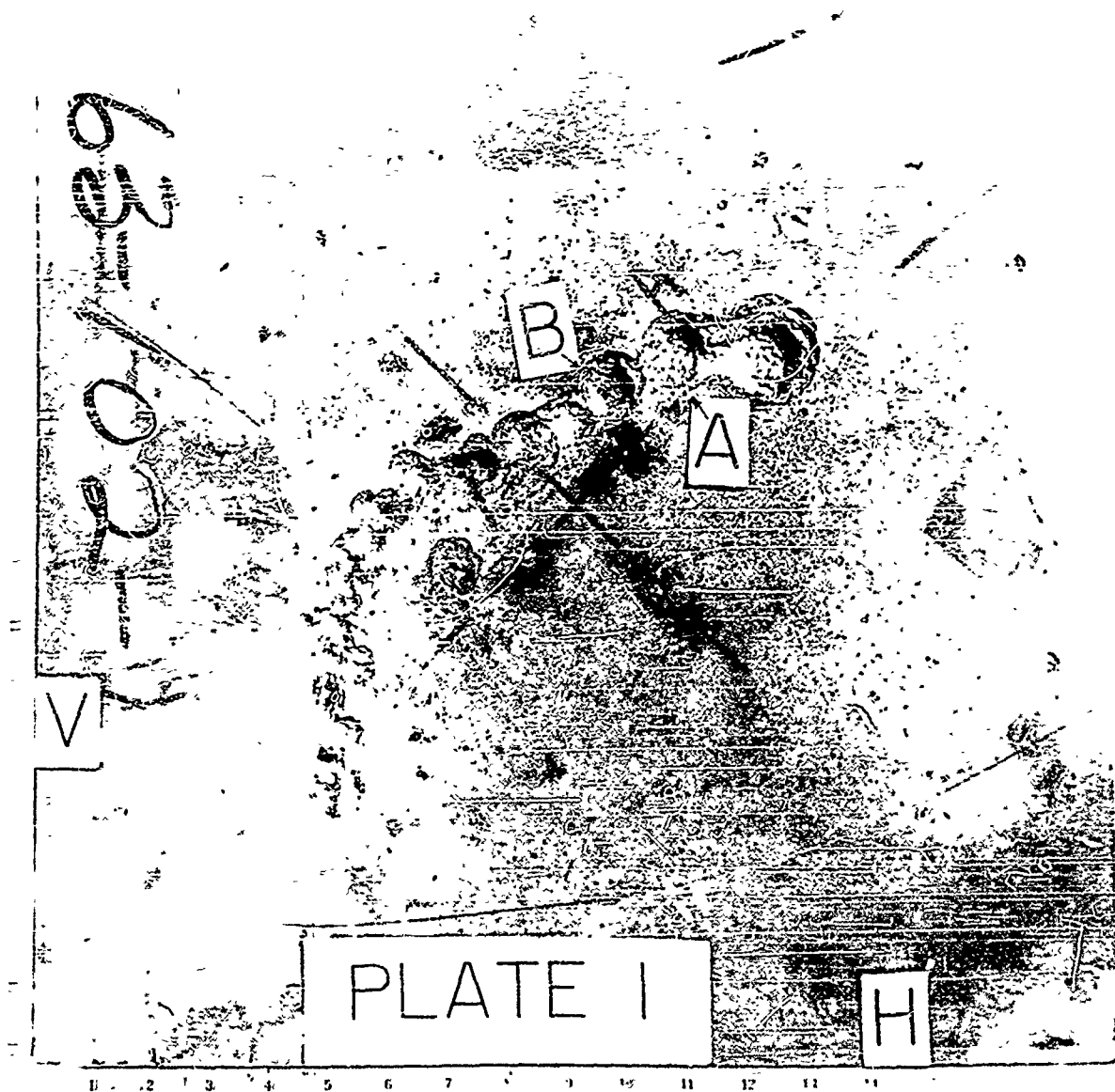
FIGURE 38   TARGET 63-102, 2024-T351 ALUMINUM,
2.0 INCH THICK

FIGURE 39 CRATER A, TARGET 63-102, 2024-T351
ALUMINUM, 2.0 INCH THICK (2.5X)

FIGURE 40 TARGET 62 109, 2024 T351 ALUMINUM,
2.0 INCH THICK
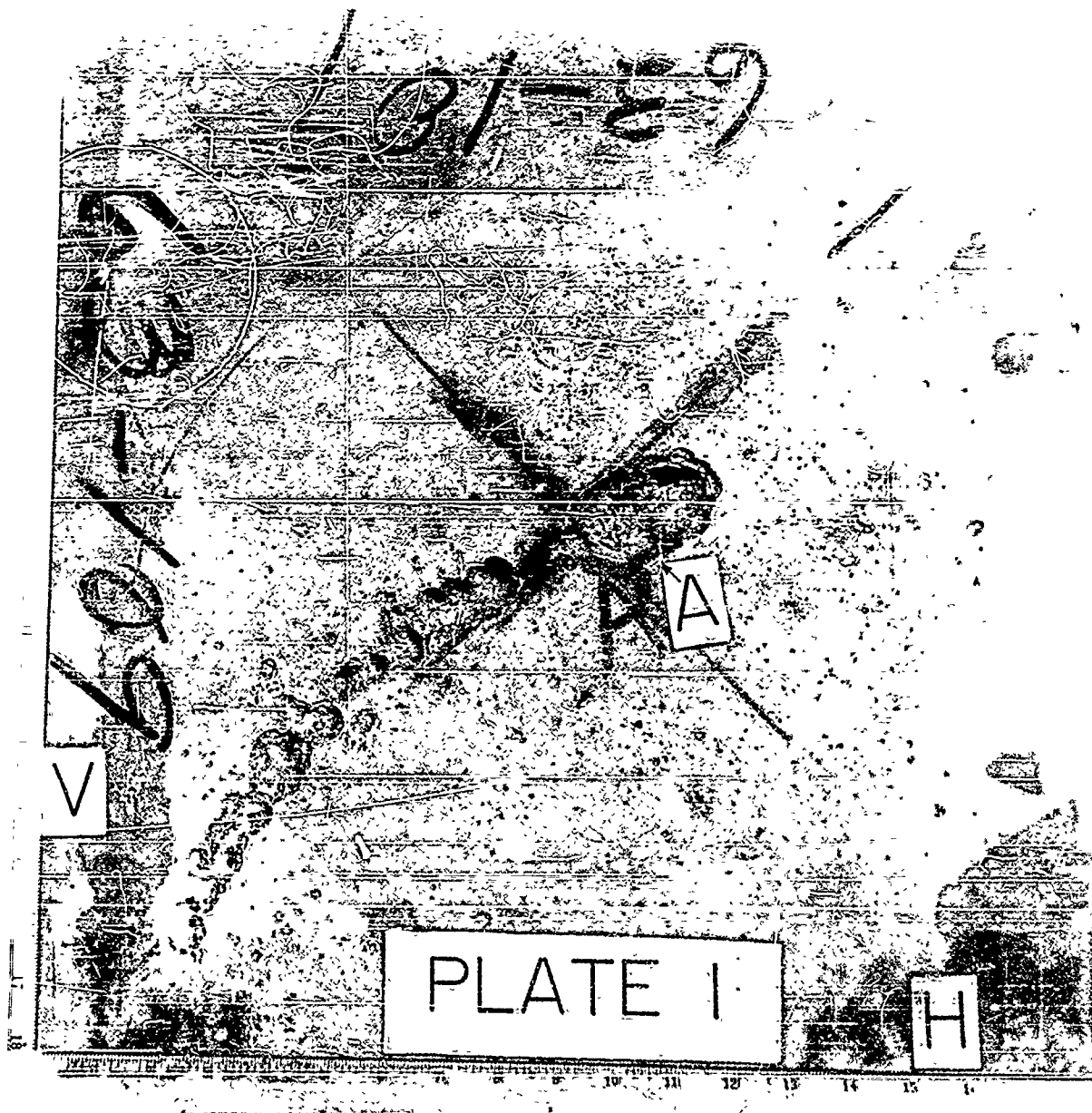
FIGURE 41 CRATER A. TARGET 63-109, 2024-T351
ALUMINUM, 2.0 INCH THICK (2X)
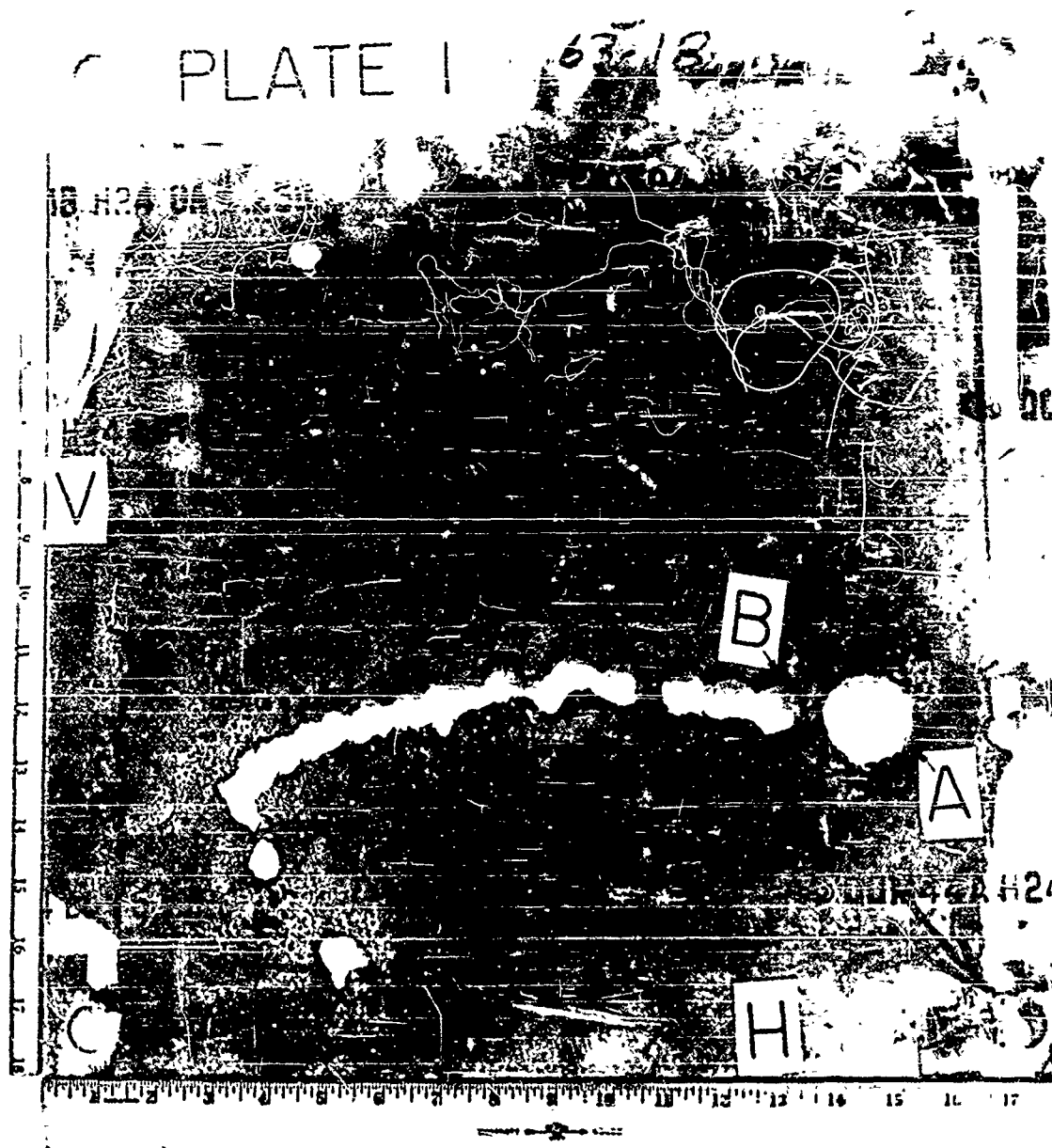
FIGURE 42   TARGET 63-18, PLATE 1, AZ31B-H24
MAGNESIUM, 0.25 INCH THICK
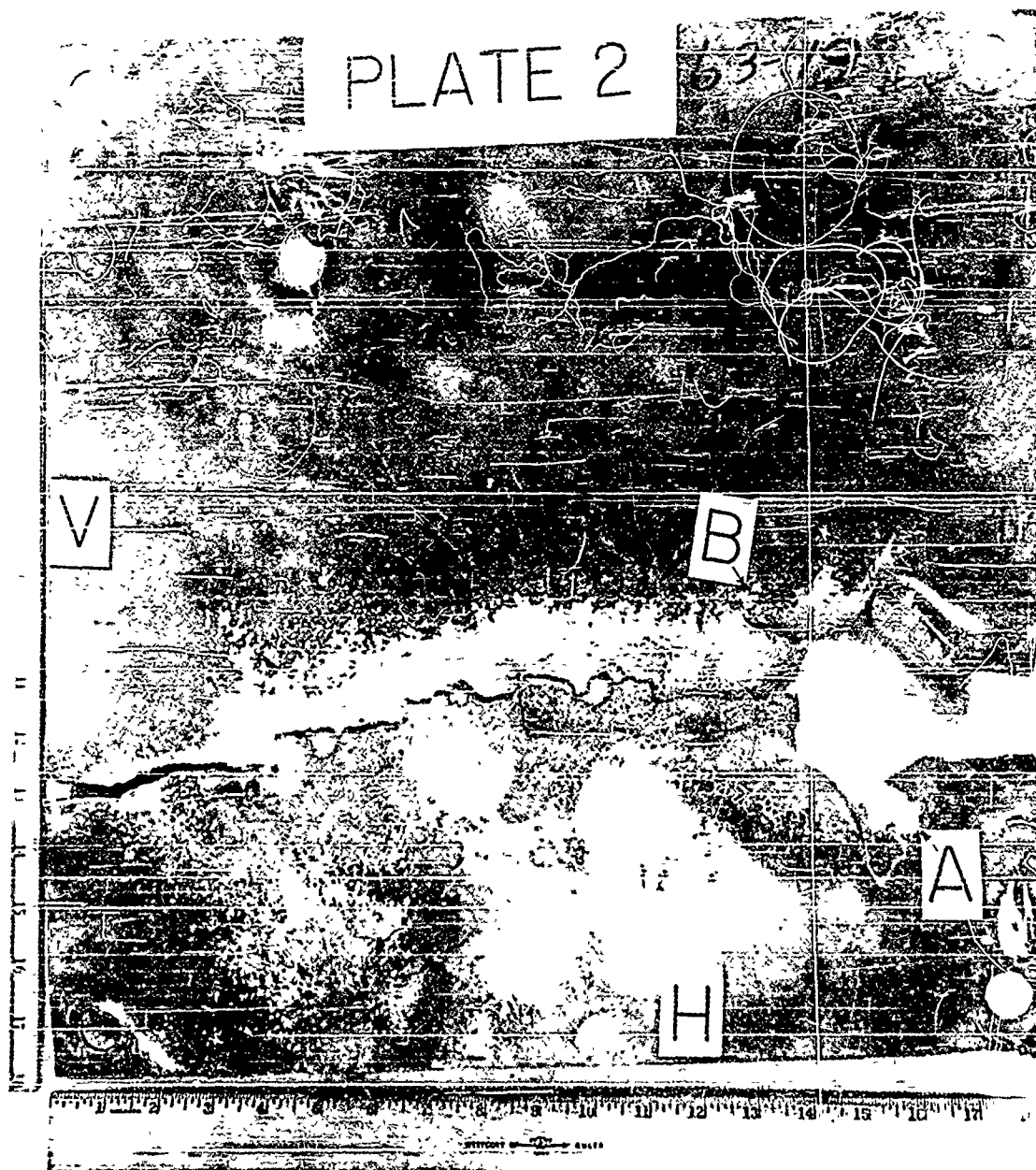
FIGURE 43   TARGET 63-18, PLATE 2, 2024-T3
ALUMINUM, 0.1 INCH THICK
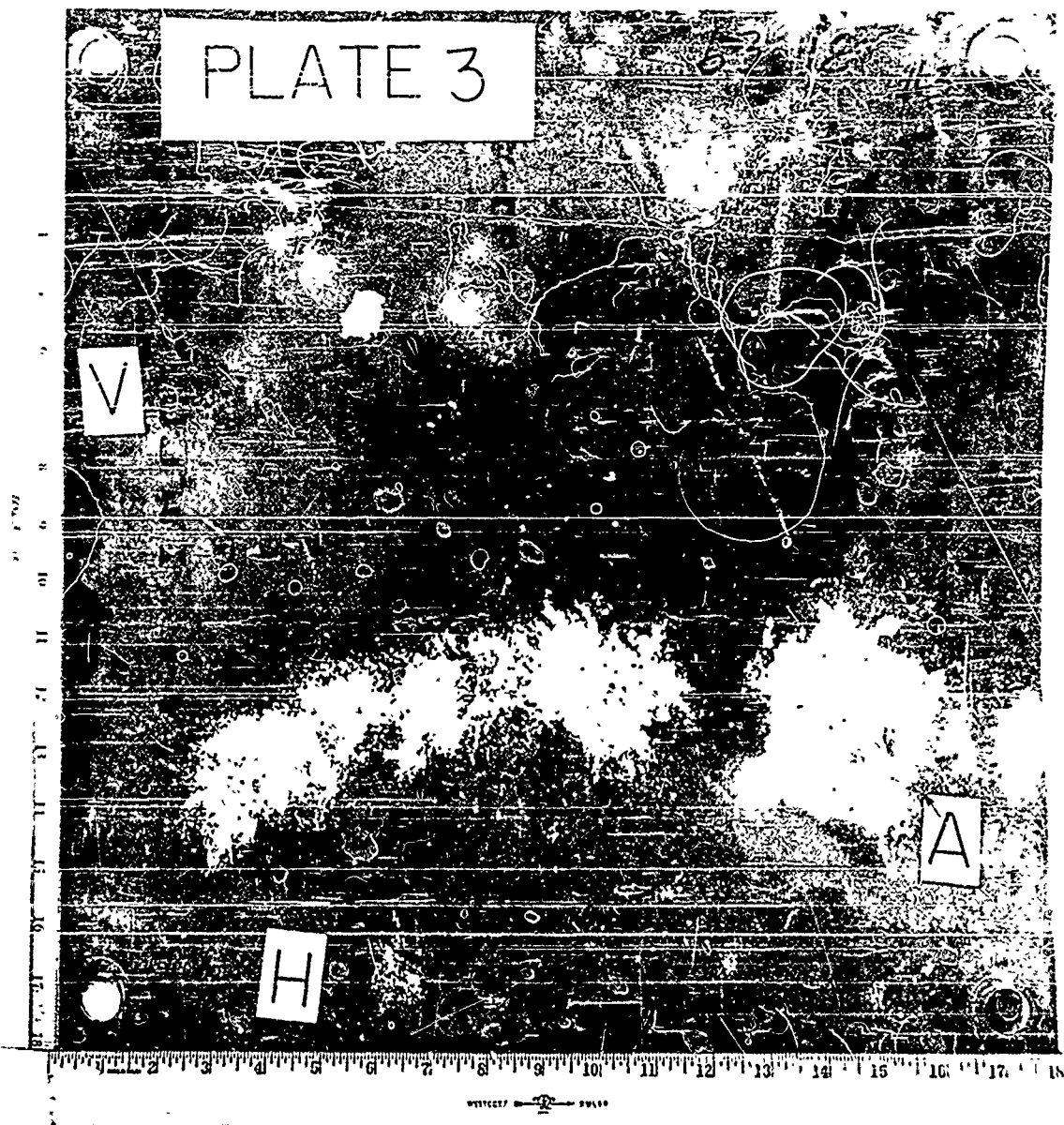
FIGURE 44   TARGET 63-18, PLATE 3, 2024-T3
ALUMINUM, 0.1 INCH THICK
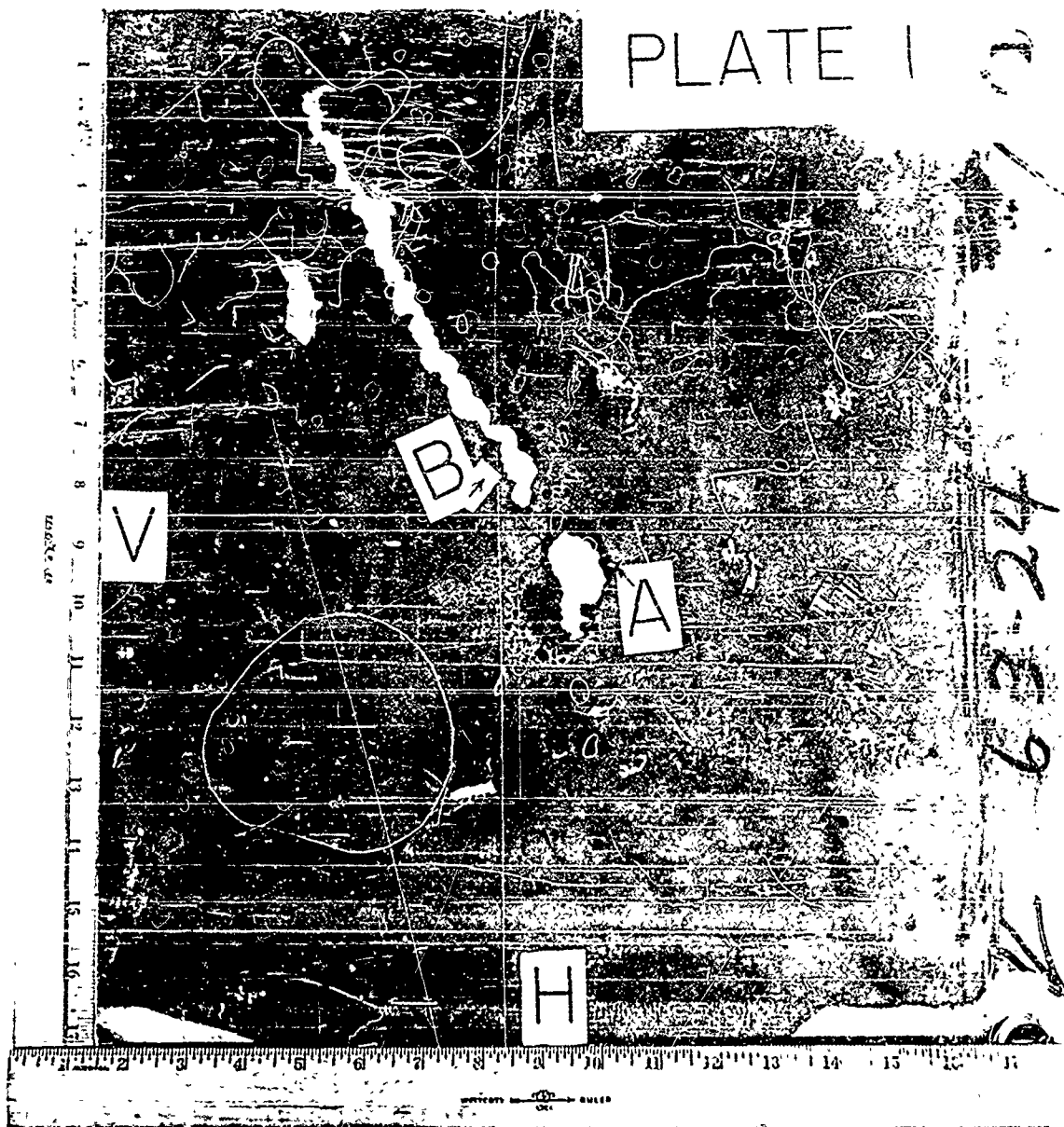
FIGURE 45   TARGET 63-24, PLATE 1, AZ31B-H24
MAGNESIUM, 0.1 INCH THICK
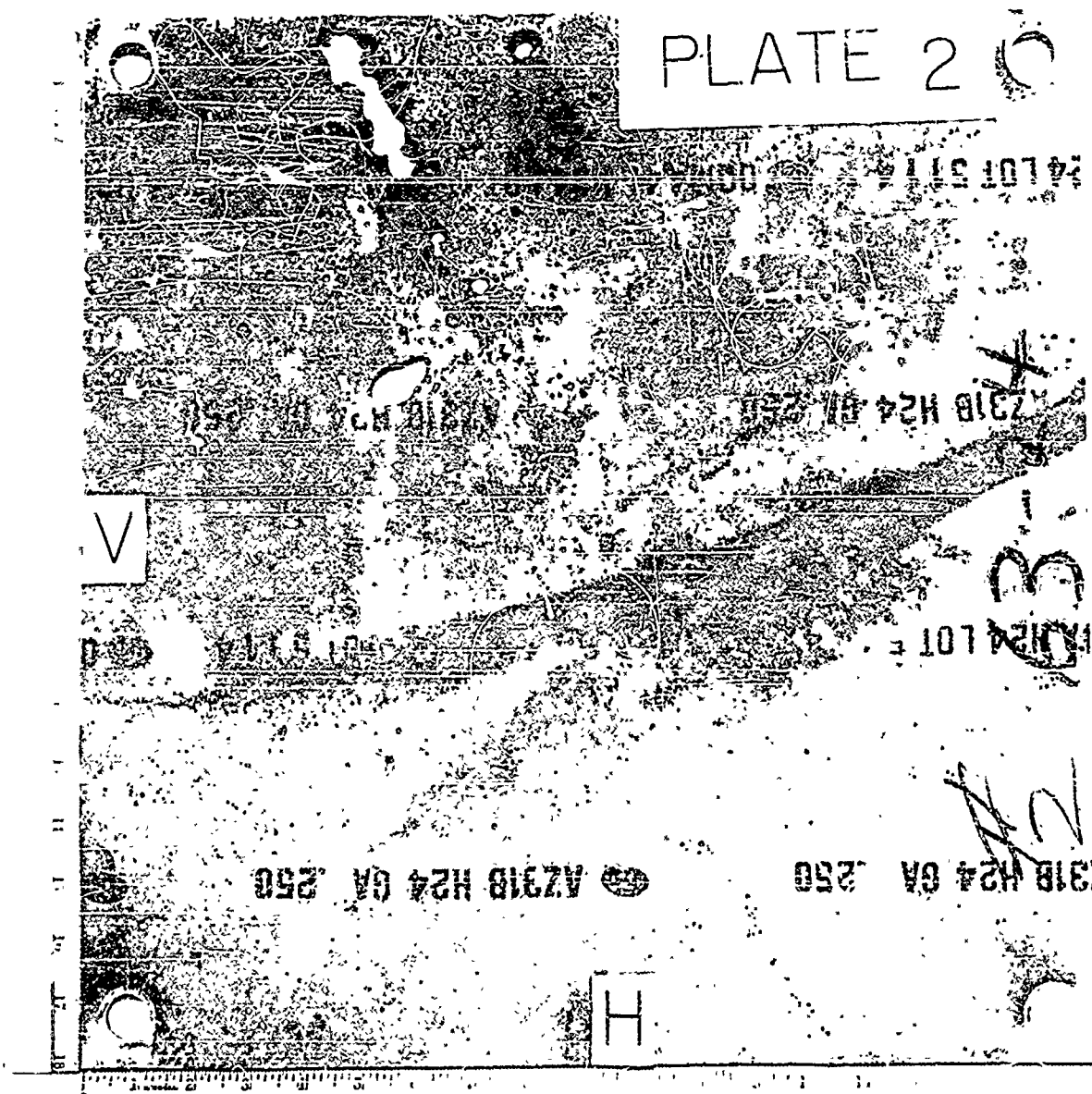
FIGURE 46   TARGET 63-24, PLATE 2, AZ31B-H24
MAGNESIUM, 0.25 INCH THICK
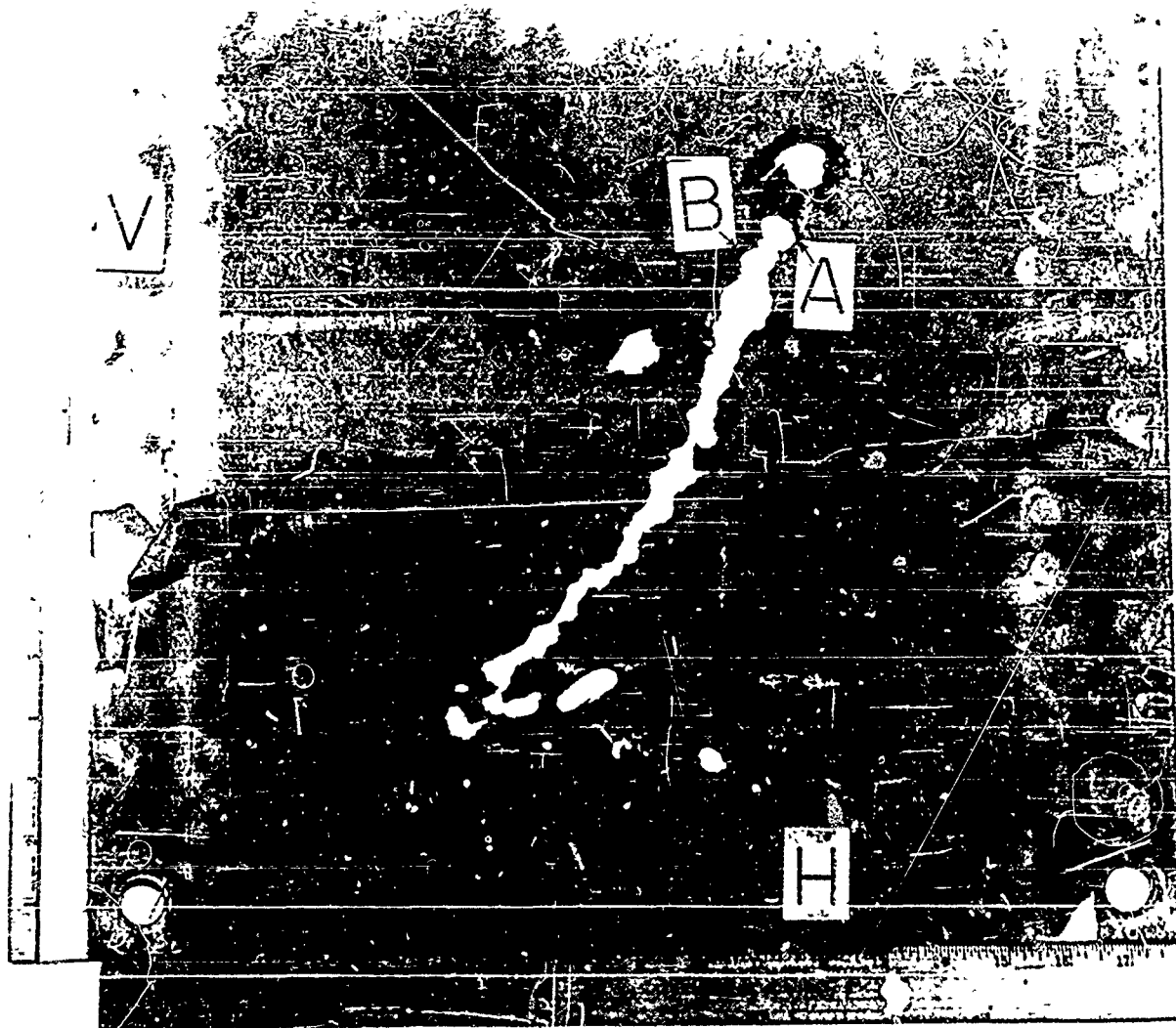
FIGURE 47   TARGET 63-30, PLATE 1, AZ31B-H24
MAGNESIUM, 0.1 INCH THICK
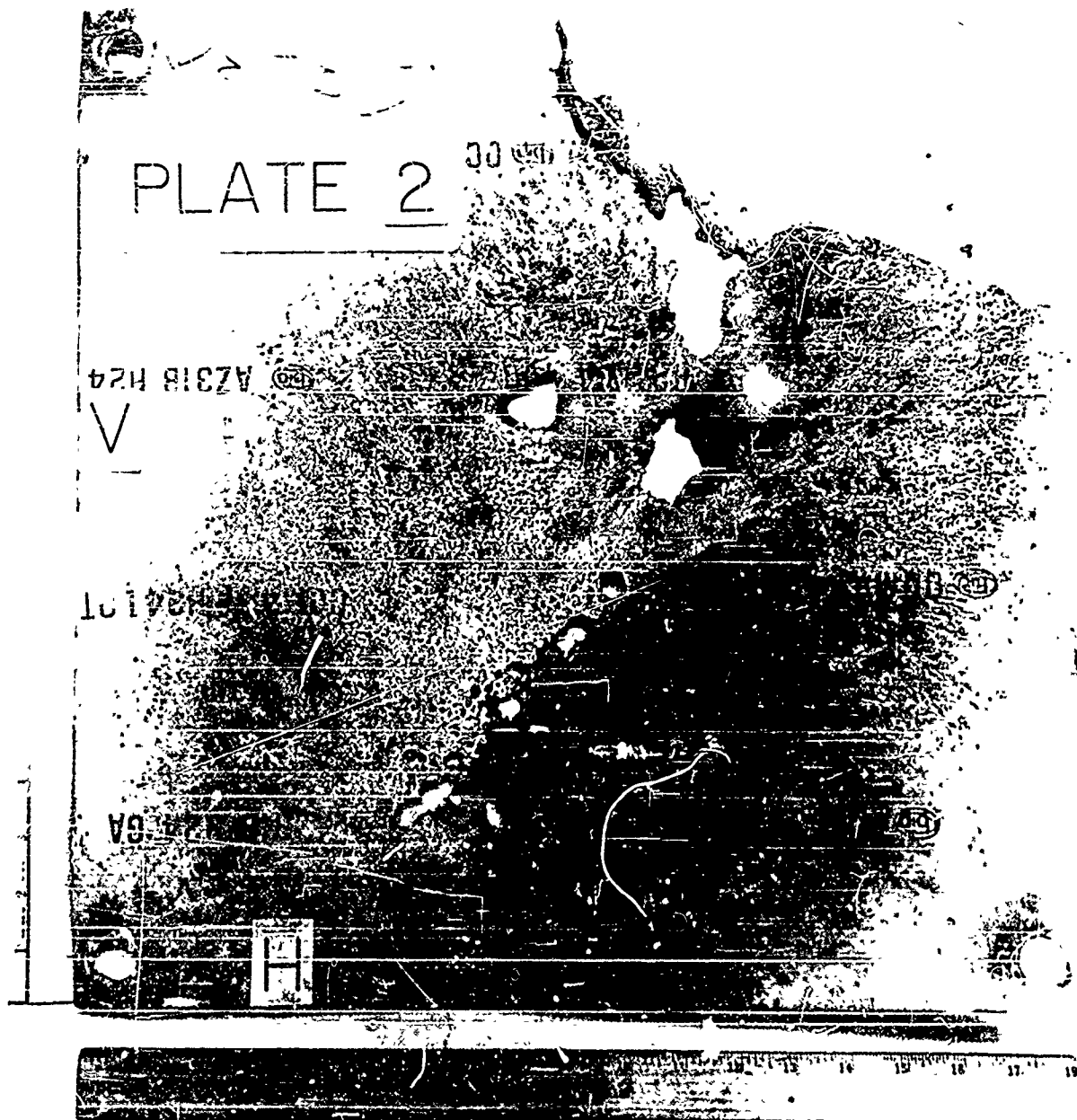
FIGURE 48   TARGET 63-30, PLATE 2, AZ31B-H24
MAGNESIUM, 0.1 INCH THICK
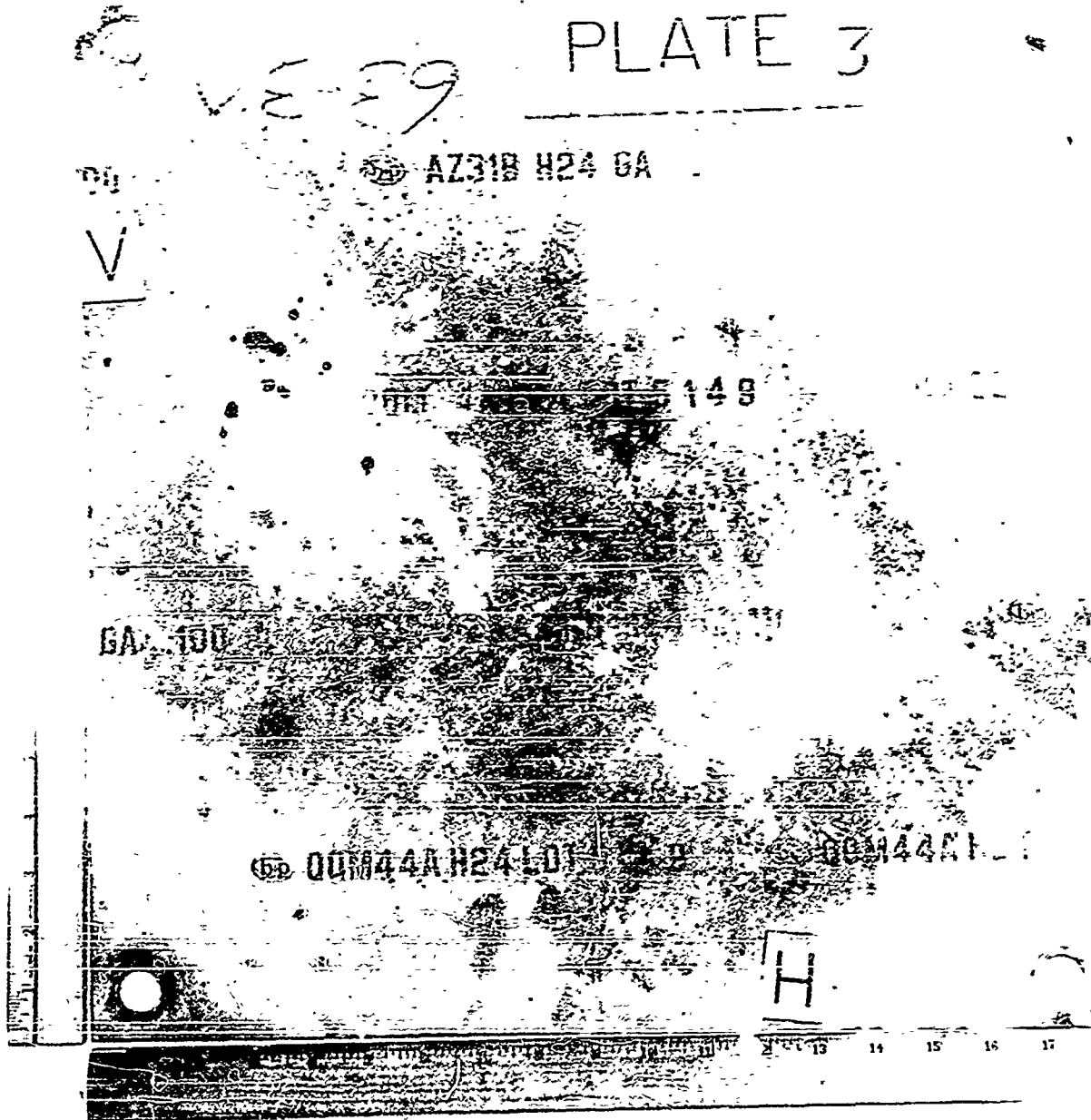
FIGURE 49 TARGET 63-30, PLATE 3, AZ31B-H24
MAGNESIUM, 0.1 INCH THICK
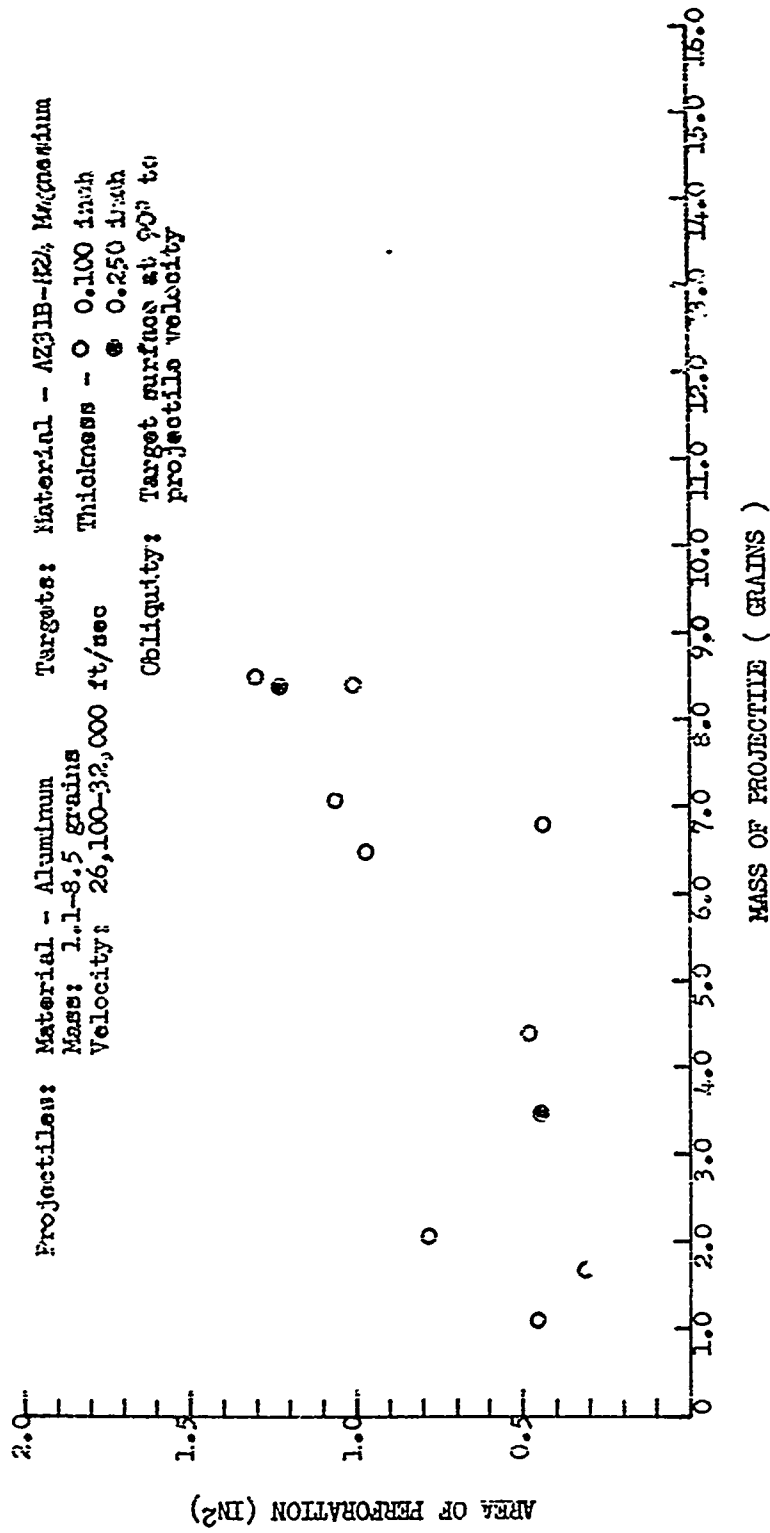
FIGURE 50 PERFORATION AREA AS A FUNCTION OF PROJECTILE
MASS FOR MAGNESIUM TARGETS

Projectiles: Material – Aluminum
Mass – 1.1-8.5 grains
Velocity – 26,100-32,000 ft/sec

Targets: Material – AZ31B-EW4 Magnesium
Thickness – ○ 0.1 inch
⊕ 0.2ˮ inch

Obliquity: Target surface at 90° to
projectile velocity

PROJECTED AREA (IN²)

AREA OF PERFORATION (IN²)
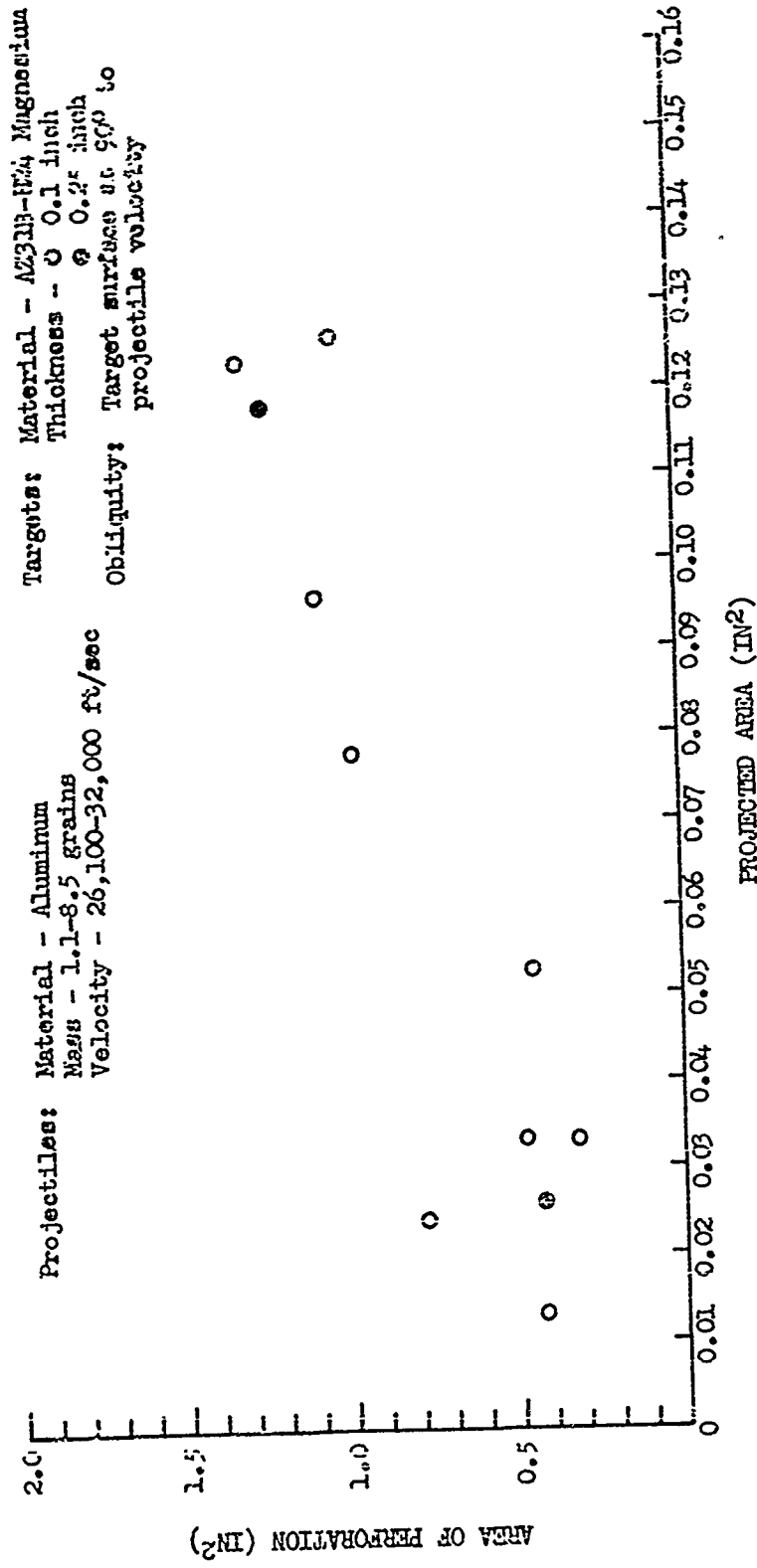
FIGURE 51   PERFORATION AREA AS A FUNCTION OF PROJECTED AREA
OF PROJECTILES ON MAGNESIUM TARGETS
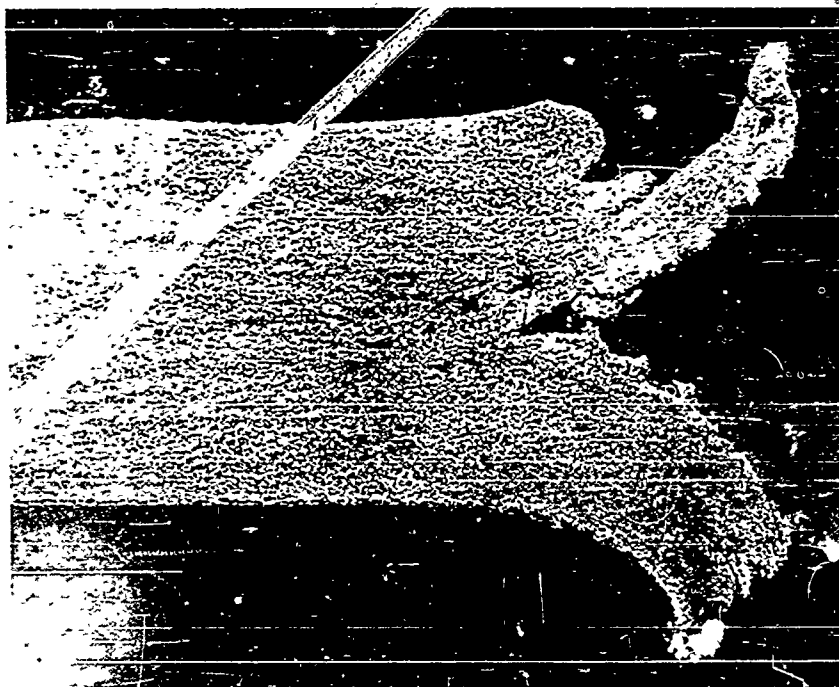
FIGURE 52   PERFORATION A, TARGET 63-21, AZ31B-H24
MAGNESIUM, 0.1 INCH THICK (20X)
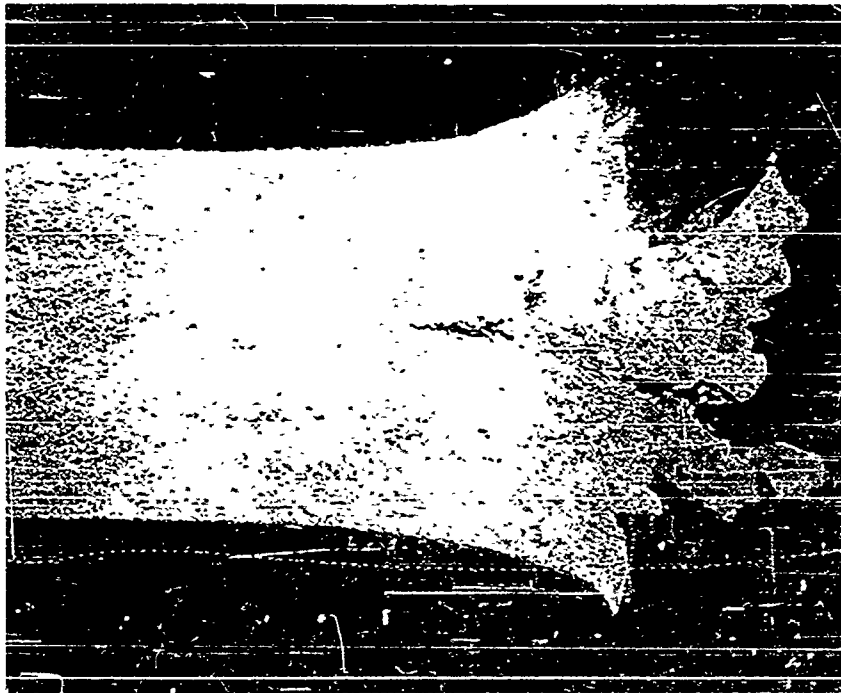
FIGURE 53   PERFORATION B, TARGET 63-24, AZ31B-H24
MAGNESIUM, 0.1 INCH THICK (20X)
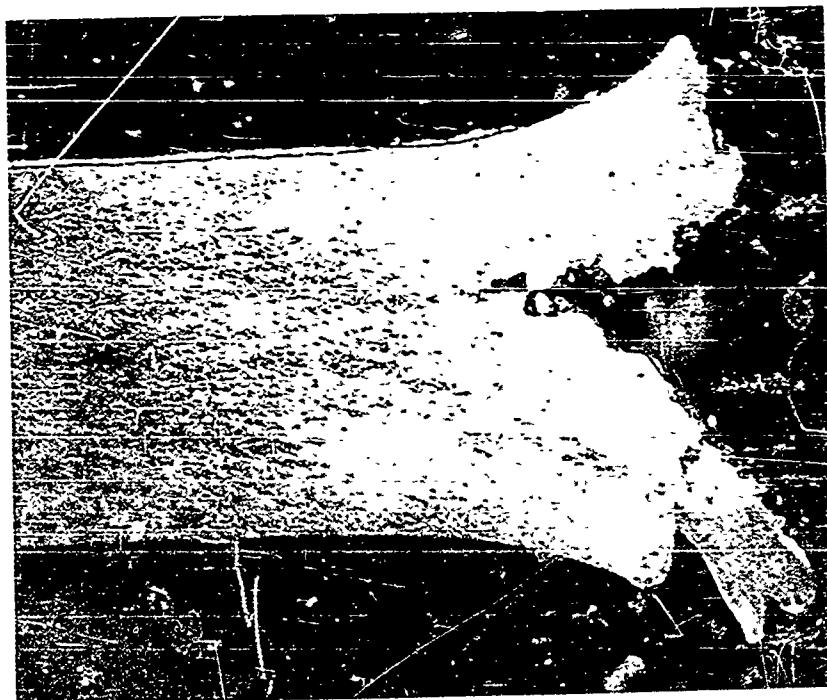
FIGURE 54   PERFORATION A, TARGET 63-47, AZ31B-H24
MAGNESIUM, 0.1 INCH THICK (2CX)

Durimet Microhardness Tester
Load: 100g

HARDNESS (VICKERS SCALE)

DISTANCE FROM EDGE (IN)

FIGURE 55   HARDNESS AS A FUNCTION OF DISTANCE FROM THE EDGE OF
PERFORATION B, TARGET 18-63

Magnification: 500X
Etchant: Acetic Acid-Nickel Nitrate

FIGURE 56   MICROSTRUCTURE IN AN UNAFFECTED AREA (UPPER) AND
AN AREA NEAR PERFORATION B (LOWER) OF TARGET 63-L,
AZ31B-H24 MAGNESIUM, 0.25 INCH THICK

$\overline{1\mu}$

FIGURE 57 ELECTRON MICROGRAPH OF STRUCTURE NEAR PERFORATION B,
TARGET 63-18, AZ31B-H24 MAGNESIUM, 0.25 INCH THICK (9900X)

$1\,\mu$

FIGURE 58 ELECTRON MICROGRAPH OF STRUCTURE NEAR PERFORATION B,
TARGET 63-18, AZ31B-H24 MAGNESIUM, 0.25 INCH THICK (30,700X)

|— ——— |
$1\,\mu$
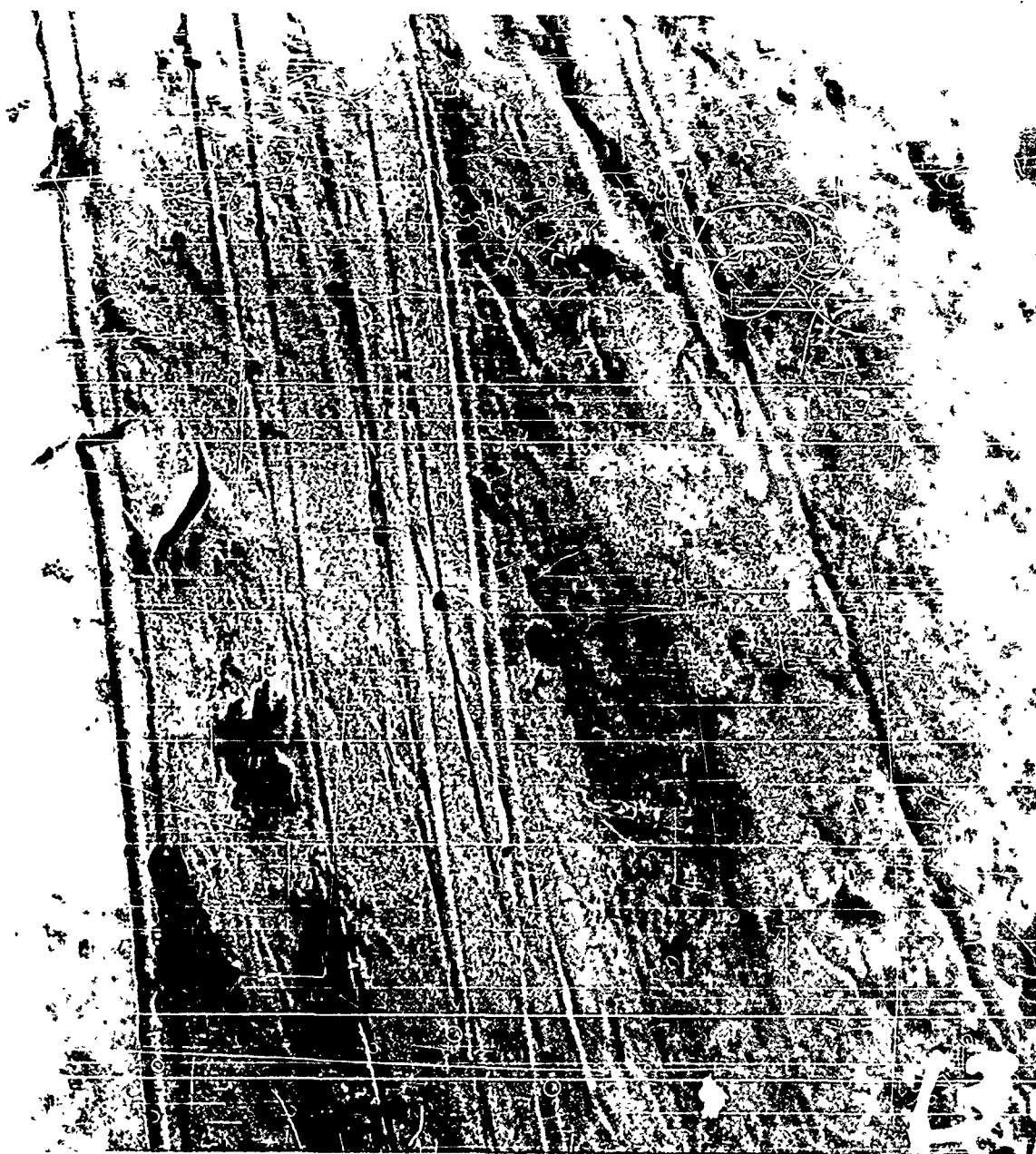
FIGURE 59   ELECTRON MICROGRAPH OF STRUCTURE NEAR PERFORATION 5,
TARGET 63-18, AZ31B-H24 MAGNESIUM, 0.25 INCH THICK (30,700X)
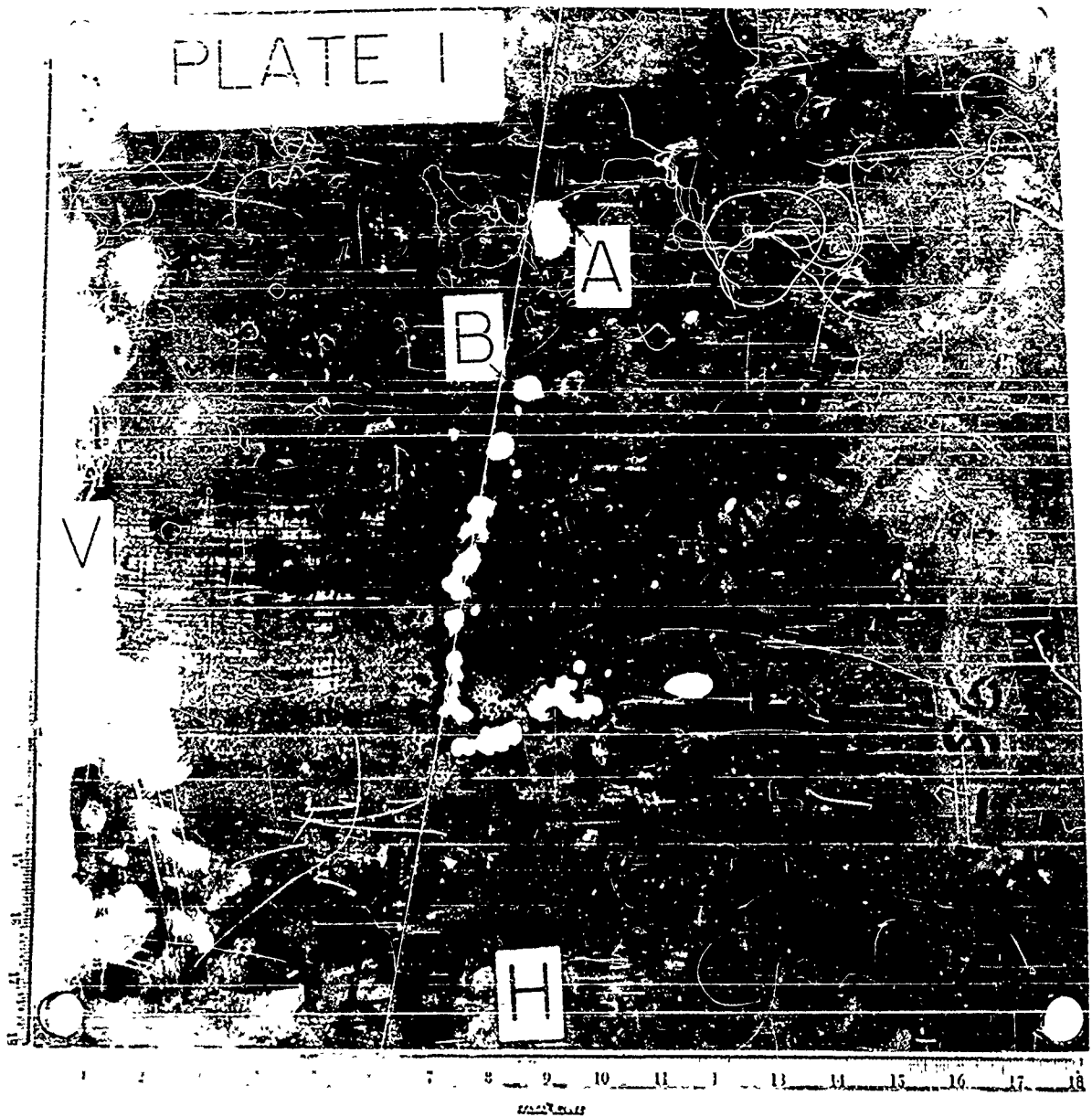
FIGURE 60   TARGET 63-86, PLATE 1, 4130 STEEL,
0.1 INCH THICK
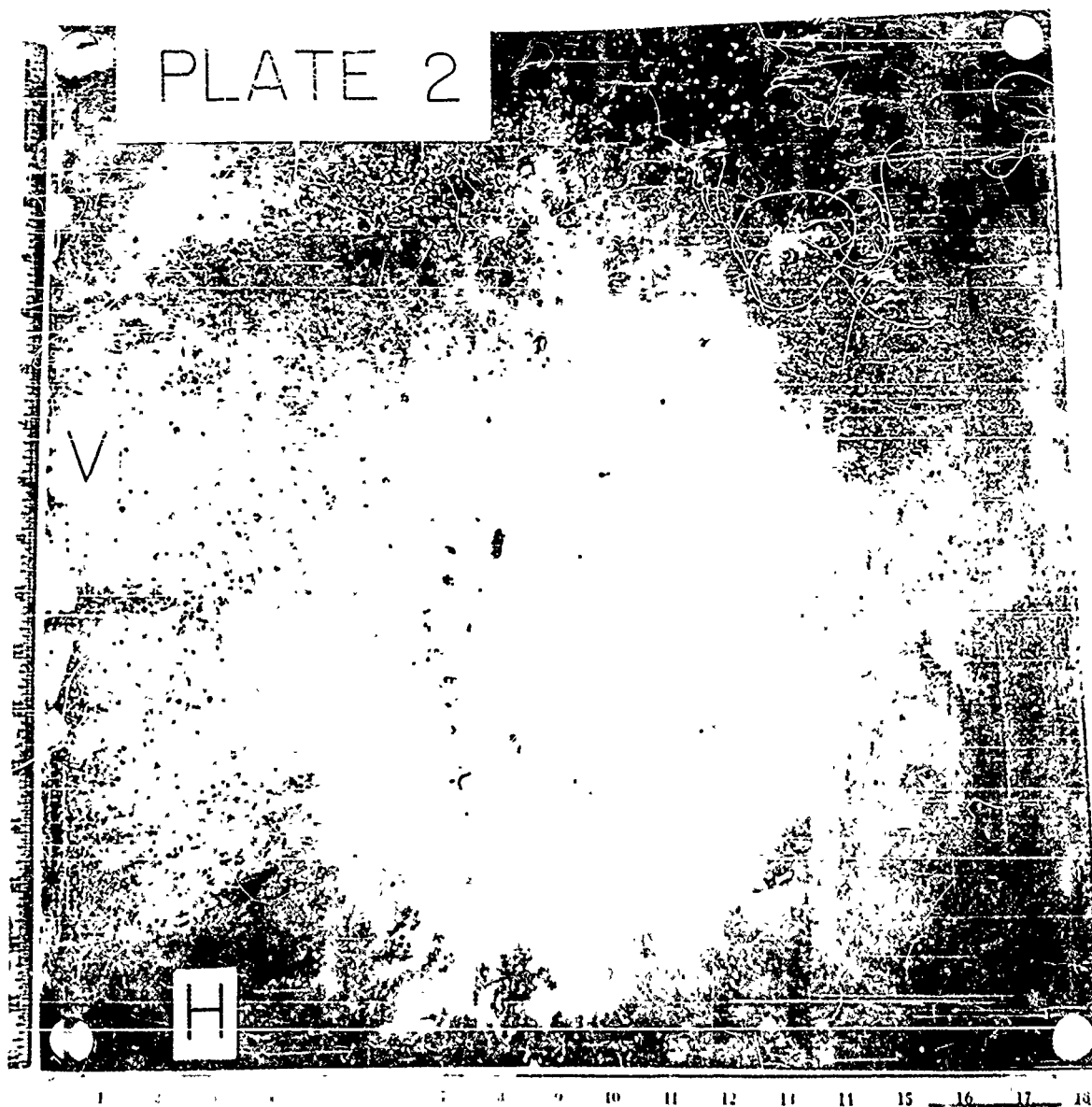
PLATE 2

FIGURE 61 TARGET 63-36, PLATE 2, 4130 STEEL,
0.1 INCH THICK
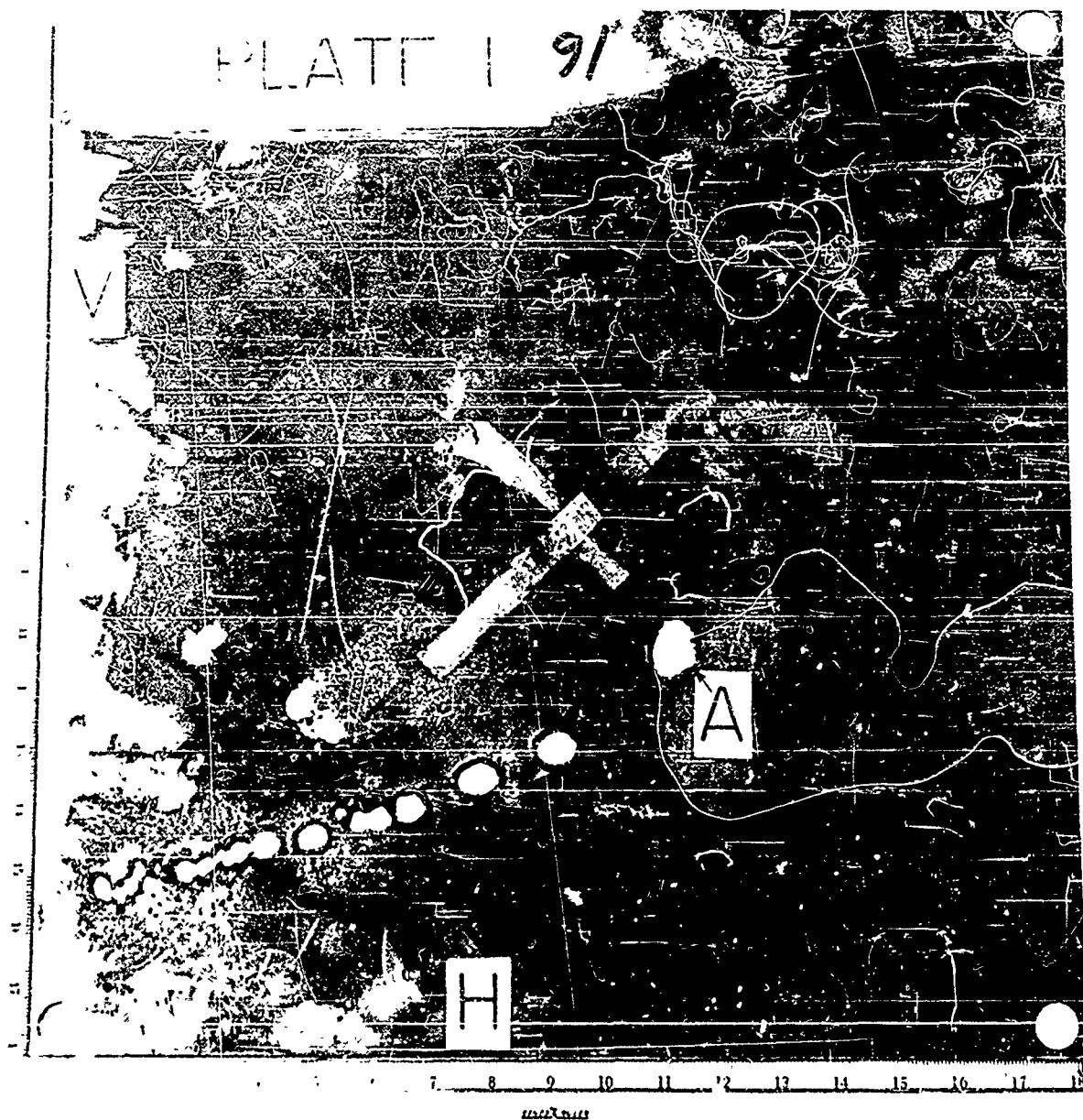
FIGURE 62   TARGET 63-97, PLATE 1, 4130 STEEL,
0.1 INCH THICK
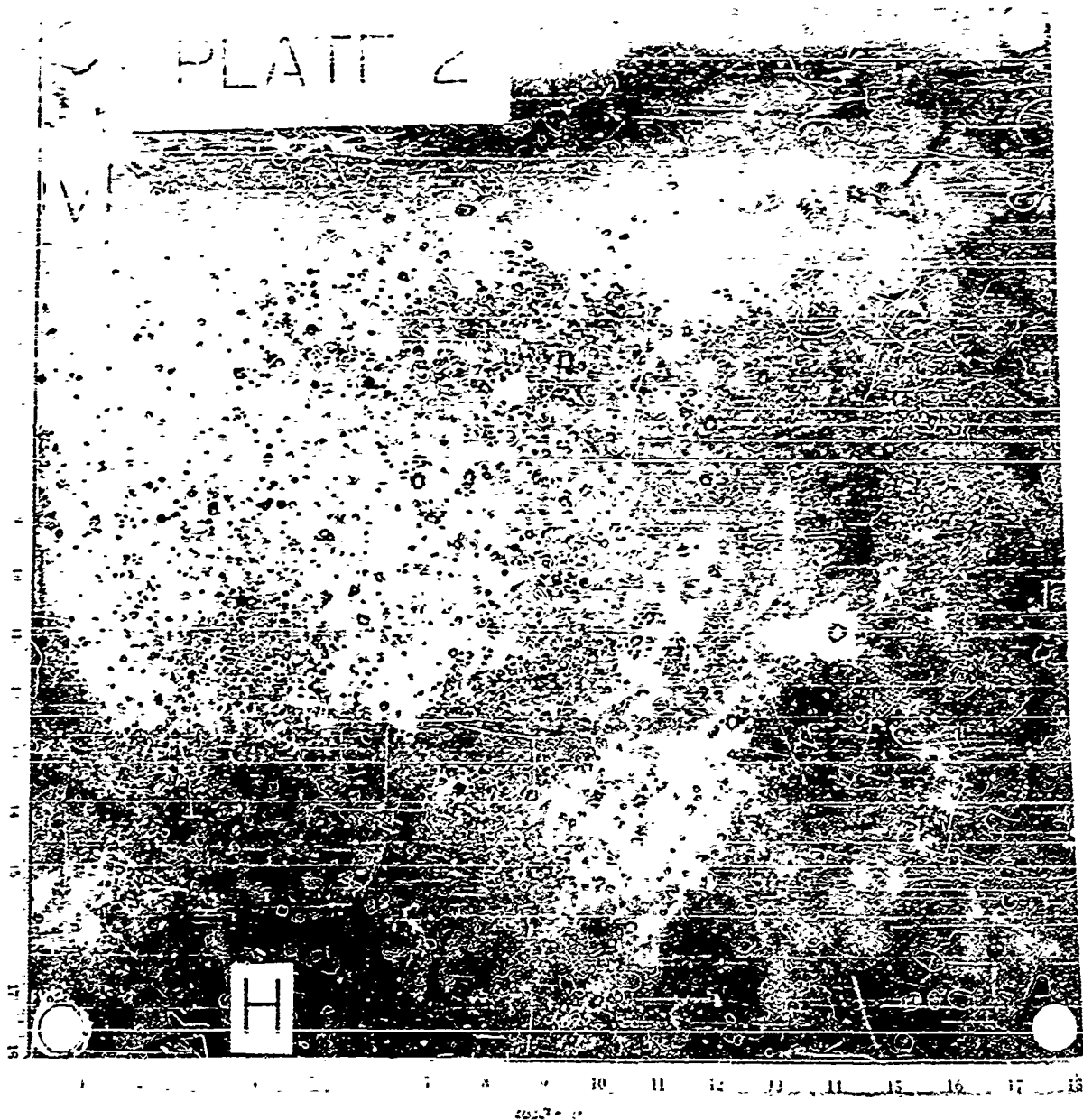
FIGURE 63   TARGET 63-87, PLATE 2, 4130 STEEL,
0.1 INCH THICK
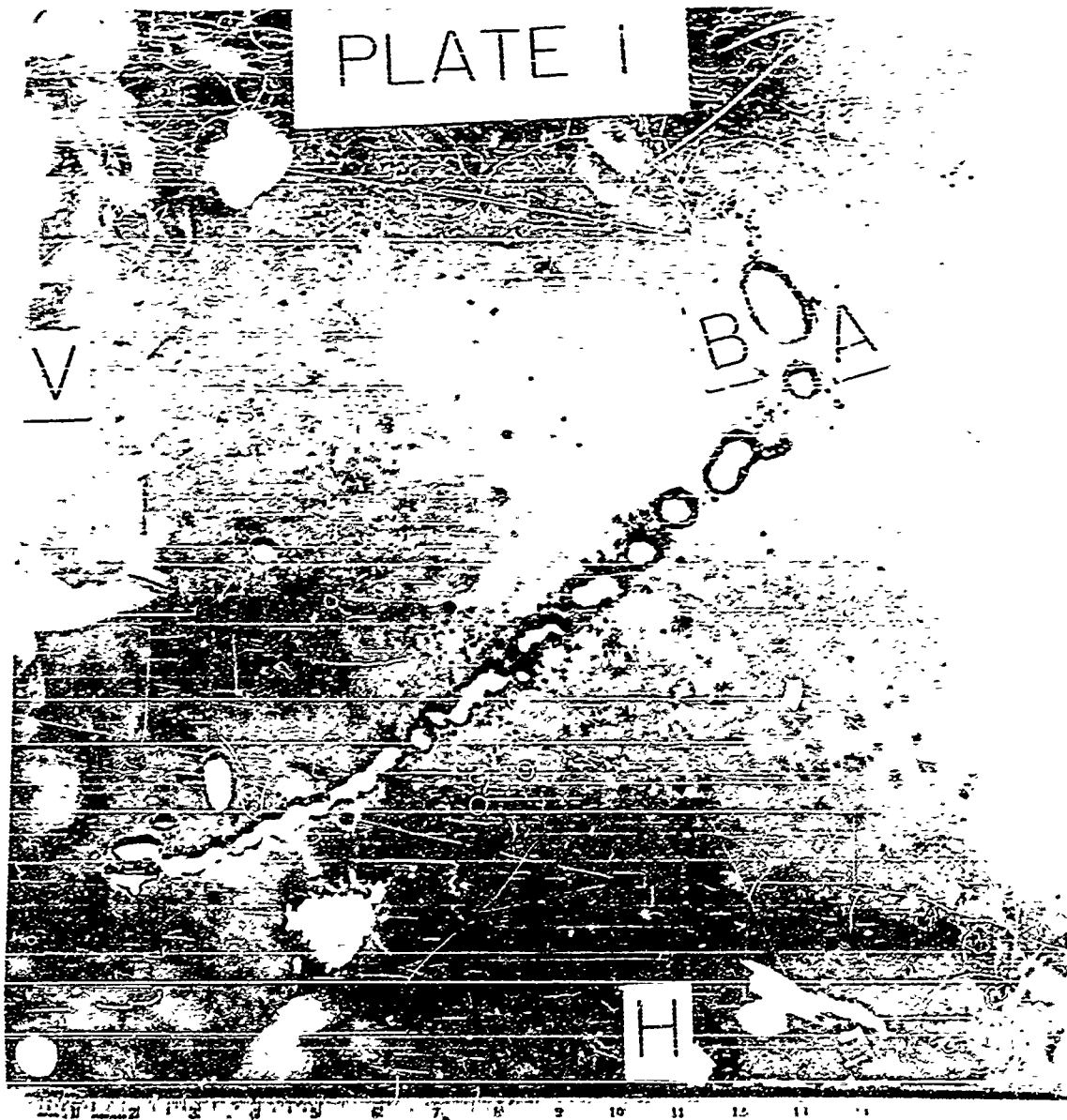
FIGURE 64 TARGET 63-88, PLATE 1, 4130 STEEL,
0.1 INCH THICK
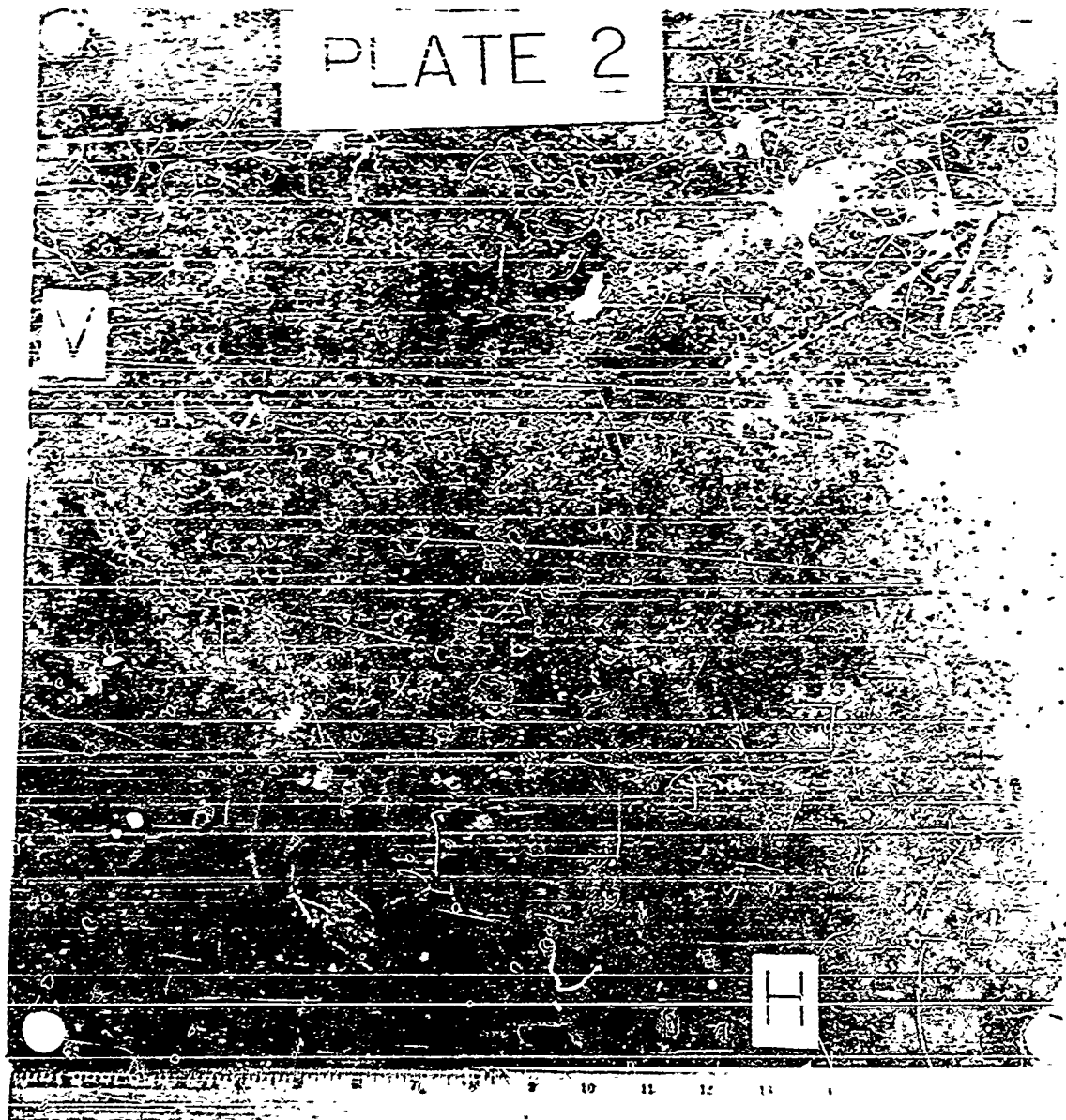
FIGURE 65   TARGET 63-88, PLATE 2, 4130 STEEL,
0.1 INCH THICK
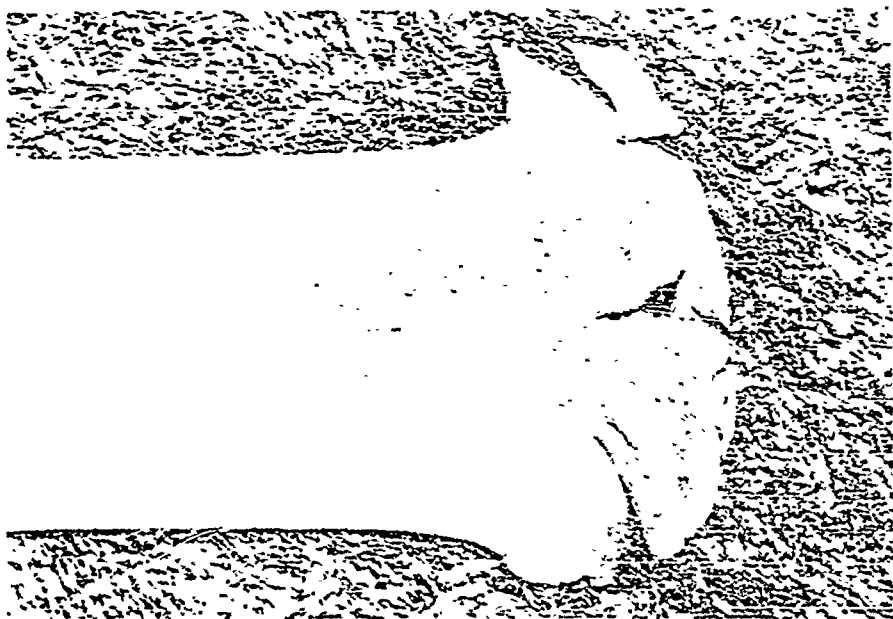
FIGURE 66   PERFORATION A, TARGET 63-86, 4130 STEEL,
0.1 INCH THICK (20X)

Durimet Microhardness Tester
Load: 100 grams
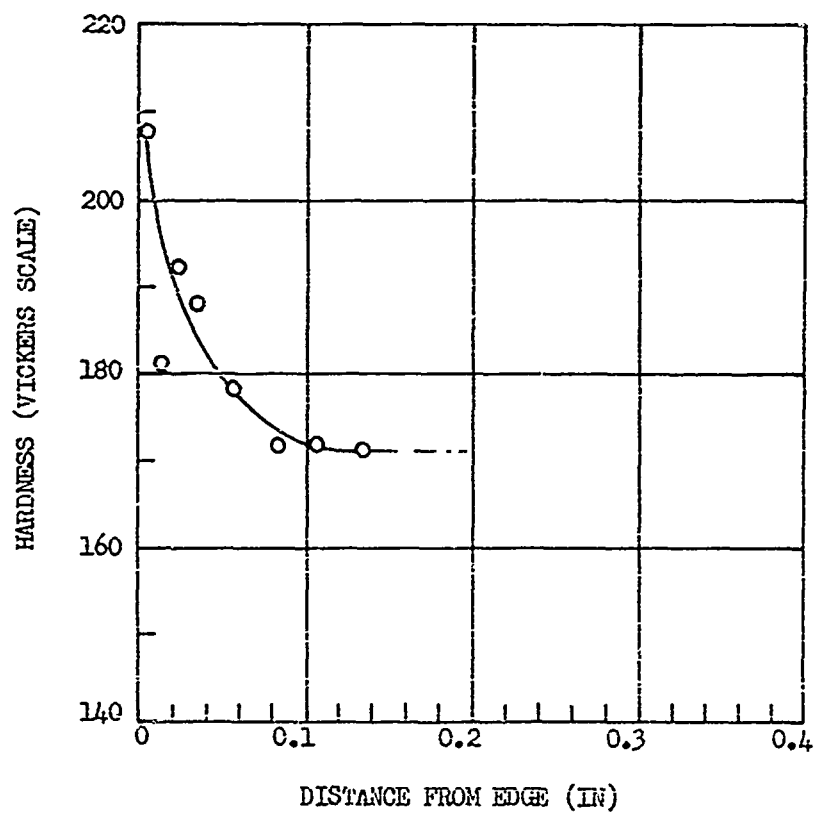
FIGURE 67   HARDNESS AS A FUNCTION OF DISTANCE FROM
             EDGE OF PERFORATION A, TARGET 63-37
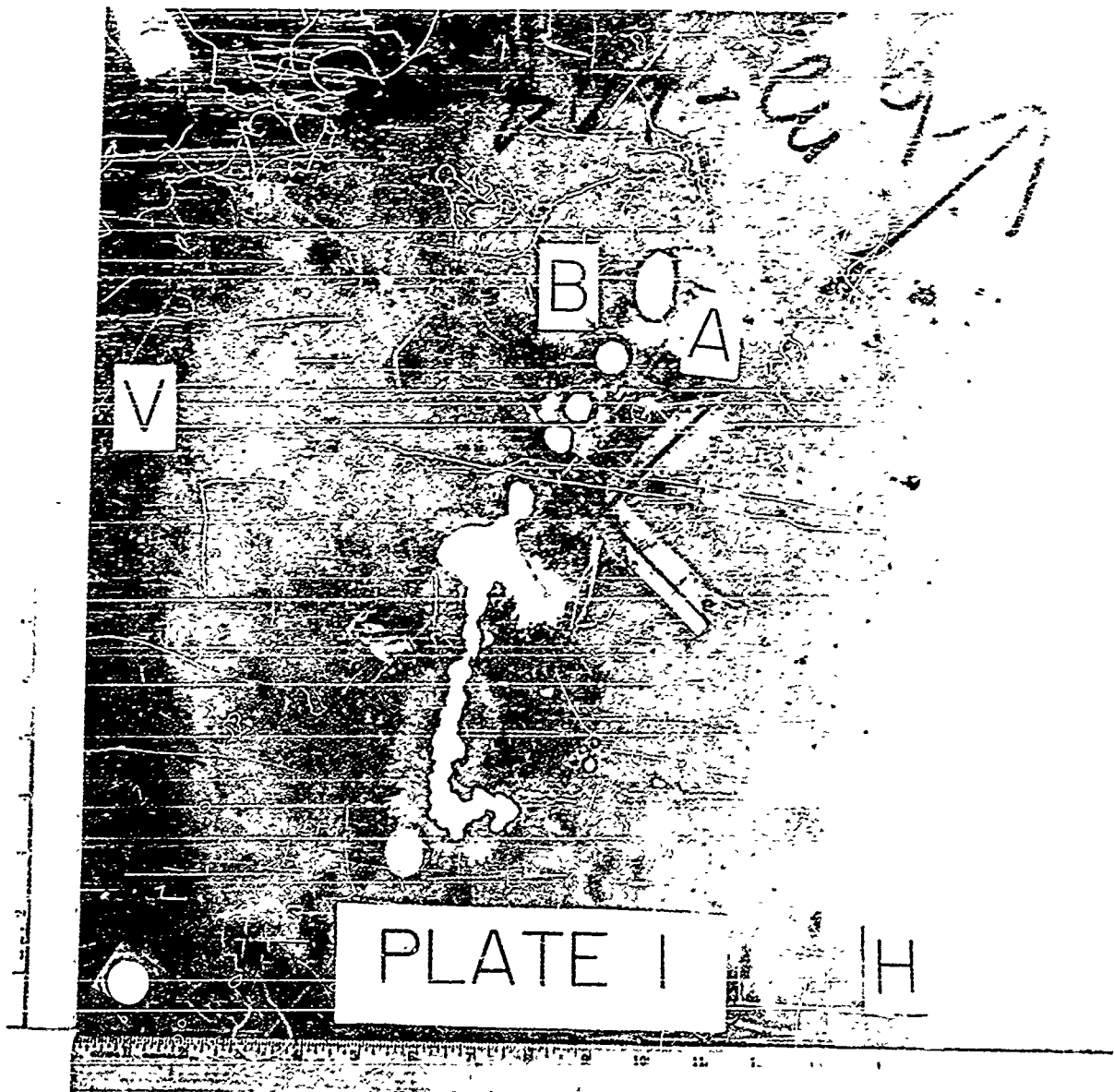
FIGURE 68   TARGET 63-104, PLATE 1, TYPE 410
STAINLESS STEEL, 0.1 INCH THICK

FIGURE 69   TARGET 63-104, PLATE 1, TYPE 410
STAINLESS STEEL, 0.1 INCH THICK
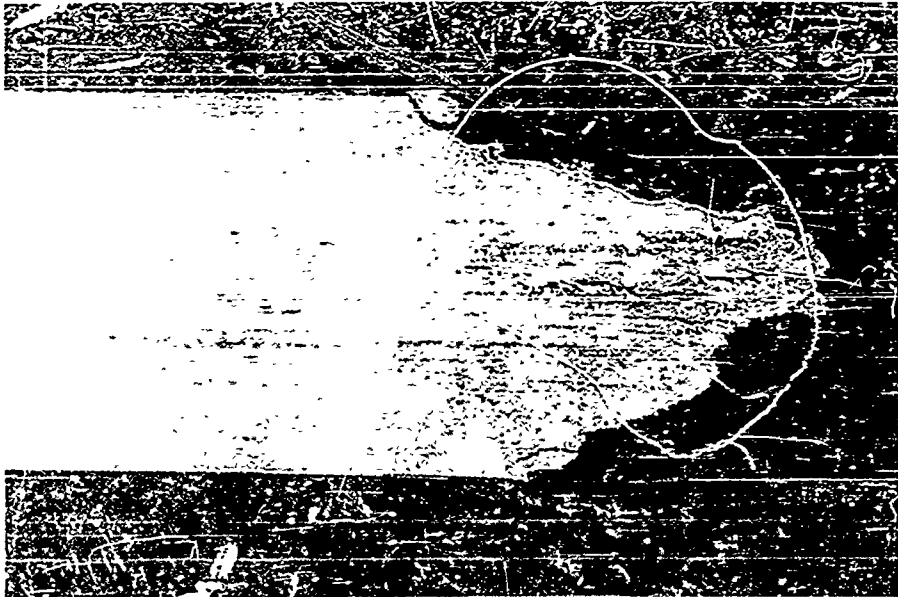
FIGURE 70   PERFORATION A, TARGET 63-104, TYPE 410
            STAINLESS STEEL, 0.1 INCH THICK (20X)
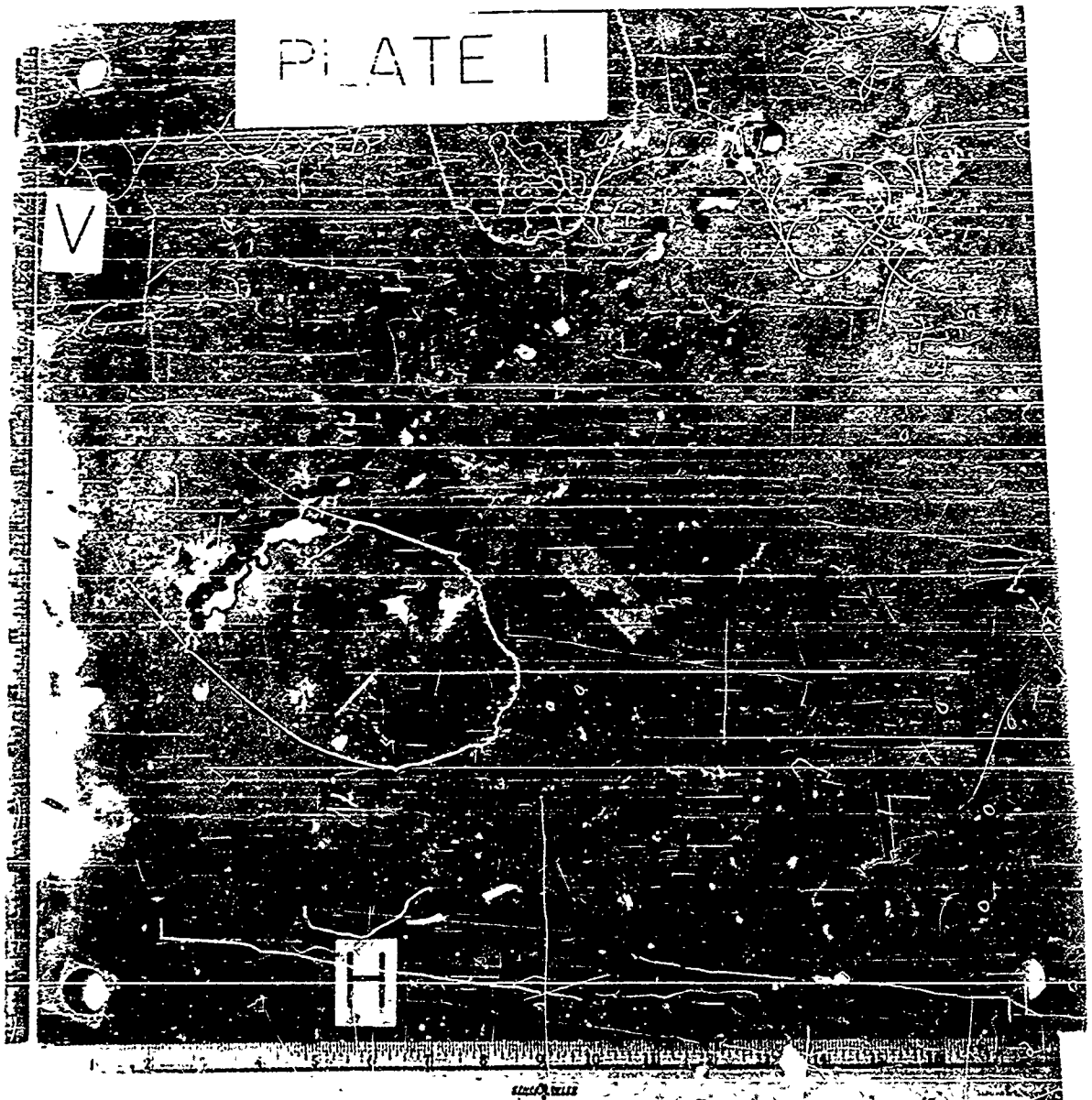
TARGET 71   TARGET 63-97, PLATE 1, TITANIUM
(6AL, 4V), 0.1 INCH THICK
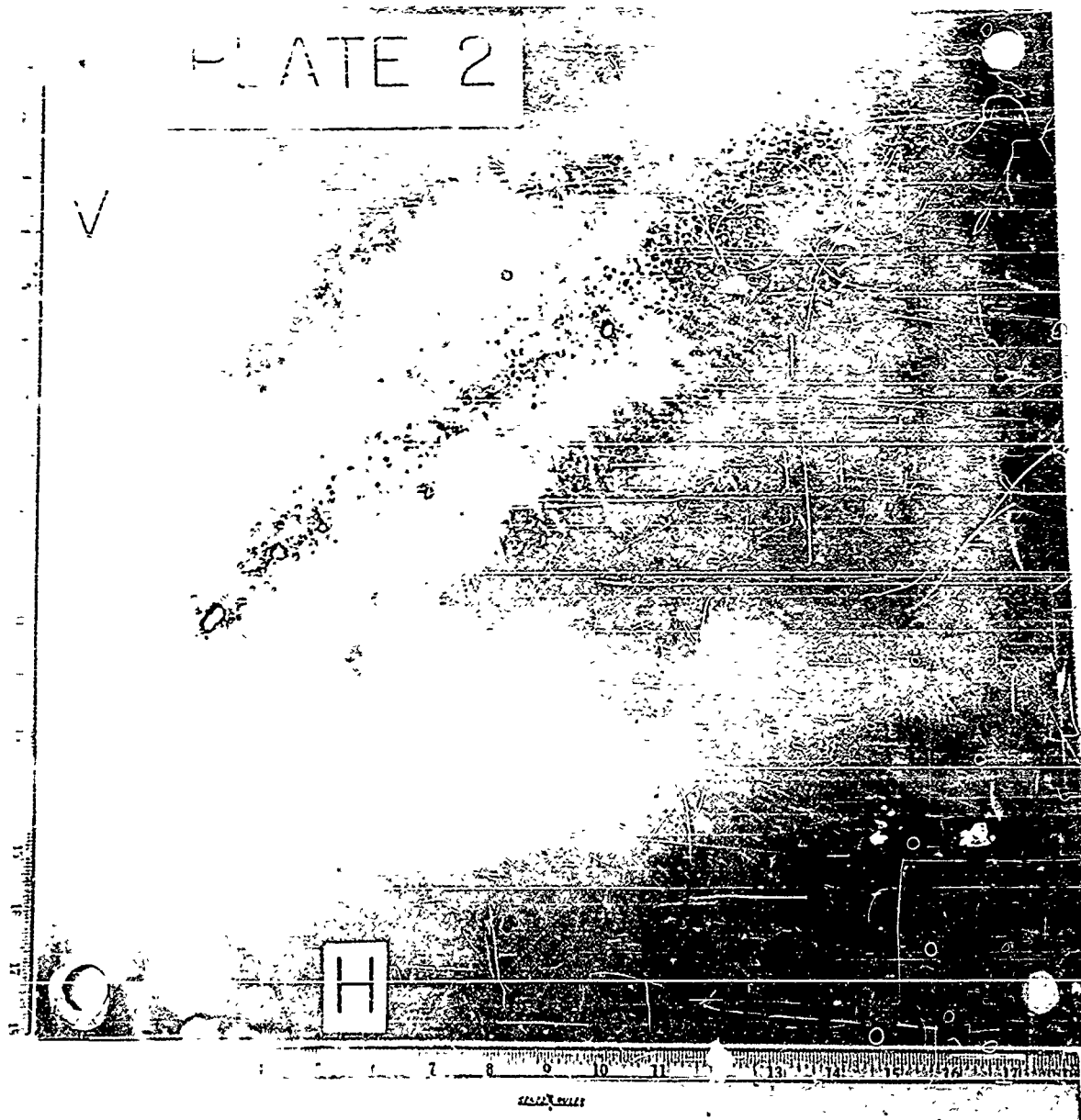
FIGURE 72   TARGET 63-97, PLATE 2, TITANIUM
(6AL, 4V), 0.? INCH THICK
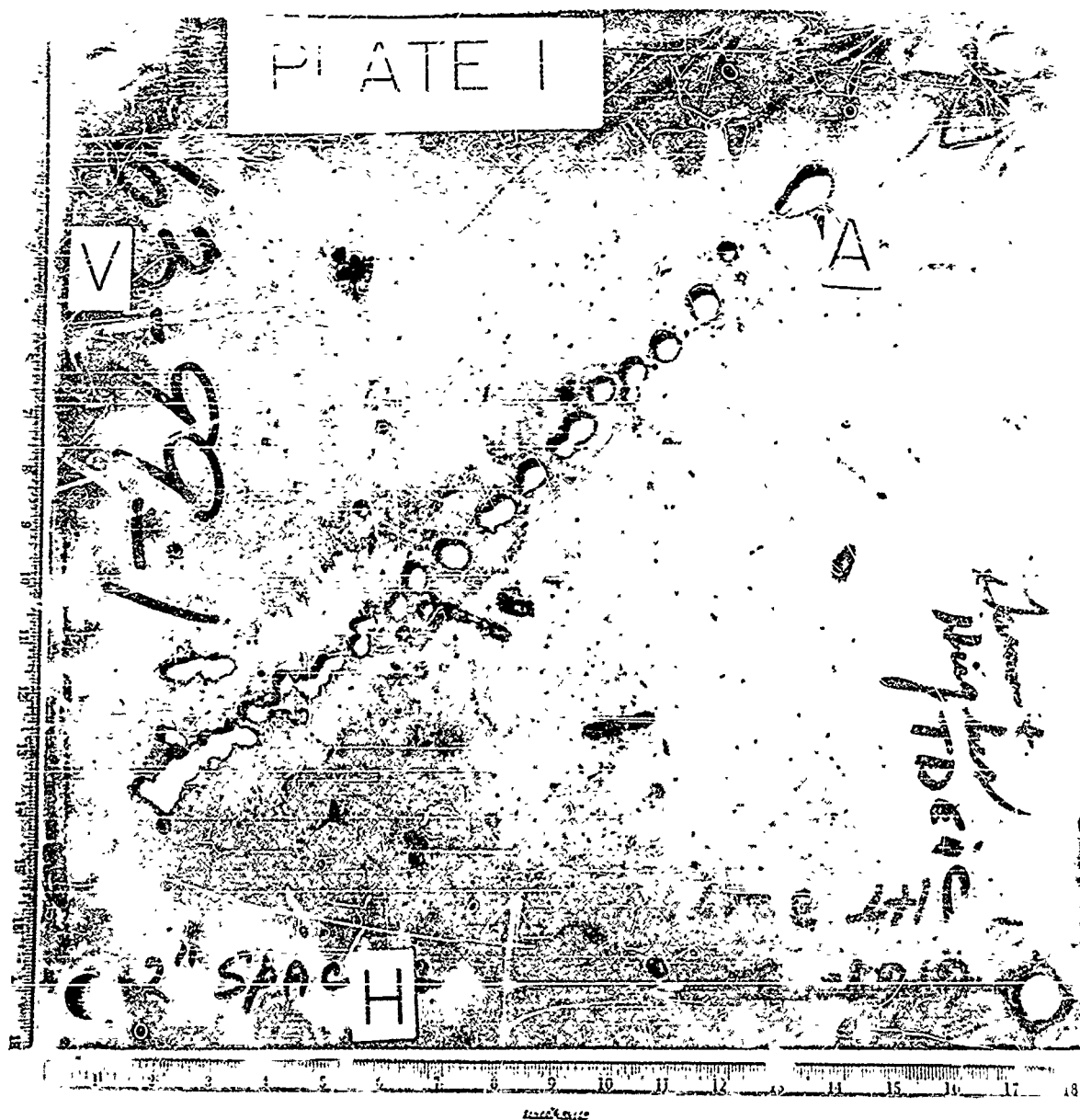
FIGURE 73   TARGET 63-99, PLATE 1, TITANIUM
(6AL, 4V), 0.1 INCH THICK
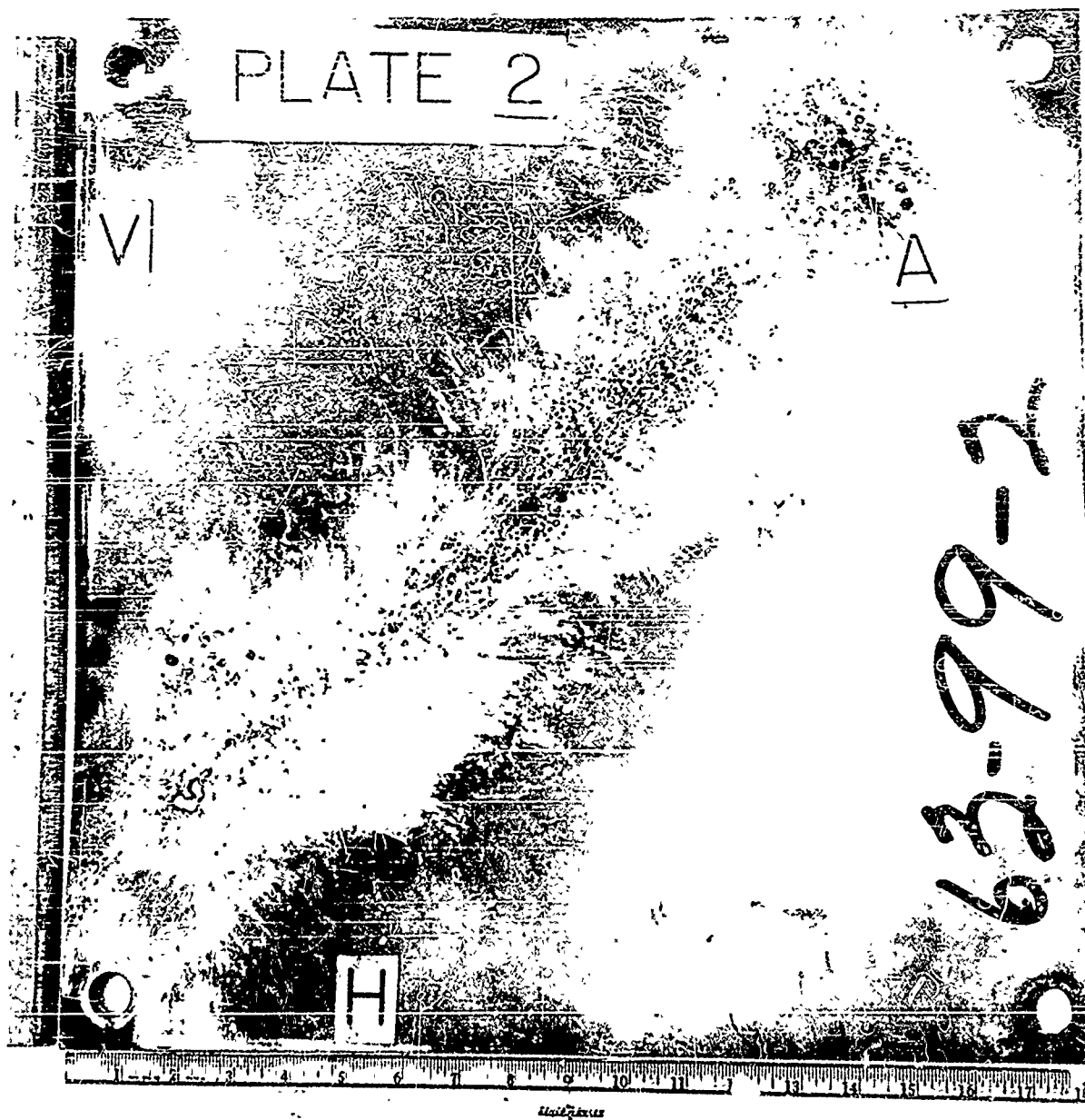
FIGURE 74 TARGET 63-99, PLATE 2, TITANIUM
(6AL, 4V), 0.1 INCH THICK
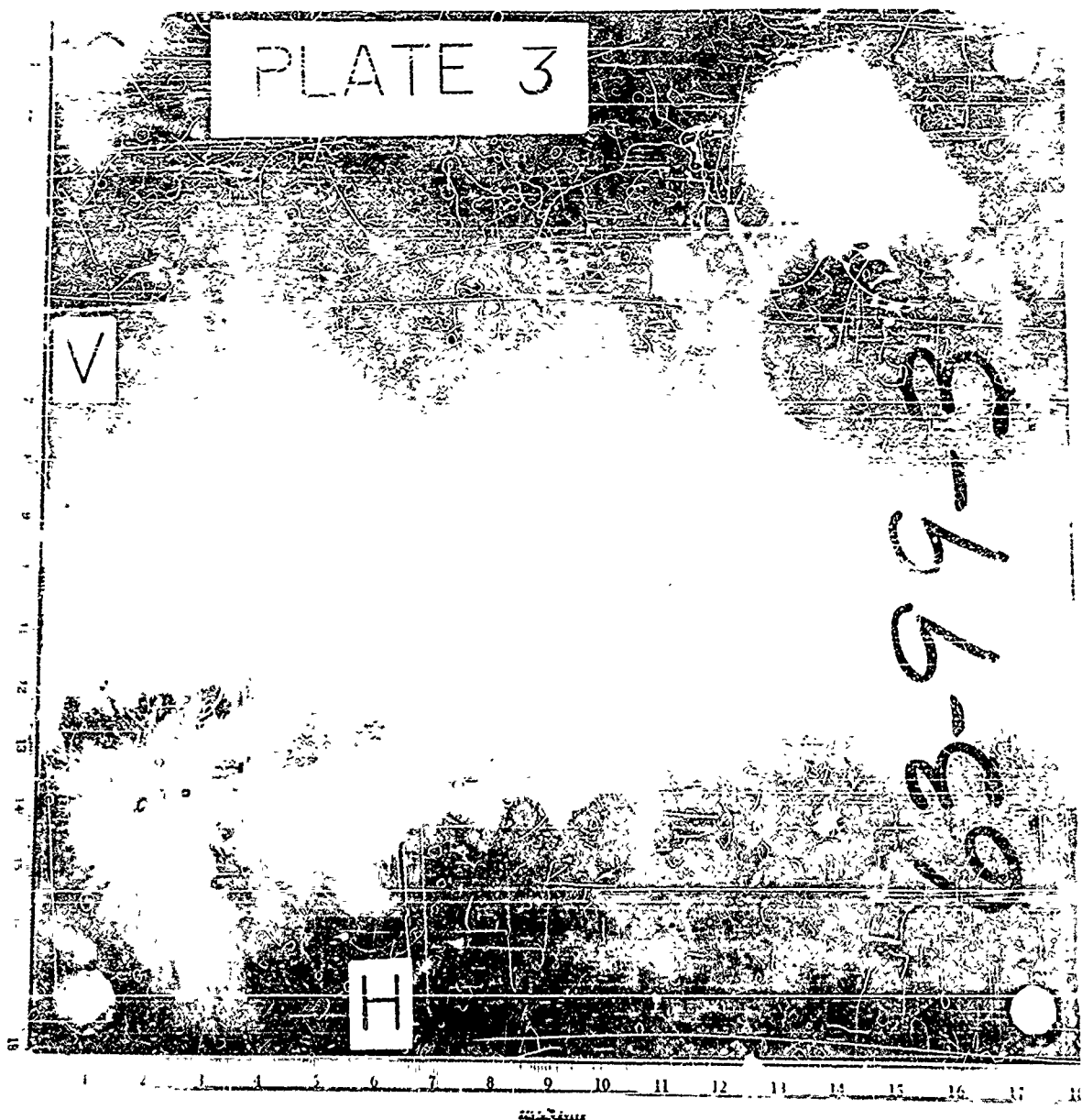
FIGURE 75 TARGET 63-99, PLATE 3, TITANIUM
(6AL, 4V), 0.1 INCH THICK
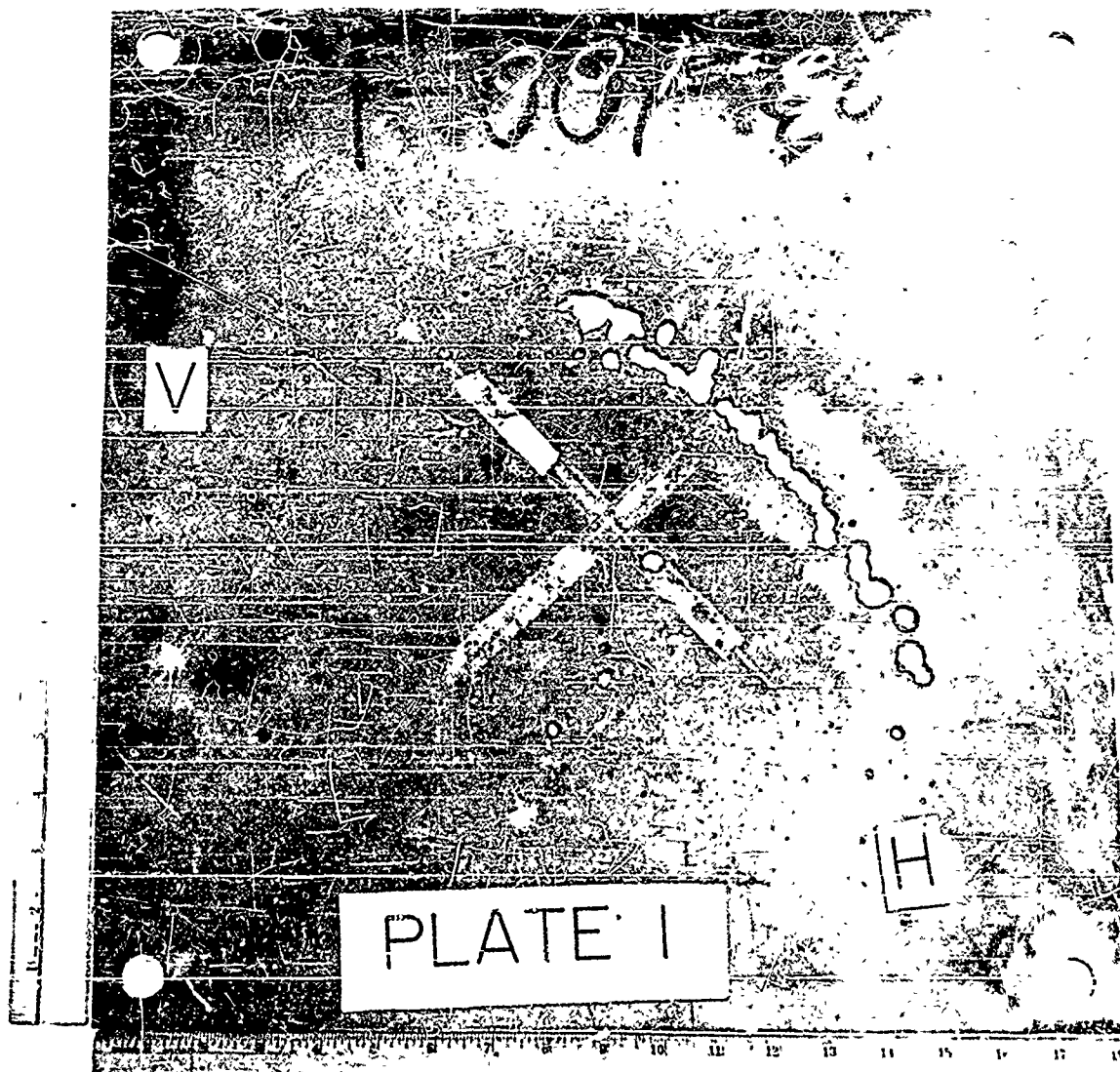
FIGURE 76   TARGET 63-100, PLATE 1, TITANIUM
(6AL, 4V), 0.1 INCH THICK

FIGURE 77   TARGET 63-100, PLATE 2, TITANIUM
(6AL, 4V), 0.1 INCH THICK

FIGURE 78 PERFORATION X, TARGET 63-100, TITANIUM
(6AL, 4V), 0.1 INCH THICK (25X)
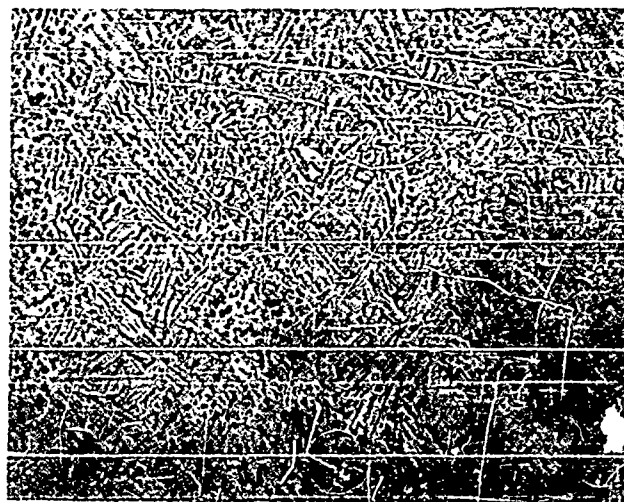
FIGURE 79   MICROSTRUCTURE NEAR A PERFORATION IN
            TARGET 63-100, TITANIUM, 0.1 INCH THICK

TABLE 1   DESCRIPTION OF TARGETS

Target Number	Material	Panel Thickness (in.)				Spacing (in.)
		1	2	3	4	

I. Thin Aluminum

Target Number	Material	1	2	3	4	Spacing (in.)
EB-61	2024-T3	0.1	0.1	0.1	0.1	2
63-12	2024-T3	0.1	0.1	0.1	0.1	2
63-15	2024-T3[1]	0.1	0.5	0.1		2
63-46	2024-T3	0.1	0.1			24
63-51	2024-T3	0.1	0.25	0.25		4
63-52	2024-T3	0.1	0.25	0.25	0.25	2
63-53	2024-T3	0.1	0.25	0.25		8
63-54	2024-T3	0.1	0.25			8
63-59	2024-T3	0.1	0.25	0.25		16
63-62	2024-T3[1]	0.1	0.5			2
63-63	2024-T3[1]	0.1	0.5			24
63-70	2024-T3	0.1	0.25	0.25		4
63-79	2024-T3[1]	0.1	0.5			16
63-82	2024-T3	0.1	0.25			8
63-83	2024-T3	0.1	0.25			24
63-91	2024-T3[2]	0.1	0.25			2
63-94	2024-T3[1]	0.1	1.0			2
63-02	2024-T3[1]	0.1	1.0			8
64-03	2024-T3[1]	0.1	1.0			4
64-04	2024-T3[1]	0.1	1.0			4
64-05	2024-T3[1]	0.1	1.0			16
64-06	2024-T3[1]	0.1	1.0			24
64-09	2024-T3[3]	0.1	2.0			4

II. Thick Aluminum

Target Number	Material	1	2	3	4	Spacing (in.)
63-9	2024-T4	0.5				
63-10	2024-T4	0.5				
63-95	2024-T4	1.0				
63-98	2024-T351	2.0				
63-102	2024-T351	2.0				
63-109	2024-T351	2.0				

III. Magnesium

Target Number	Material	1	2	3	4	Spacing (in.)
63-17	AZ31B-H24[4]	0.1	0.1	0.1	0.1	2
63-18	AZ31B-H24[4]	0.25	0.1	0.1	0.1	2
63-19	AZ31B-H24[4]	0.25	0.5	0.1	0.1	2
63-20	AZ31B-H24	0.1	0.25	0.25		
63-21	AZ31B-H24	0.1	0.25	0.25		4
63-22	AZ31B-H24	0.1	0.25	0.25		
63-23	AZ31B-H24	0.1	0.25	0.25		

TABLE 1 (Continued) DESCRIPTION OF TARGETS

Target Number	Material	Panel Thickness (in.)				Spacing (in.)
		1	2	3	4	
III. Magnesium (Continued)						
63-24	AZ31B-H24	0.1	0.25	0.25		24
63-25	AZ31B-H24	0.1	0.25	0.25		16
63-30	AZ31B-H24	0.1	0.1	0.1		8
63-47	AZ31B-H24	0.1	0.1	0.1	0.1	4
63-48	AZ31B-H24	0.1	0.1	0.1		
63-49	AZ31B-H24	0.1	0.1			24
IV. Steel						
63-86	AISI 4130	0.1	0.1			8
63-87	AISI 4130	0.1	0.1			16
63-88	AISI 4130	0.1	0.1			
63-104	410 Stainless	0.1	0.1	0.1		2
V. Titanium						
63-97	Titanium	0.1	0.1			2
63-99	Titanium	0.1	0.1	0.1		2
63-100	Titanium	0.1	0.1			4

1. Panel 2 is 2024-T4 aluminum.
2. Panel 2 is 4130 steel.
3. Panel 2 is 2024-T351 aluminum.
4. Panels 2, 3, and 4 are 2024 aluminum.

TABLE 2 SUMMARY OF PROJECTILE AND TARGET DAMAGE DATA

Target	Identity	Length (in)	Diameter (in)	Mass (grains)	Velocity (ft/sec)	Pitch	Yaw	Angle of Incidence	Projected Area (in²)	Depth (in)	Diameter (in) (Crater/Hole Dimensions)	Area (in²)	Vol (in³)
EB-61	A	--	--	4.6	31,000	--	--	--	--	hole	0.72	.41	
	B	--	--	2.6	30,800	--	--	--	--	"	0.61	.29	
63-12	A	0.31	0.10	1.5	31,400	-12°	-15°	72°	0.017	"	0.63	.31	
63-15	A	0.76	0.12	8.5	31,400	-25°	-45°	43°	0.095	"	1.25/0.60	.59	
63-46	A	0.86	0.13	8.9	31,500	-73°	60°	15°	0.120	"	1.01/0.81	.90	
63-51	A	0.82	0.12	5.2	31,200	77°	72°	11°	0.090	"	1.25/0.9	.48	
	B	0.21	0.08	1.1	31,200	12°	0°	79°	0.010	"	0.50	.20	
63-52	A	1.00	0.16	13.9	31,700	-24°	-51°	38°	0.153	"	1.25/0.75	.74	
63-53	A	0.72	0.15	7.5	31,600	7°	20°	79°	0.048	"	1.25/0.75	.74	
63-54	A	0.96	0.13	9.7	32,200	90°	78°	0°	0.132	"	1.45/0.90	1.02	
	B	0.42	0.11	2.8	31,500	0°	-08°	82°	0.016	"	0.40	.13	
63-59	A	0.85	0.14	8.8	31,500	0°	-46°	46°	0.097	"	1.0	.79	
	B	0.37	0.12	1.8	32,000	-30°	-51°	37°	0.033	"	0.63	.31	
63-62	A	0.78	0.12	6.0	32,100	-70°	80°	9°	0.093	"	1.25/0.84	.82	
63-63	A	0.80	0.10	5.5	31,500	-47°	-75°	24°	0.077	"	1.63/0.81	1.32	
	B	0.44	0.12	4.5	32,200	-8°	-19°	70°	0.028	"	0.50/0.38	.15	
63-70	A	-.31	0.13	9.8	30,200	87°	-62°	3°	0.156	"	1.56/0.81	.99	
63-79	A	0.33	0.12	2.4	31,300	0°	90°	0°	0.023	"	1.25/0.75	.74	
	B	0.47	0.13	3.4	30,200	0°	-19°	71°	0.037	"	0.56	.25	
	C	0.20	0.15	1.7	30,000	54°	-46°	20°	0.029	"	0.53	.22	
	D	0.27	0.12	1.9	30,200	-33°	-29°	50°	0.033	"	0.53	.22	
63-82	A	1.12	0.12	7.3	30,800	-80°	80°	7°	0.129	"	1.38/0.94	1.02	
63-83	A	0.16	0.12	4.5	31,200	26°	-51°	37°	0.057	"	0.94/0.63	.46	
63-91	A	0.9?	0.19	11.8	30,500	-39°	-69°	21°	0.104	"	0.78	.48	
63-94	A	0.97	0.15	12.0	31,200	55°	43°	32°	0.129	"	1.19/0.78	.73	
64-02	A	1.10	0.12	11.7	31,800	-75°	90°	0°	0.148	"	1.24/0.94	.94	
64-03	A	0.59	0.13	5.9	31,800	-16°	17°	67°	0.042	"	0.59	.27	
	B	0.43	0.10	1.8	30,600	12°	-5°	75°	0.016	"	0.50	.20	
64-04	A	0.86	0.14	5.2	31,700	8°	5°	81°	0.039	"	0.44	.15	
	B	0.28	0.10	1.2	31,100	-32°	-32°	49°	0.039	"	0.50	.20	
64-05	A	0.87	0.14	7.7	31,800	61°	6°	29°	0.100	"	1.28/0.81	.81	
64-06	A	0.84	0.13	7.2	30,800	0°	-13°	77°	0.034	"	0.50	.20	
	E	0.29	0.09	1.5	31,000	-86°	90°	0°	0.023	"	0.50	.20	
64-09	A	0.95	0.13	9.8	31,100	-2°	-22°	68°	0.050	"	0.88/0.63	.44	
	B	0.52	0.08	1.8	30,000	12°	63°	27°	0.036	"	0.59/0.75	.35	

I. Thin Aluminum Targets

TABLE 2 SUMMARY OF PROJECTILE AND TARGET DAMAGE DATA (Cont'd)

Target	Identity	Projectile Length (in)	Diameter (in)	Mass (grains)	Velocity (ft/sec)	Pitch	Yaw	Angle of Incidence	Projected Area (in²)	Depth (in)	Diameter (in)	Area (in²)	Vol. (in³)
II. Thick Aluminum Targets													
63-9	A	0.20	0.09	1.0	27,800	-21°	29.5°	55.6°	0.02	Hole	0.7	0.38	--
63-10	A	0.45	0.11	2.0	29,700	0°	3°	90°	0.020	"	0.75	0.44	--
63-95	B	0.33	0.12	7.6	29,700	0°	0°	0°	0.23	"	1.50	1.76	--
63-98	A	0.70	0.14	6.4	31,400	56°	-3°	20.6°	0.034	"	1.63	--	--
				No data obtained									
63-102	A	0.81	0.16	7.8	31,000	31.5°	-28.5°	50.7°	0.074	.63	1.38	"	7.7 ml
	B	0.37	0.09	1.7	30,800	-9.0°	-10.5°	76.3°	0.013	.5	1.13	--	4.0 ml
63-109	A	0.57	0.14	3.9	31,500	0°	-23.5°	61.5°	.037	.75	1.75	--	Intersecting craters
III. Magnesium Targets													
63-17	A	0.89	0.12	8.4	31,700	-28°	-60°	29°	0.126	Hole	1.36/0.94	1.02	
	B	0.56	0.15	4.4	30,600	14°	14.5°	70°	0.033	"	1.25/.5	0.49	
63-18	A	0.92	0.14	8.4	32,000	-66°	78.5°	90°	0.118	"	1.25	1.23	
	B	0.55	0.10	3.5	30,500	-6.5°	18.5°	90°	0.026	"	0.75	0.44	
63-19	A	0.90	0.13	7.9	30,200	-57.5°	0.0°	90°	0.093	"	Observed by Interconnecting Perforations		
63-20				No data obtained									
63-21	A	0.59	0.14	6.5	31,300	90°	74°	0°	0.078	"	1.25/1.0	0.93	
63-22				No data obtained									
63-23				No data obtained									
63-24	A	0.7	0.13	8.5	31,500	-84°	90°	0°	0.123	"	1.56/1.06	1.30	
	B	0.2	0.09	1.1	30,900	0°	20.5°	70°	0.013	"	0.94/0.63	0.46	
63-25	A	0.24	0.13	1.3	30,700	-19.5°	5°	70°	0.016	"	Not identified on plate		
	B	0.17	0.13	1.2	30,300	65°	32.5°	25°	0.021	"	Not identified on plate		
	C	0.21	0.10	0.3	30,200	18.5°	0°	72°	0.012	"	Not identified on plate		
63-30	A	0.82	0.11	6.9	27,500	-24°	41.5°	45°	0.054	"	0.75	0.44	
	B	0.35	0.09	1.7	26,100	-68°	4.3°	22°	0.035	"	0.63	0.31	
	C	0.35	0.11	2.1	27,100	-51°	11°	39°	0.024	"	1.0	0.79	
63-47	A	0.71	0.13	7.1	31,900	58°	75°	14°	0.096	"	1.38/1	1.08	
63-48				No data obtained									
63-49	A	1.09	0.12	9.6	31,400	37.5°	61°	27°	0.123	"	Observed by interconnecting perforations		

TABLE 2   SUMMARY OF PROJECTILE AND TARGET DAMAGE DATA (Cont'd)

Target	Identity	Projectile Length (in)	Diameter (in)	Mass (grains)	Velocity (ft/sec)	Orientation Pitch	Yaw	Angle of Incidence	Projected Area (in²)	Target Damage (Crater/Hole Dimensions) Depth (in)	Diameter[1] (in)	Area (in²)	Vol. (in³)
IV. Steel Targets													
63-86	A	1.09	0.13	9.0	32,000	10°	-38°	51°	0.091	Hole	Intersecting perforations		
	B	0.42	0.09	3.1	31,000	0°	9°	81°	0.015	"	0.5	0.20	
63-87	A	0.96	0.14	7.5	30,800	0°	-44°	46°	0.106	"	1.0/0.75	0.59	
63-88	A	0.87	0.16	7.3	31,500	74°	-69°	13°	0.112	"	1.5/0.75	0.88	
	B	0.16	0.14	0.9	31,100	36°	19°	5°	0.011	"	0.44	0.15	
63-104	A	0.74	0.11	5.1	31,100	9°	11°	76°	0.037	"	1.25/0.63	0.61	
V. Titanium Targets													
53-97				No data obtained									
63-99	A	0.95	0.13	7.1	30,900	-26°	-64°	26°	0.082	"	1.13/0.63	0.56	
65-100				No data obtained									

1   Where two values are shown for a perforation, the perforation was elliptical. The values are the lengths of the major and minor axes.

INITIAL DISTRIBUTION

1	DOD (DIAAP-1K2)
1	Hq USAF (AFTAC)
1	Hq USAF (AFCIN-3K2)
2	Hq USAF (AFRDC)
1	Hq USAF (AFRAE-E, L/C Hicks)
1	Hq USAF (AFTST-EL/CS, Maj Myers)
1	USAF (AFRST-PM/ME, Maj Geiseman)
1	Hq USAF (AFXPDK-NI)
1	AFSC (SCKMA)
1	AFSC (SCTA, Mr R Fiek)
2	BSD (Col Brassfield)
1	ASD (SEPRR)
1	AFFDL (FDTS, Mr. Parmley)
2	ASD (ASAD-Lib)
1	ASD (ASRNGW, Don Lewis)
2	AFSWC (Tech Info Div)
1	AFCRL (CRQST-2)
1	AFOSR
1	AFOSR (SRHP, Dr M M Slawsky)
1	AFOSR (SRHP, Dr J F Masi)
1	AFOSR (Dr A G Horney)
1	AFOSR (SRHP, Dr R Reed)
1	AFOSR (Dr M A Cook)
1	OOAMA (OOYD)
1	NASA
1	NASA (Ofc of Adv Rsch)
2	NASA (Tech Lib)
1	NASA, Rsch Ctr (W H Kinard)
1	NASA, Rsch Ctr (J Stack)
4	NASA, Ames Rsch Ctr (Tech Lib)
1	Marshall Space Flight Center (W D Murphree)
1	Marshall Space Flight Center Adv Rsch Proj Lab (Dr W Johnson)
1	Adv Rsch Proj Agency (Dr C Bates)
1	Dir of Def Rsch & Engr (Tech Lib)
2	Dir of Def Rsch & Engr (Dr R M Yates)
2	ARO (Scientific Info Br)
1	Armour Rsch Foundation (Mr G H Strohmeir)
1	Aberdeen Proving Ground (Tech Lib)
1	White Sands Missile Range

1	Univ of Chicago (Lib)
2	Franklin Institute of the State of Penn
2	SSD (SSTRG/LC W Levin)
1	Calif Inst of Tech, Jet Propulsion Lab
2	John Hopkins Univ (Applied Rsch Lab)
1	OAR (RROSA/Maj Davis
1	OAR (RROSA/Maj Stalk)
20	DDC
3	Lewis Rsch Ctr
2	Dir, IDA/WPNS Sys Eval Gp
1	Dir, USAF PROJ RAND (Tech Lib)
3	Army Materiel Command Rsch Directorate (MCR)
2	Picatinny Arsenal (SMUPA-DW5)
1	Aberdeen Proving Ground (Dr Eichelberger)
1	Aberdeen Proving Ground (J Kineke)
1	Aberdeen Proving Ground (F E Allison)
1	Redstone Scientific Info Ctr
1	Frankford Arsenal (Lib)
1	Frankford (Pitman-Dunn Lab)
2	Springfield Armory (R&D Div)
2	Watervliet Arsenal (Col C A Conlon)
2	Watertown Arsenal
1	Rock Island Arsenal
1	Army Engr Rsch and Dev Lab (Tech Doc Ctr)
1	Dir of Spec Wpns Div (C. I. Peterson)
1	Army Rsch Ofc – Durham (Dr A S Galbraith)
4	Bureau of Naval Weapons (R 12)
4	Bureau of Naval Weapons (RM)

1 US Naval Rsch Lab
    (Code 130/MR WJ Atkins)
2 US Naval Ord Test Stn
    (Mr L Cosner)
2 US Naval Ord Test Stn)
    (Tech Lib)
2 US Naval Ord Lab
    (Tech Lib)
2 US Naval Wpns Lab
    (Tech Lib)
1 US Naval Wpns Lab (Dr Soper)
1 AFMTC   (MTBAT)
4 TAC   (DORQ)
5 Hayes International Corp
2 General Electric Co
  APGC
    1   PGOM
    2   PGBAP-1
    3   PGEH
    1   PGOW
  RTD, Det 4
    2   ATWR
    1   ATWW
    1   ATTR
    1   ATB
    20   ATBT